GALLIUM ARSENIDE - GALLIUM ALUMINUM ARSENIDE DISTRIBUTED FEEDBACK AND DISTRIBUTED BRAGG REFLECTOR LASERS

Thesis by

Huan-wun Yen

In Partial Fulfillment of the Requirements

for the Degree of

Doctor of Philosophy

California Institute of Technology

Pasadena, California

1976

(Submitted May 11, 1976)

To my dear parents

ACKNOWLEDGMENT

I would like to express my sincere gratitude to my research advisor, Professor Amnon Yariv, for his excellent guidance and constant encouragement throughout the course of this work. It has been a very pleasant and fruitful five years for me to be part of the quantum electronics group. I enjoyed every minute of it.

During this study we were very fortunate to enjoy the cooperation from the Central Research Laboratory of Hitachi, Tokyo, Japan. In particular I would like to thank Dr. Michiharu Nakamura for his technical advice and helpful discussions. His contributions and friendship are greatly treasured. Also I would like to acknowledge Dr. Hugh Garvin of Hughes Research Laboratories in Malibu, California. His professional assistance and stimulating discussions on the fabrication of corrugations are most helpful. I am also indebted to Dr. Elsa Garmire for introducing me to the Laboratory work and epitaxial crystal growth.

It is a pleasure to acknowledge the skillful technical assistance of Desmond Armstrong with the experimental apparatus. Special thanks go to Ms. Dian Rapchak and Mrs. Ruth Stratton for doing such a wonderful job of typing the manuscript.

Financial support received from the International Business Machines Corporation, the National Science Foundation, the Office of Naval Research, and the California Institute of Technology is greatly appreciated.

Finally my thanks go to my wife, Julie, for her love and support.

ABSTRACT

This work describes theoretical and experimental studies of GaAs-GaAlAs distributed feedback and distributed Bragg reflector lasers. These lasers are strong candidates as the light source in integrated optical circuits and optical communication systems.

A coupled-mode formalism is used to study the propagation of electromagnetic waves in a dielectric waveguide with periodic surface corrugation. The reflection and transmission characteristics of both passive and active periodic waveguides are found as a function of wavelength.

These results are used to derive the oscillation conditions of two different laser structures: (1) the distributed feedback laser - where a corrugated active waveguide section is the basic structure, (2) the distributed Bragg reflector laser - where an active region is flanked by two sections of passive periodic waveguides.

The procedure of determining the lasing wavelength is outlined. The merits and disadvantages of various laser structures are compared and discussed.

Experimental results on fabrication and measurements of GaAs-GaAlAs distributed feedback and distributed Bragg reflector lasers are presented and compared with the theory. Various fabrication and measurement techniques developed during the course of the investigation are described in some detail.

TABLE OF CONTENTS

CHAPTER 1

INTRODUCTION

1-1 Integrated Optics and Optical Communications

From the beginning of radio communications it has been the goal of electrical engineers to explore higher carrier frequency ranges for better signal quality and larger information capability. The evolution started with AM radio in the KHz range, proceeded to FM transmission in MHz range, and on to microwaves in the GHz range. It was not until about 1960 with the advent of lasers that communications in the optical frequency regime began to be considered seriously. Some of the potential advantages of optical communication systems are: (a) extremely large bandwidth and therefore high data rates, (b) very wide spectral ranges, (c) small system components. Optical communication, however, did not receive serious attention since propagation through the atmosphere involves high transmission losses and low loss optical waveguides did not exist.

During the last few years the situation has changed radically. Techniques for fabricating very low loss waveguide—optical fibers were developed, and transmission losses as low as 2 db/km at near infrared wavelengths were achieved[1]. This technological breakthrough stimulated once again the interest in optical communications, in particular the communications through optical fibers.

Besides their large bandwidth potential, the fiber communication system has the merits of small size and light weight, no ground loop problem exists, and the channels are essentially free of any

interference and pick-up problems. It is expected that fiber channels will provide both short range and long range high data density communication. For these applications we will need terminals at both ends and repeaters along the line to complete the system. Fig. 1-1 shows a simplified diagram of such a link. At the terminals signals are either generated and modulated for launching or detected, amplified and demodulated for processing. In repeaters the signals are detected, amplified, and used to modulate another source for relaunching. These terminals and repeaters should be reliable and have dimensions comparable to those of the fibers. While most of the conventional optical systems in use today are bulky and extremely sensitive to alignment, it is essential that a new kind of technology be developed for this purpose. And this is where "Integrated Optics"[2] comes in.

The technology of integrated optics centered around the study of optical dielectric waveguides and devices made using such waveguides. These devices include grating filters, Bragg reflectors, grating couplers, taper couplers, lenses, prisms, directional couplers, lasers, modulators, polarizers and detectors, all in planar form. It is thus conceivable that one could fabricate on a common substrate all the necessary components which will be interconnected by waveguides to form a small, rugged integrated optical circuit in very much the same way as electronic integrated circuits. Most of the work done so far in the area of integrated optics, however, involves the demonstration of individual components and the technology of integration is only in its very beginning. There is

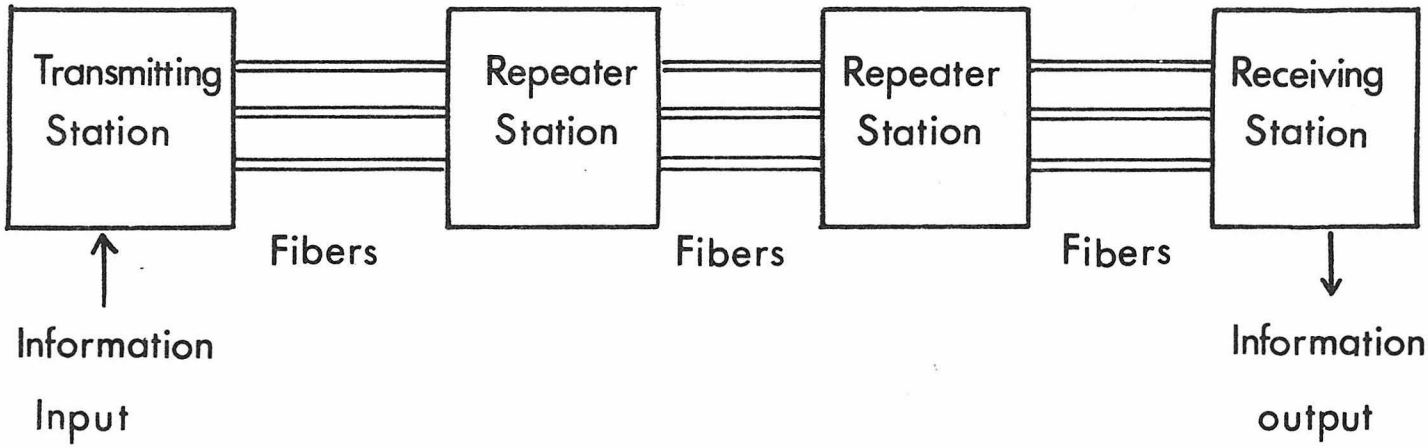

Fig. 1-1 Block diagram of an optical fiber communication link.

no apparent obstacle, however, for achieving such an integration in the near future. There remains the difficult problem of interconnecting the fibers and the optical circuits which will be addressed in Chapter 4.

1-2 GaAs-GaAlAs System for Monolithic Integrated Optical Circuits

Many different materials were used in fabricating optical components during the past few years. Each particular device requires the optimization of certain parameters which dictate the choice of material. In the integration process one could use the "hybrid" approach, in which several different materials are incorporated in one circuit so that each individual component performance can be optimized. In practice this approach poses a major problem, which is that of interfacing different components. The coupling efficiency between components of different material is usually low unless some precautions are taken in designing and manufacturing. This process can become very complicated even for a simple circuit. Hence it is important to search for materials suitable for monolithic optical circuits for simplicity and reliability.

First let us examine some of the basic functions to be performed by an optical circuit. These include (a) light generation, (b) light detection, (c) modulation and switching, (d) waveguiding, (e) coupling. The versatility of GaAs in terms of electrical and optical properties makes it a very strong candidate for the basic material of integrated optics[3,4]. Let us examine GaAs against the basic requirements listed above: (a) GaAs is the only material to

date from which small size cw lasers that operate at room temperature can be made. (b) A reversely biased p-n junction or an ion implanted region in GaAs are known to be reasonably good detectors[5,6]. (c) GaAs possesses one of the largest electro-optic and acousto-optic figures of merit and has been used in making efficient modulators[7]. (d) GaAs can be alloyed with AlAs to form $Ga_{1-x}Al_xAs$. The index of refraction of this material varies with x, the mole fraction of Al. The larger x the smaller the index of refraction. Hence it is convenient to form dielectric waveguides with layers of GaAs and $Ga_{1-x}Al_xAs$. (e) Directional couplers[8], grating couplers[9] and taper couplers[10] have been fabricated with high quality in GaAs.

Moreover GaAs technology such as liquid phase, vapor phase, and molecular beam[11] epitaxial crystal growth, ion implantation, ion beam etching, chemical etching, diffusion, doping, ohmic contacting Schottky barriers, etc. are being pursued and developed to a very high technical quality necessary for making optical circuits.

Another important factor that favors GaAs is that GaAs injection lasers emit light with wavelength in the region of 0.8 - 0.9 μm which coincides with the low loss window of the fiber transmission spectrum[1].

Recently several new techniques in liquid phase epitaxy have been developed. These include the growth of tapered waveguides[10] and the selective growth through masks[12,13]. These two techniques are essential to the integration of components. It is the author's opinion that the successive selective epitaxial growth is going to play a vital role in integrated optics as the selective diffusion

does in electronic integrated circuits.

1-3 Distributed Feedback and Distributed Bragg Reflector Lasers

The most important component in a transmitting terminal or a repeater of the fiber communication system is the light source. The conventional miniature light source is the GaAs-GaAlAs injection laser. The reflection feedback in these lasers is usually obtained by cleaving the crystal along a pair of parallel crystal planes. Because of the dielectric constant difference between GaAs and the air finite reflectivity is achieved on both ends. This fabrication process is discrete and therefore not compatible with the planar technology. A novel "mirror-less" laser structure was suggested by Kogelnik and Shank[14] which utilizes the spatial periodic modulation of the properties of the lasing medium to cause coupling between waves going in opposite directions. Such a feedback mechanism is not localized but rather distributed along the length of the medium and is referred to as distributed feedback.

A periodic surface corrugation of a waveguide can be viewed as a periodic modulation of the waveguide's effective index of refraction. If a wave propagates in the waveguide with a guide wavelength $\lambda_g = 2\Lambda$ then the backward scattered wave from the corrugations will add up in phase as depicted in Fig. 1-2. We shall call this phenomenon backward Bragg scattering (or reflection) and the condition $\Lambda = \lambda_g/2$, the Bragg condition since it is analogous to x-ray scattering by crystal planes. A section of a waveguide which is corrugated can thus be used as a mirror (Bragg reflector) with reflectivity which is

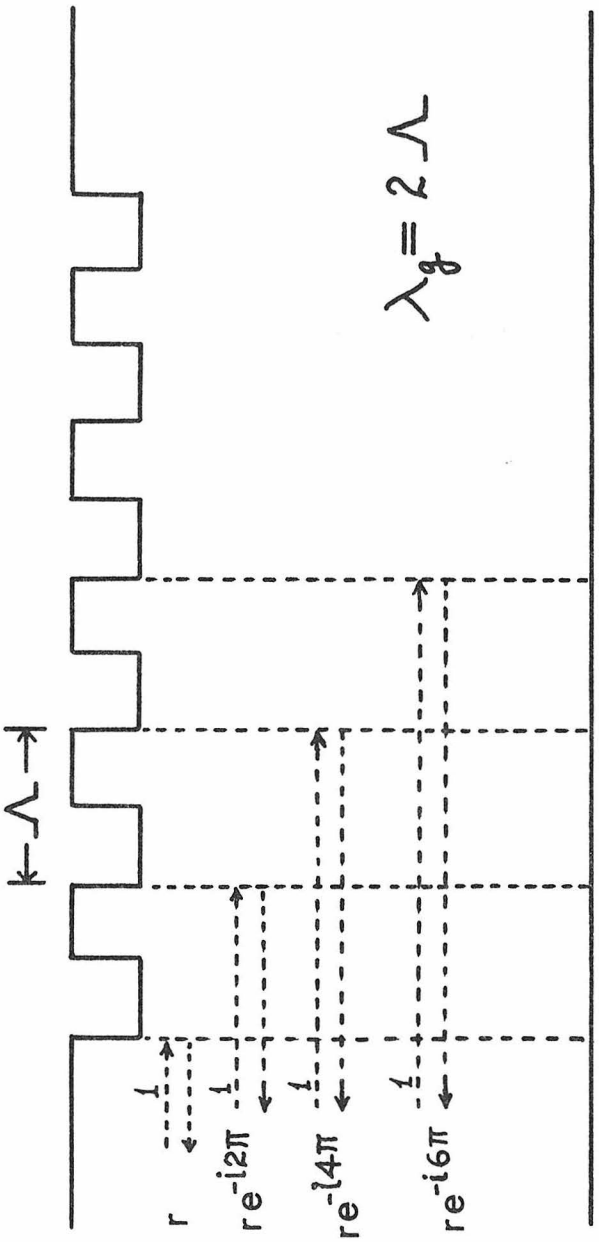

Fig. 1-2 Backward Bragg scattering in a periodic waveguide.

a strong function of the frequency of the incident wave.

If this type of periodic structure is incorporated into a conventional GaAs injection laser it results in reflection feedback without a need for cleaved end mirrors. Two approaches to achieve this feedback are shown in Fig. 1-3. In (a) the corrugation (or grating) extends over the whole length of the active region. This structure is called distributed feedback (DFB) laser. In (b) the corrugations are present on both sides of the active region and serve as mirrors. Such a structure is referred to as the distributed Bragg reflector (DBR) laser[15].

The advantages of using DFB and DBR lasers are four-fold:
(a) The fabrication process is compatible with planar technology.
(b) Better laser longitudinal and transverse mode control[14,16] result from the frequency selective nature of the feedback.
(c) Better frequency stability against temperature variation[17].
(d) The presence of the gratings makes possible new schemes of coupling laser output into fibers[18] or other optical circuits.
There is still the reliability (operating lifetime) problem which needs to be solved before any practical applications of these lasers are possible.

In Chapters 2, 3, and 4 we will describe the theoretical and experimental studies of DFB and DBR lasers and their potential applications in integrated optical circuits.

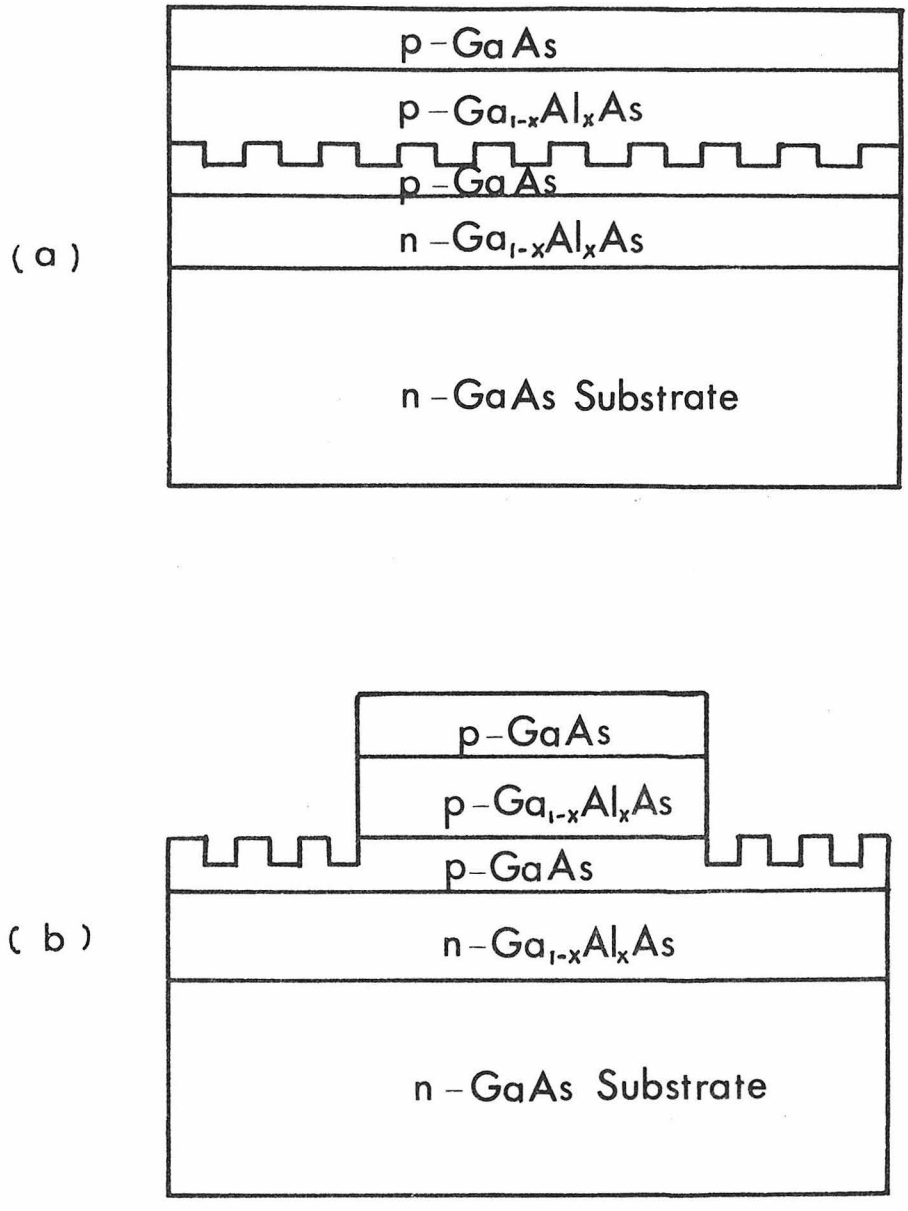

Fig. 1-3 Schematic diagram of double-heterostructure GaAs lasers. (a) Distributed feedback laser (b) Distributed Bragg reflector laser.

1-4 Experimental Techniques

Because of the small dimensions of the optical circuits and because of the strict requirement of edge smoothness of certain components special fabrication techniques are needed. In order to produce reliable long-life, low loss devices it is important that one knows the limitations of each technique. In Chapter 5 we will describe some of the techniques used during the course of studying GaAs-GaAlAs DFB and DBR lasers. These include:

(a) Liquid phase epitaxial crystal growth -- probably the most important single technique in fabricating GaAs lasers, waveguides, and other related components.

(b) Grating fabrication -- for use in DFB and DBR lasers, wire-grid polarizers, couplers, and filters. Grating period ranges from 0.1 μm to 1 μm.

(c) Ion beam etching and sputtering -- combined with photolithography is capable of fabricating complex circuits on a single substrate.

(d) Optical measurements -- photoluminescence measurements, laser spectroscopy, and waveguide parameter measurements are used for sample and device characterization.

(e) Other device fabrication techniques such as diffusion, ohmic contact formation, chemical etching, etc.

CHAPTER 1 REFERENCES

(1) D. B. Keck, R. D. Maurer, and P. C. Schultz, "On the ultimate lower limit of attenuation in glass optical waveguides," Appl. Phys. Lett. 22, 307 (1973).

(2) "Special issue on integrated optics and optical waveguides," IEEE Trans. Microwave Theory Tech. 23, January (1975).

(3) A. Yariv, "Active integrated optics," Fundamental and Applied Laser Physics, Proceedings of the Esfahan Symposium, John Wiley & Sons, New York, p. 897 (1971).

(4) V. Evtuhov and A. Yariv, "GaAs-GaAlAs devices for integrated optics," IEEE Trans. Microwave Theory Tech. 23, 44 (1975).

(5) F. K. Reinhart, "Electroabsorption in $Al_yGa_{1-y}As$-$Al_xGa_{1-x}As$ double heterostructures," Appl. Phys. Lett. 22, 372 (1973).

(6) H. Stoll, A. Yariv, R. G. Hunsperger, and G. L. Tangonan, "Proton-implanted optical waveguide detectors in GaAs," Appl. Phys. Lett. 23, 664 (1973).

(7) F. K. Reinhart and B. I. Miller, "Efficient GaAs-$Al_xGa_{1-x}As$ double-heterostructure light modulators," Appl. Phys. Lett. 20, 36 (1972).

(8) S. Somekh, E. Garmire, and A. Yariv, "Channel optical waveguiding directional couplers," Appl. Phys. Lett. 22, 46 (1973).

(9) F. K. Reinhart, R. A. Logan, and C. V. Shank, "GaAs-$Al_xGa_{1-x}As$ injection lasers with distributed Bragg reflectors," Appl. Phys. Lett. 27, 45 (1975).

(10) J. L. Merz, R. A. Logan, W. Wiegmann, and A. C. Gossard, "Taper couplers for GaAs-$Al_xGa_{1-x}As$ waveguide layers produced by liquid

phase and molecular beam epitaxy," Appl. Phys. Lett. 26, 337 (1975).

(11) A. Y. Cho, "Film deposition by molecular-beam techniques," J. Vac. Sci. Technol. 8, S31 (1971).

(12) T. Tsukada, "GaAs-$Ga_{1-x}Al_xAs$ buried heterostructure injection lasers," J. Appl. Phys. 45, 4899 (1974).

(13) I. Samid, C. P. Lee, A. Gover, and A. Yariv, "Embedded heterostructure epitaxy: A technique for two dimensional thin-film definition," Appl. Phys. Lett. 27, 405 (1975).

(14) H. Kogelnik and C. V. Shank, "Coupled-wave theory of distributed feedback lasers," J. Appl. Phys. 43, 2327 (1972).

(15) S. Wang, "Principles of distributed feedback and distributed Bragg-reflector lasers," IEEE J. Quantum Electron. 10, 413 (1974).

(16) S. Somekh, "Transverse mode control in a distributed feedback semiconductor laser," Proc. IEEE (Lett.), 62, 277 (1974).

(17) M. Nakamura, K. Aiki, J. Umeda, A. Katzir, A. Yariv, and H. W. Yen, "GaAs-GaAlAs double-heterostructure injection lasers with distributed feedback," IEEE J. Quantum Electron. 11, 436 (1975).

(18) H. W. Yen, W. Ng, I. Samid, and A. Yariv, "GaAs distributed Bragg reflector lasers," to be published in Optics Communication.

CHAPTER 2

COUPLED-MODE THEORY IN PERIODIC WAVEGUIDES

2-1 Introduction

The name "periodic waveguide" refers to a waveguide with parameters which are periodically modulated along the length of the guide. Before treating periodic waveguides let us review some of the basic properties of an ordinary slab waveguide as shown in Fig. 2-1(a).

The waveguide consists of a thin layer of thickness t and an index of refraction n_2 sandwiched between two media of indices of refraction n_1 and n_3. Assuming that there is no variation in the y-dimension, i.e. $\partial/\partial y = 0$, one can show that[1] such a structure can guide a finite number of confined TE modes with field components E_y, H_x, H_z and TM modes with components H_y, E_x, and E_z. There is also a continuum of radiation modes associated with this structure. These radiation modes are referred to as unguided modes because they are not confined to the inner layer. We shall disregard the radiation modes for the time being and proceed with the discussions on guided modes.

Let us consider TE modes first. The field component $E_y(x,z,t)$ obeys the wave equation

$$\nabla^2 E_y = \frac{n_i^2}{c^2} \frac{\partial^2 E_y}{\partial t^2} \tag{2-1}$$

where i = 1,2,3 indicates the three different regions with indices n_1, n_2, and n_3 respectively. We take $E_y(x,z,t)$ in the form

$$E_y(x,z,t) = \mathcal{E}_y(x) e^{i(\omega t - \beta z)} \tag{2-1a}$$

The transverse function $\mathcal{E}_y(x)$ is taken as

$$\mathcal{E}_y(x) = \begin{cases} C \exp(-qx) & 0 \leq x < \infty \\ C[\cos(hx) - (q/h)\sin(hx)] & -t \leq x \leq 0 \\ C[\cos(ht) + (q/h)\sin(ht)]\exp[P(x+t)] & -\infty \leq x \leq -t \end{cases} \qquad (2\text{-}1b)$$

Substituting (2-1a) and (2-1b) in (2-1) for regions 1,2,3 yields

$$\begin{aligned} h &= (n_2^2 k^2 - \beta^2)^{1/2} \\ q &= (\beta^2 - n_1^2 k^2)^{1/2} \\ p &= (\beta^2 - n_3^2 k^2)^{1/2} \end{aligned} \qquad (2\text{-}1c)$$

where $k = \omega/c$.

The solutions for $\mathcal{E}_y(x)$ and $\mathcal{H}_z(x) = (i/\omega\mu)\, \partial\, \mathcal{E}_y(x)/\partial x$ must be continuous at both $x = 0$ and $x = -t$. By imposing these continuity conditions we get from (2-1b)

$$\tan(ht) = \frac{h(p+q)}{h^2 - pq} \qquad (2\text{-}1d)$$

At a given frequency (i.e. a given k), the eigenvalue equation (2-1d) can be satisfied only at a finite number of β values. For each such β we solve using (2-1c) for the corresponding p, q and h and therefore for the field components in (2-1b). Each field configuration resulting from a given eigenvalue β corresponds to a guided mode of the waveguide. The arbitrary constant C appearing in Equation (2-1b) can be defined such that the field $\mathcal{E}_y(x)$ corresponds to a power flow of one watt (per unit width in the y-direction) in the mode. A mode for which $E_y = A\,\mathcal{E}_y(x)$ will thus correspond to a power flow of $|A|^2$ Watts/m.

For TM modes the field components are

$$H_y(x,z,t) = \mathcal{H}_y(x)e^{i(\omega t-\beta z)}$$

$$E_x(x,z,t) = \frac{i}{\omega\varepsilon}\frac{\partial H_y}{\partial z} \qquad (2\text{-}2)$$

$$E_z(x,z,t) = -\frac{i}{\omega\varepsilon}\frac{\partial H_y}{\partial x}$$

where the function $\mathcal{H}_y(x)$ is taken as

$$\mathcal{H}_y(x) = \begin{cases} -C[\frac{h}{\bar{q}}\cos(ht) + \sin(ht)]\exp[p(x+t)] & x < -t \\ C[-\frac{h}{\bar{q}}\cos(hx) + \sin(hx)] & -t \leq x \leq 0 \\ C(-\frac{h}{\bar{q}})\exp(-qx) & x > 0 \end{cases} \qquad (2\text{-}2a)$$

The continuity of H_y and E_z at $x = 0$ and $x = -t$ requires that

$$\tan(ht) = \frac{h(\bar{p} + \bar{q})}{h^2 - \bar{p}\bar{q}} \qquad (2\text{-}2b)$$

where

$$\bar{p} = \frac{n_2^2}{n_3^2}p \text{ and } \bar{q} = \frac{n_2^2}{n_1^2}q \qquad (2\text{-}2c)$$

The normalization constant C is chosen so that the field $\mathcal{H}_y(x)$ represents, as in the case of TE modes, a power flow of one watt (per unit width in the y-direction) in the mode. The constants C for TM mode and TE mode are different.

In an ideal waveguide, that is one with homogeneous media and smooth boundaries, the guided modes once launched will propagate down the guide independently of each other. In other words there will be no energy transfer among the guided modes. The situation is quite

different once a perturbation is introduced. The perturbation in general will cause scattering or coupling of the original guided modes to the other guided modes and (or) the unguided radiation modes. If the perturbation is introduced along the guide and arranged in such a way that the scattering or coupling effect adds up coherently, then such a waveguide section acts as reflector or coupler. This situation is possible when the perturbation is periodic. The perturbation can consist of a periodic variation of the index of refraction or the gain (or loss) coefficient[2] of the guiding structure, or of the waveguide height. In our study we will confine ourselves to the latter case. In a real device this is achieved by a periodic corrugation of one of the waveguide interfaces as shown in Fig. 2-1(b).

If we define the dielectric function of the unperturbed waveguide [Fig. 2-1(a)] as

$$\varepsilon(\bar{r}) = \begin{cases} \varepsilon_1 & x > 0 \\ \varepsilon_2 & 0 > x > -t \\ \varepsilon_3 & -t > x \end{cases}$$

then the dielectric function of the perturbed waveguide [Fig. 2-1(b)] can be written as

$$\varepsilon'(\bar{r}) = \varepsilon(\bar{r}) + \Delta\varepsilon(\bar{r})$$

where (for a square wave corrugation)

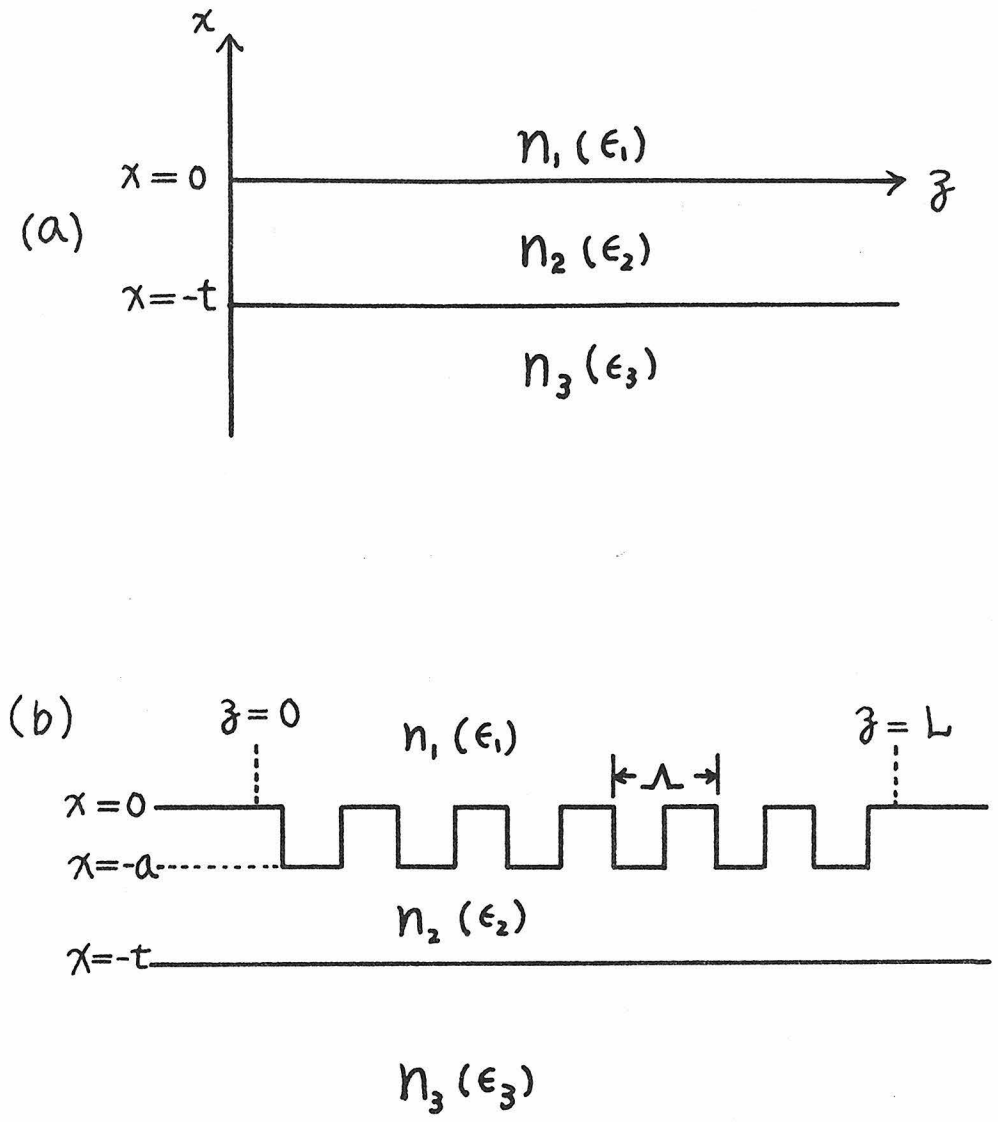

Fig. 2-1 Schematic diagrams of (a) perfect slab waveguide (b) slab waveguide with square wave corrugation.

$$\Delta\varepsilon(\bar{r}) = \begin{cases} 0 & x > 0 \\ (\varepsilon_1-\varepsilon_2)\left\{\frac{1}{2} + \sum_{\substack{\ell=-\infty \\ \ell\neq 0}}^{\infty} \frac{\sin\frac{\ell\pi}{2}}{\pi\ell} \exp(i\,\frac{2\pi\ell}{\Lambda}\,z)\right\} & 0 > x > -a \\ 0 & x < -a \end{cases}$$

and Λ is the period of the corrugation perturbation.

To study the properties of wave propagation in the structure described above we can use the coupled-mode formalism[3] which leads to a set of coupled differential equations which describe the rate of change of the amplitudes of the modes involved. In most of our analysis we are interested in the interaction of two waves; one is the forward going wave and the other is the backward going wave of the same mode number. Let

$$E_i^m(\bar{r}) = B(z)\mathcal{E}_y^m(x)e^{-i\beta_m z}$$

and

$$E_r^m(\bar{r}) = A(z)\mathcal{E}_y^m(x)e^{i\beta_m z}$$

be these two waves, where $\mathcal{E}_y^m(x)$ is the normalized m-th TE mode of the unperturbed waveguide and A(z) and B(z) are the complex mode amplitudes. The coupled-mode equations

$$\frac{dA}{dz} = i\kappa B e^{-i2\Delta\beta z}$$

$$\frac{dB}{dz} = -i\kappa A e^{i2\Delta\beta z} \qquad (2\text{-}3)$$

can be derived through a perturbation analysis[2,3] where

$$\Delta\beta \doteq \beta - \beta_o = \beta - \frac{\pi}{\Lambda} \qquad (2\text{-}4)$$

According to equation (2-3) the rate of change of A along z is proportional to the value of B at z and vice versa. The proportional constant κ is called the "coupling coefficient." In general κ depends on the shape of the periodic surface corrugation and the modes $E_i^m(z)$ and $E_r^m(z)$. It can be calculated from the overlap integral

$$\kappa_\ell^m = - \frac{\omega\varepsilon_o \sin\frac{\pi\ell}{2}}{4\pi\ell} \int_{-\infty}^{\infty} (\varepsilon_1 - \varepsilon_2) |\mathcal{E}_y^m(x)|^2 dx$$

where m designates the m-th waveguide mode and ℓ denotes the ℓ-th order harmonic of the corrugation function that is responsible for the coupling. Hence κ is the quantity that measures the strength of interaction between the two opposite going waves.

One can solve equation (2-3) with the proper boundary conditions to obtain $E_i(z)$ and $E_r(z)$. It can be shown that when a waveguide mode with $\Delta\beta = 0$, i.e., the mode with wavelength $\lambda_g = 2\Lambda$ (twice the corrugation period) propagates down the guide and enters the corrugated section it will be strongly coupled to the backward going mode. So the incident wave will evanesce as it propagates down the waveguide. At the same time there is a build-up of the reflected wave. Thus effectively a corrugated waveguide section acts as a "reflector" or "mirror" whose reflectivity can be varied by adjusting the corrugation height and length. This behavior of periodic waveguide makes possible the realization of DFB and DBR semiconductor lasers.

It should be noted that the gratings not only couple the forward going guided modes to the backward going guided modes but also couple the guided modes to the radiation modes. This will be regarded as

radiation loss[4] if the periodic waveguide is used as a reflector or laser. If the periodic waveguide is used as an input-output coupler[5,6] the coupling between guided and radiation modes is a useful phenomenon.

In this chapter we shall study the properties of the coupled-mode equations, derive the coupling constant for waveguides with periodic surface corrugation and apply the coupled-mode formalism to study the reflection and transmission characteristics of a section of periodic waveguide.

2-2 Coupled-mode Formalism

The problem of electromagnetic wave propagation in periodic structures has been studied extensively[7]. One of the most common methods used in deriving useful analytical expressions is the coupled-mode formalism. We shall outline the procedures in obtaining the coupled mode equations and the overlap integral, equation (2-4), that determines the coupling constant κ for a periodic waveguide.

Fig. 2-1(a) shows a regular slab waveguide with dielectric constants ε_1, ε_2, and ε_3 in three different regions. We define

$$\varepsilon(\bar{r}) = \begin{cases} \varepsilon_1 & x > 0 \\ \varepsilon_2 & 0 > x > -t \\ \varepsilon_3 & -t > x \end{cases} \qquad (2\text{-}5)$$

as the dielectric function of this unperturbed waveguide. Fig. 2-1(b) shows a slab waveguide with square wave perturbation at the x = 0 boundary. If we let

$$\Delta\varepsilon(\bar{r}) = \begin{cases} 0 & x > 0 \\ (\varepsilon_1-\varepsilon_2)\{\frac{1}{2} + \sum_{\substack{\ell=-\infty \\ \ell\neq 0}}^{\infty} \frac{\sin\frac{\pi\ell}{2}}{\pi\ell} \exp(i\,\frac{2\pi}{\Lambda}\,\ell z)\} & 0 > x > -a \\ 0 & -a > x \end{cases} \qquad (2\text{-}6)$$

where a is the height of the square wave perturbation, then the dielectric function of the perturbed waveguide is given by

$$\varepsilon'(\bar{r}) = \Delta\varepsilon(\bar{r}) + \varepsilon(\bar{r}) \qquad (2\text{-}7)$$

Now the field vector $\bar{D}(\bar{r},t)$ becomes

$$\begin{aligned} \bar{D}(\bar{r},t) &= \varepsilon'(\bar{r})\bar{E}(\bar{r},t) \\ &= [\varepsilon(\bar{r}) + \Delta\varepsilon(\bar{r})]\bar{E}(\bar{r},t) \\ &= \varepsilon_o\bar{E}(\bar{r},t) + \bar{P}(\bar{r},t) \\ &= \varepsilon_o\bar{E}(\bar{r},t) + \bar{P}_o(\bar{r},t) + \Delta\bar{P}(\bar{r},t) \end{aligned}$$

where

$$\bar{P}_o(\bar{r},t) \equiv [\varepsilon(\bar{r}) - \varepsilon_o]\bar{E}(\bar{r},t)$$

and

$$\Delta\bar{P}(\bar{r},t) = \Delta\varepsilon(\bar{r})\bar{E}(\bar{r},t) \qquad (2\text{-}8)$$

Equation (2-8) is then used in the wave equation

$$\nabla^2\bar{E}(\bar{r},t) = \mu\varepsilon_o \frac{\partial^2\bar{E}(\bar{r},t)}{\partial t^2} + \mu \frac{\partial^2\bar{P}(\bar{r},t)}{\partial t^2}$$

to obtain

$$\nabla^2\bar{E}(\bar{r},t) - \mu\varepsilon(\bar{r}) \frac{\partial^2\bar{E}(\bar{r},t)}{\partial t^2} = \mu \frac{\partial^2\Delta\bar{P}(\bar{r},t)}{\partial t^2} \qquad (2\text{-}9)$$

This is the wave equation that describes the propagation of electromagnetic waves in a slab waveguide with boundary perturbation represented by $\Delta\bar{P}(\bar{r},t)$ which is given by equation (2-6) and (2-8).

The field $\bar{E}(\bar{r},t)$ of the periodic waveguide can be expanded in terms of the modes of the unperturbed smooth waveguide. Consider, as an example the case of TE modes. The y-component of $\bar{E}(\bar{r},t)$ can be written as

$$E_y(\bar{r},t) = \frac{1}{2}\sum_m A_m(z)\mathcal{E}_y^m(x)e^{i(\omega t-\beta_m z)} + \text{complex conjugate} \qquad (2\text{-}10)$$

where $\mathcal{E}_y^{(m)}(x)e^{i(\omega t-\beta_m z)}$ is the y component of the electric field of the m-th eigenmode of the unperturbed waveguide. We substitute equation (2-10) into (2-9), and with the help of (2-6) and (2-8), and limiting ourselves to the case of coupling between the positive and negative going m-th mode we obtain

$$\begin{aligned}\frac{dA_m}{dz} &= i\kappa B_m e^{-i2\Delta\beta z}\\ \frac{dB_m}{dz} &= -i\kappa A_m e^{i2\Delta\beta z}\end{aligned} \qquad (2\text{-}11)$$

where

$$\kappa = \frac{-\omega\varepsilon_o \sin\frac{\pi\ell}{2}}{4\pi\ell}\int_{-\infty}^{\infty}\Delta\varepsilon(x)[\mathcal{E}_y^m(x)]^2dx \qquad (2\text{-}12)$$

$$\Delta\beta = \beta_m - \frac{\ell\pi}{\Lambda} = \beta_m - \beta_o$$

and ℓ is the order of the corrugation (or grating) harmonics responsible for the coupling.

The electric fields associated with the coupled incident and reflected modes are

$$E_i^m(\bar{r}) = B_m(z)\mathcal{E}_y^m(x)e^{i(\omega t-\beta_m z)}$$

and

$$E_r^m(\bar{r}) = A_m(z)\mathcal{E}_y^m(x)e^{i(\omega t+\beta_m z)}$$

respectively. A simple calculation using equation (2-11) shows that

$$\frac{d}{dz}\left(|B_m|^2 - |A_m|^2\right) = 0$$

This is merely a description of the conservation of power since the waveguide is assumed to be lossless and $|B_m|^2$, $|A_m|^2$ are proportional to the power (per unit width) carried by the forward and backward going waves respectively.

2-3 The Coupling Constant

Equation (2-12) defines the coupling constant κ which appears in the coupled-mode equation (2-11). In a square wave corrugation $\Delta\varepsilon(\bar{r})$ is

$$\Delta\varepsilon(x) = \begin{cases} 0 & x > 0 \\ n_1^2 - n_2^2 & 0 > x > -a \\ 0 & -a > x \end{cases}$$

So the integral reduces to

$$\kappa = \frac{\omega\varepsilon_o \sin\frac{\ell\pi}{2}}{4\pi\ell}\int_{-a}^{o}(n_2^2-n_1^2)[\mathcal{E}_y^m(x)]^2dx$$

Using the eigenmode function of the m-th TE mode[8] we have

$$\kappa = \frac{k^2\sin\frac{\ell\pi}{2}}{\beta\pi\ell}\,\frac{h_m^2(n_2^2-n_1^2)}{t_{eff}(h_m^2+q_m^2)}\int_{-a}^{o}\left[\cos(h_m x) - \frac{q_m}{h_m}\sin(h_m x)\right]^2dx$$

If we carry out the actual integration κ becomes

$$\kappa = \frac{\sin\frac{\pi\ell}{2}}{\pi\ell\beta_m t_{eff}}\left\{\frac{a}{2}(n_2^2-n_1^2)k^2 + \frac{\sin 2h_m a}{4h_m}(h_m^2-q_m^2) + \frac{q_m}{2}(1-\cos 2h_m a)\right\} \tag{2-13}$$

where p, q, h, β are given by equations (2-1c), (2-1d), and $t_{eff} = t + 1/p_m + 1/q_m$ is the effective waveguide thickness for the m-th mode of the unperturbed waveguide. If $a \ll t$ we can find an approximate expression for κ to first order in a as

$$|\kappa| = \frac{h_m^2 a}{\pi\ell\beta_m t_{eff}} \qquad \ell = 1,3,5,\ldots \tag{2-14}$$

It is seen that κ is different for different transverse modes m. In Fig. 2-2 we plot $|\kappa|$ as a function of waveguide thickness t for several transverse modes. We see that for each m, κ reaches a maximum for t slightly above its cutoff value and then decreases rapidly as t increases. In a thick waveguide higher order modes have larger coupling constants than the lower order modes as evident from the figure.

Equation (2-14) is valid only in the case of square wave corrugation where the x and z dependence of $\Delta\varepsilon(x,z)$ are separable. In corrugations with shapes other than squarewave we have to expand $\Delta\varepsilon(x,z)$ in a Fourier series with x dependent coefficients and then use the series in the following integral

$$\frac{k^2 h_m^2}{\beta(h_m^2+q_m^2)t_{eff}} \int_{-\infty}^{\infty} \Delta\varepsilon(x,z)[\mathcal{E}_y^m(x)]^2 dx$$

and pick out the proper term corresponding to the ℓ-th order grating operation. The details of this procedure have been worked out by Streifer et al[9].

Up to this point we limited our discussion to TE modes. The

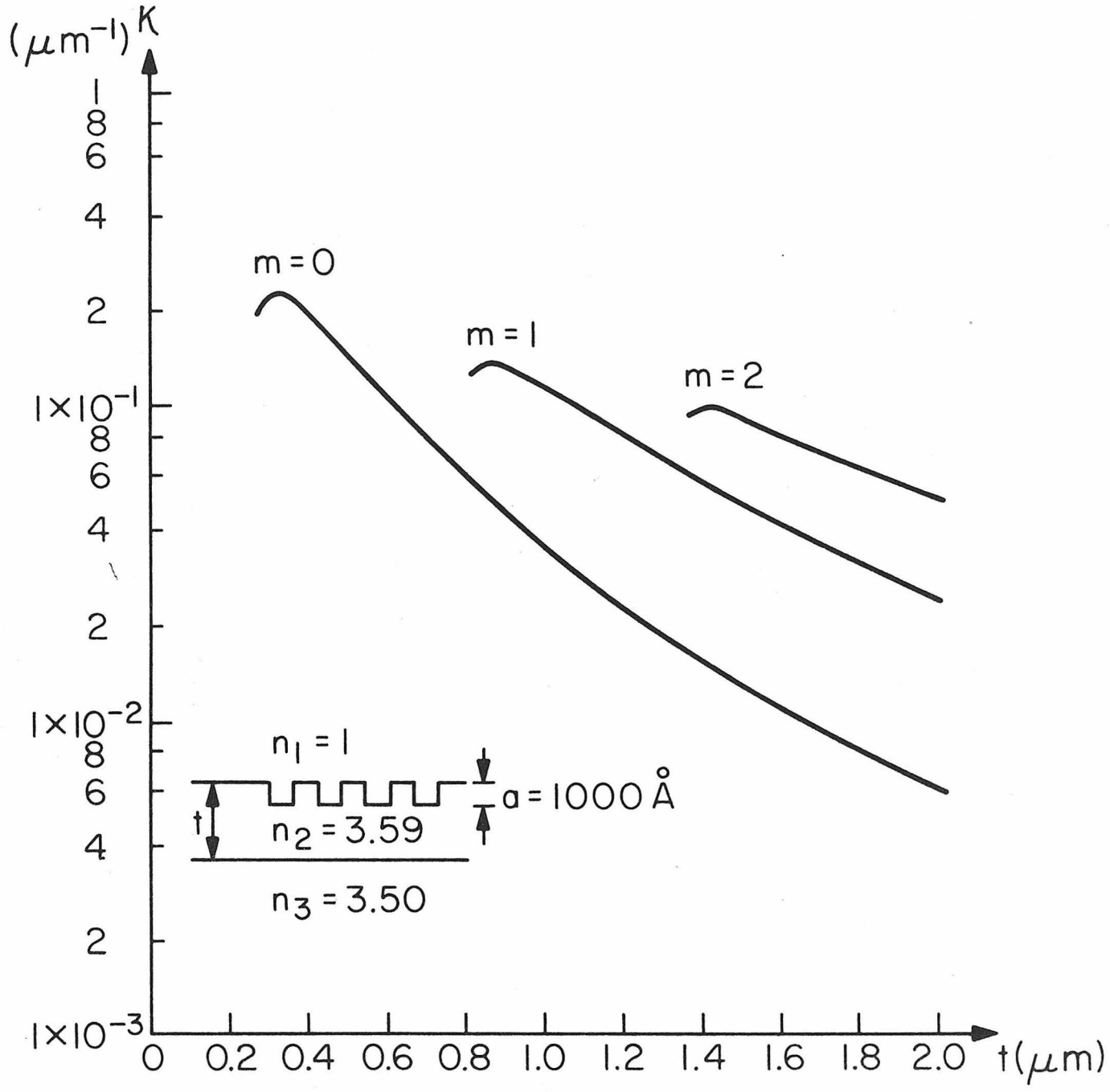

Fig. 2-2 Coupling constant versus waveguide thickness for different transverse TE modes.

procedure for finding κ in the case of TM modes is similar except the calculation of the integral is considerably more complicated[10].

In the rest of this section we will introduce a different approach to derive the coupling constants which will help us understand better the origin of the coupling. From the coupled-mode equation (2-11), if set $\Delta\beta = 0$ then

$$|\kappa| = |\frac{1}{B}\frac{dA}{dz}|$$

so physically κ is the amplitude reflection coefficient per unit interaction length. Let us apply this simple idea to the case of wave propagation through an infinite periodic dielectric medium whose index of refraction is described by the function n(z) as

$$n(z) = n + n_1 \cos\frac{2\pi}{\Lambda} z \qquad (2\text{-}15)$$

We are not going to solve this problem directly but rather consider the special case shown in Fig. 2-3. The medium consists of alternating layers of index of refraction $n-n_1$ and $n+n_1$ with a period Λ. An incident wave with propagation constant $\beta = 2\pi n/\lambda = \pi/\Lambda$ will undergo a reflection at each boundary between the $n-n_1$ and $n+n_1$ layers given by

$$r = \frac{(n+n_1) - (n-n_1)}{(n+n_1) + (n-n_1)} \approx \frac{n_1}{n}$$

where we have assumed that $n_1 << n$.

Within each period we have two reflections, one is in the interface between the $n+n_1$ and $n-n_1$ medium, the other is between the $n-n_1$ medium and the $n+n_1$ medium. Although these two reflection coefficients have opposite sign, the wave propagation phase delay between these two reflected waves is exactly π at the Bragg wavelength, hence they add

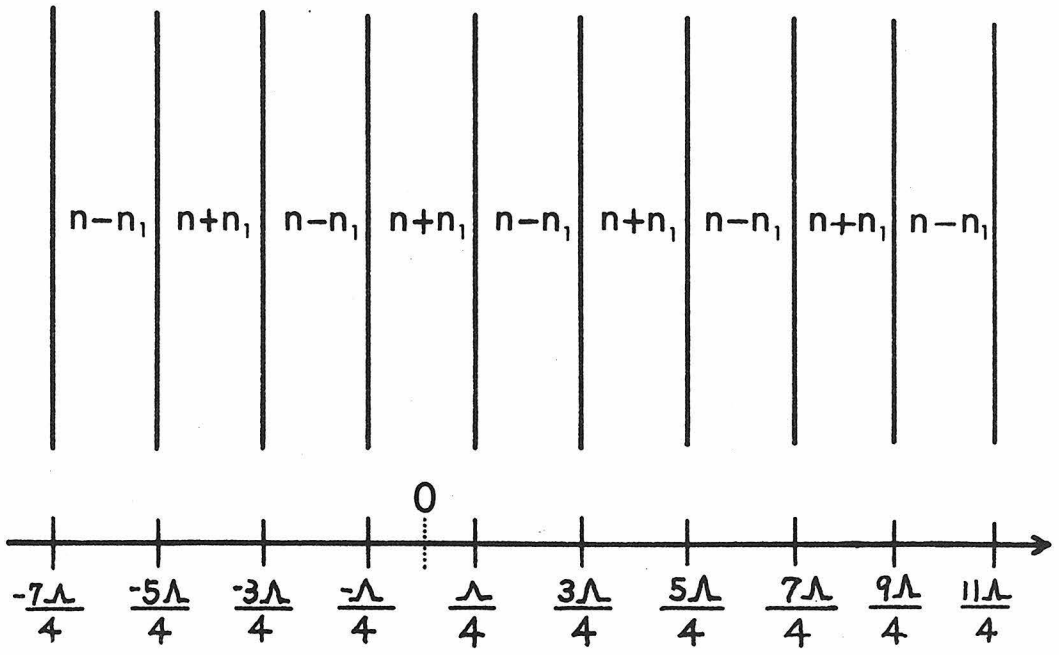

$$n(z) = n + \begin{cases} n_1 & \left(\frac{4N-1}{4}\right)\Lambda < z < \left(\frac{4N+1}{4}\right)\Lambda \\ n_1 & \left(\frac{4N+1}{4}\right)\Lambda < z < \left(\frac{4N+3}{4}\right)\Lambda \end{cases}$$

$$N = 0, \pm 1, \pm 2, \cdots\cdots\cdots$$

Fig. 2-3 An infinite periodic medium consists of layers of index of refraction $n-n_1$ and $n+n_1$ interlaced with a period Λ.

up in phase. The coupling constant κ is thus given by

$$\kappa = \frac{2r}{\Lambda} = \frac{2n_1}{n\Lambda}$$

Since $\Lambda = \frac{\lambda}{2n}$ we can rewrite κ as

$$\kappa_{square} = \frac{4n_1}{\lambda} \tag{2-16}$$

This is the coupling constant of a medium with square wave index of refraction modulation under fundamental operation. The index of refraction of such a medium can be described as

$$n(z) = n + \Delta n(z)$$

$$\Delta n(z) = \begin{cases} n_1 & \frac{(4N-1)\Lambda}{4} < z < \frac{(4N+1)\Lambda}{4} \\ -n_1 & \frac{(4N+1)\Lambda}{4} < z < \frac{(4N+3)\Lambda}{4} \end{cases} \qquad N = 0, \pm 1, \pm 2, \cdots$$

so $n(z)$ can be expanded in a Fourier series. Let us pick out the fundamental harmonic term

$$n(z) = n + \frac{4n_1}{\pi} \cos \frac{2\pi}{\Lambda} z$$

$4n_1/\pi$ can be regarded as the effective sinusoidal modulation amplitude of the square wave modulation. So to find the coupling constant in a medium with an index of refraction $n(z)$ given by equation (2-15) all we have to do is multiply κ_{square} by $\pi/4$, or

$$\kappa_{sinusoidal} = \frac{4n_1}{\lambda} \times \frac{\pi}{4} = \frac{\pi n_1}{\lambda} \tag{2-17}$$

This is identical to the result given by Kogelnik and Shank[2].

Next we shall apply this method to a periodic waveguide. Again we consider a square wave corrugation first. The surface corrugation

on a waveguide is effectively a modulation of the waveguide height. Each discontinuity along the guide will cause a partial reflection of the incident wave. Fig. 2-4 shows a step discontinuity of waveguide thickness from t to t+a. For our purpose here we choose z = 0 at the discontinuity point. The waveguide at z < 0 with thickness t is referred to as waveguide 1, the one at z > 0 with thickness t+a as waveguide 2. Let $E_1(x)e^{-i\beta_1 z}$ be the incident wave and $rE_1(x)e^{i\beta_1 z}$ be the reflected wave in waveguide 1 and $tE_2(x)e^{-i\beta_2 z}$ be the transmitted wave in waveguide 2. Neglecting radiation losses, we can write down the field continuity equations at z = 0 as

$$(1+r)E_1(x) = TE_2(x) \tag{2-18}$$

and

$$\beta_1(1-r)E_1(x) = \beta_2 TE_2(x) \tag{2-19}$$

where r and T are the amplitude reflection and transmission coefficients respectively. Taking the ratio of (2-18) and (2-19) we find

or

$$\frac{1 + r}{1 - r} = \frac{\beta_1}{\beta_2}$$

$$r = \frac{\beta_1 - \beta_2}{\beta_1 + \beta_2} \tag{2-20}$$

If we define $\beta_2-\beta_1 \equiv \delta\beta$ then

$$r = \frac{-\delta\beta}{2\beta_1+\delta\beta} \approx \frac{-\delta\beta}{2\beta_1}\left(1 - \frac{\delta\beta}{2\beta_1}\right) \tag{2-21}$$

where $\delta\beta$ is due to a small step change "a" in waveguide height t. The next task is to find a relation between $\delta\beta$ and a. This is done by taking the implicit derivative of equation (2-1d) with respect to t. We can rewrite equation (2-1d) for TE modes as

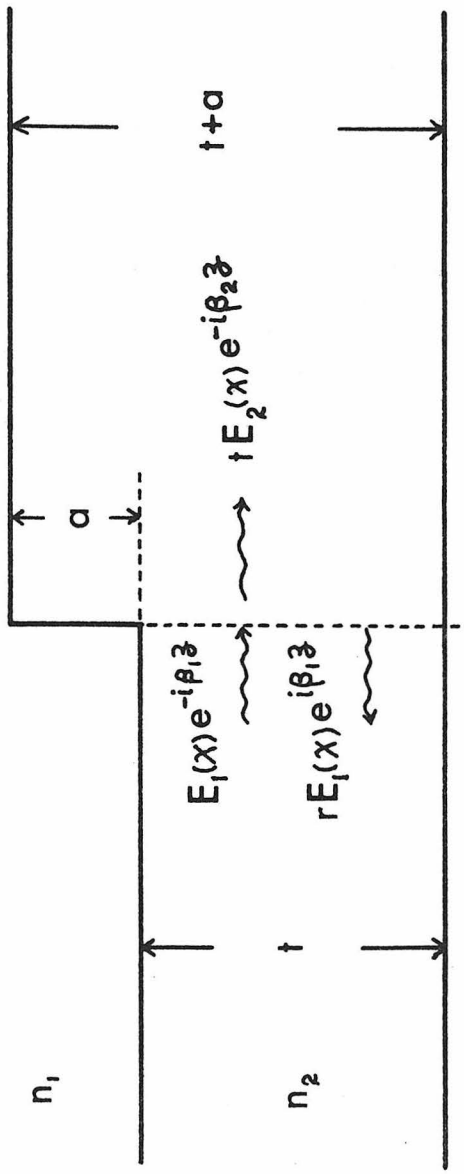

Fig. 2-4 Schematic diagram shows a step change of waveguide thickness from t to t+a at z = 0.

$$\tan(n_2^2k^2-\beta^2)^{1/2}t = \frac{[(\beta^2-n_3^2k^2)^{1/2} + (\beta^2-n_1^2k^2)^{1/2}](n_2^2k^2-\beta^2)^{1/2}}{(n_2^2k^2-\beta^2) - (\beta^2-n_3^2k^2)^{1/2}(\beta^2-n_1^2k^2)^{1/2}} = f(\beta)$$

Hence

$$\frac{\partial\beta}{\partial t} = \frac{h}{\frac{\beta t}{h} + \cos^2 ht\, f'(\beta)}$$

and

$$f'(\beta) = \frac{\beta(p+q)(h^2+q^2)(h^2+p^2)}{hpq(h^2-pq)^2}$$

After simplification we have

$$\frac{\partial\beta}{\partial t} = \frac{h^2}{\beta(t + \frac{1}{p} + \frac{1}{q})} = \frac{h^2}{\beta t_{eff}} \qquad (2\text{-}22)$$

and

$$\frac{\partial^2\beta}{\partial t^2} = -\frac{\partial\beta}{\partial t}\left[\frac{3}{t_{eff}} + \frac{h^2}{\beta^2 t_{eff}} - \frac{h^2}{t_{eff}^2}\left(\frac{1}{p^3} + \frac{1}{q^3}\right)\right]$$

$\beta(t+a)$ can be expanded into a Taylor's series as

$$\beta(t+a) = \beta(t) + a\frac{\partial\beta}{\partial t} + \frac{a^2}{2}\frac{\partial^2\beta}{\partial t^2} + \cdots$$

$$\therefore \delta\beta = \beta(t+a) - \beta(t) = a\frac{\partial\beta}{\partial t}\left\{1 - \frac{a}{2t_{eff}}\left[3 + \frac{h^2}{\beta^2} - \frac{h^2}{t_{eff}}\left(\frac{1}{p^3} + \frac{1}{q^3}\right)\right]\right\}$$

After substituting this result into equation (2-21) we have

$$r = -\frac{h^2 a}{2\beta^2 t_{eff}}\left\{1 + \frac{1}{2}\left[3 - \frac{h^2(p^3+q^3)}{p^3q^3t_{eff}}\right]\left(\frac{a}{t_{eff}}\right)\right\}$$

For a periodic waveguide with square wave corrugation the coupling constant can be found as

$$|\kappa| = \frac{2|r|}{\Lambda} = \frac{2\beta|r|}{\pi} = \frac{h^2 a}{\pi\beta t_{eff}}\left\{1 + \frac{1}{2}\left(\frac{a}{t_{eff}}\right)\left[3 - \frac{h^2(p^3+q^3)}{p^3q^3t_{eff}}\right]\right\} \qquad (2\text{-}23)$$

The first order term (in a) is

$$|\kappa| = \frac{h^2 a}{\pi\beta t_{eff}} \qquad (2\text{-}24)$$

This is identical to equation (2-14) with $\ell = 1$.

The effective sinusoidal modulation coefficient of the square wave surface corrugation with height a can be found to be

$$\frac{2a}{\pi} \cos \frac{2\pi}{\Lambda} z$$

Hence a sinusoidal surface corrugation with peak to peak height "a" will have a coupling constant

$$|\kappa|_{sinusoidal} = \frac{\pi}{4} |\kappa|_{square}$$

The extension of this method to corrugations of arbitrary profiles is obvious. All we need to do is to calculate the appropriate Fourier coefficient and compare with that of the square wave corrugation. Then the coupling constant is given by

$$|\kappa|_{arb.} = |\kappa|_{square} \times \left| \frac{C^{\ell}_{arb}}{C^{\ell}_{square}} \right| \qquad \ell = 1,3,5,... \qquad (2\text{-}25)$$

where C^{ℓ}_{arb} is the amplitude of the ℓ-th Fourier component of the arbitrary corrugation and C^{ℓ}_{square} is that of the square wave corrugation. For ℓ even this method fails because there are no even Fourier components in a square wave. But we can always approximate an arbitrary tooth shape by a series of step functions and obtain the reflectivity r of one period Λ and calculate κ from the ratio r/Λ. As an example let us calculate the first order (ℓ=1) and second order (ℓ=2) coupling

constants of a corrugation as shown in Fig. 2-5(a). For first order coupling

$$2\beta = \frac{2\pi}{\Lambda}$$

or

$$\beta\Lambda = \pi$$

Refer to Fig. 2-5(b), the reflectivity summed up at z = 0 for one period (from z = 0 to z = Λ) is

$$r = r_1 + r_2 e^{-i\frac{\pi}{2}} + (-r_2)e^{-i\pi} + (-r_1)e^{-i\frac{3\pi}{2}}$$

$$= (r_1+r_2)(1-i)$$

$$\therefore \left|\kappa\right|_{\ell=1}^{\sim} = \left|\frac{r}{\Lambda}\right| = \sqrt{2}\left|\frac{r_1+r_2}{\Lambda}\right|$$

where

$$r_1 = \frac{\beta(t) - \beta(t+a/2)}{\beta(t) + \beta(t+a/2)}, \qquad r_2 = \frac{\beta(t+a/2) - \beta(t+a)}{\beta(t+a/2) + \beta(t+a)}$$

and

$$r_1 + r_2 = \frac{2\beta(t+a/2)\,[\beta(t+a) - \beta(t)]}{[\beta(t)+\beta(t+a/2)][\beta(t+a/2)+\beta(t+a)]} \simeq \frac{\delta\beta}{2\beta}$$

where

$$\delta\beta = \beta(t+a) - \beta(t) = \frac{h^2 a}{\beta t_{eff}}$$

$$\therefore \left|\kappa\right|_{\ell=1}^{\sim} = \frac{\sqrt{2}\,h^2 a}{2\beta^2 t_{eff}\Lambda} = \frac{h^2 a}{\sqrt{2}\,\pi\beta t_{eff}}$$

It is educational to double check this result by finding the fundamental Fourier coefficient of this corrugation

$$C_1^{\sim} = \frac{4}{\Lambda}\left[\int_0^{\Lambda/8} a\cos\frac{2\pi}{\Lambda}z\,dz + \int_{\Lambda/8}^{3\Lambda/8}\frac{a}{2}\cos\frac{2\pi}{\Lambda}z\,dz\right] = \frac{\sqrt{2}a}{\pi}$$

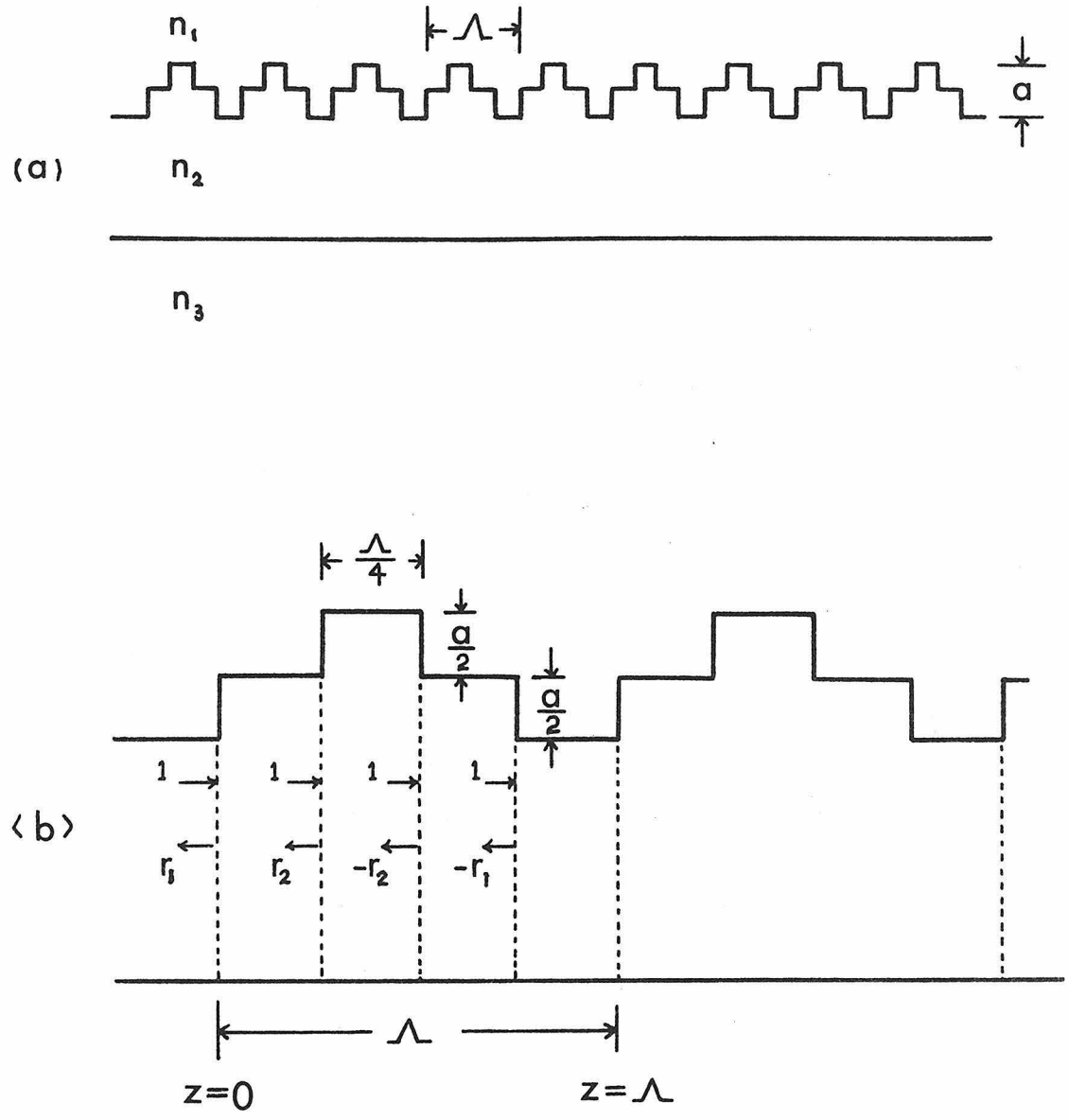

Fig. 2-5 Schematic diagram of a periodic waveguide with surface corrugations being represented by step functions.

Using equation (2-25) we obtain

$$|\kappa|^{\wedge}_{\ell=1} = \frac{h^2 a}{\pi\beta t_{eff}} \times \frac{\sqrt{2}\, a}{\pi} \times \frac{\pi}{2a} = \frac{h^2 a}{\sqrt{2}\, \pi\beta t_{eff}}$$

We thus tested the validity of this "reflectivity summing" procedure. For second order coupling between the same forward and backward modes we double the length of the period, i.e.,

$$\beta\Lambda = 2\pi$$

Referring to Fig. 2-5(b) the phase shift associated with each step is double that of the first order case and the sum reflectivity at z = 0 is

$$r = r_1 + r_2 e^{-i\pi} + (-r_2)e^{-i2\pi} + (-r_1)e^{-i3\pi}$$

$$= 2(r_1 - r_2)$$

$$\therefore\ r = 2(r_1 - r_2) \approx -\frac{3h^2 a^2}{8\beta^2 t_{eff}^2}$$

and

$$|\kappa|^{\wedge}_{\ell=2} = \frac{3h^2 a^2}{16\pi\beta t_{eff}^2}$$

The tooth shape shown in Fig. 2-5(a) can be taken as a very rough approximation of either a symmetrical triangular or a sinusoidal corrugation. For these functions the second order coupling constants have been found[9] to have the functional dependence a^2. This is also seen in the expression for $|\kappa|^{\wedge}_{\ell=2}$. Hence the results of this method are at least qualitatively correct. To obtain quantitatively correct results we have to increase the number of step functions which are used to approximate the true function.

The method described above can be applied to TM modes as well because equation (2-20) holds also for TM modes. The only

modification is that the characteristic equation is now

$$\tan ht = \frac{\bar{p} + \bar{q}}{h(1 - \frac{\bar{p}\bar{q}}{h^2})}$$

where $$\bar{p} = \frac{n_2^2}{n_3^2} p \ , \qquad \bar{q} = \frac{n_2^2}{n_1^2} q$$

One can easily show that

$$(\frac{\partial \beta}{\partial t})_{TM} = \frac{h^2}{\beta t'_{eff}}$$

where

$$t'_{eff} = t + \frac{h^2+q^2}{h^2+\bar{q}^2} \frac{n_2^2}{n_1^2 q} + \frac{h^2+p^2}{h^2+\bar{p}^2} \frac{n_2^2}{n_3^2 p}$$

is the effective waveguide thickness for TM modes.

$$\therefore |\kappa|_{TM} = \frac{h^2 a}{\pi \beta t'_{eff}} \qquad (2\text{-}26)$$

for a square wave corrugation in first order (ℓ=1) operation. Equation (2-26) and (2-24) are identical in form except we have to use the respective values of h^2, β, and t_{eff} for TE and TM modes.

2-4 Solutions of the Coupled-mode Equations

The coupled-mode equations (2-11) are reproduced here:

$$\begin{cases} \frac{dA}{dz} = i\kappa \, Be^{-i2\Delta\beta z} \\ \frac{dB}{dz} = -i\kappa \, Ae^{i2\Delta\beta z} \end{cases} \qquad (2\text{-}27)$$

Let us look at the special case $\Delta\beta = 0$ first. The equations reduce to

$$\begin{cases} \frac{dA}{dz} = i\kappa B \\ \frac{dB}{dz} = -i\kappa A \end{cases} \tag{2-28}$$

whose solutions are

$$A(z) = C_1 \sinh \kappa z + C_2 \cosh \kappa z$$
$$B(z) = -i(C_1 \cosh \kappa z + C_2 \sinh \kappa z) \tag{2-29}$$

Let us consider an infinitely long waveguide with a corrugated section between z = 0 and z = L. The boundary conditions are $E_r(L) = 0$ and $E_i(0) = 1$. Since

$$E_i(z) = B(z)e^{-i\beta z}$$

and

$$E_r(z) = A(z)e^{i\beta z}$$

then conditions on A and B are A(L) = 0 and B(0) = 1. Under these conditions the solution becomes

$$A(z) = \frac{-i \sinh \kappa(L-z)}{\cosh \kappa L}$$

$$B(z) = \frac{\cosh \kappa(L-z)}{\cosh \kappa L}$$

Note that $|E_i(z)|^2 = |B(z)|^2$ and $|E_r(z)|^2 = |A(z)|^2$. If we carry out the calculation we will find

$$|E_i(z)|^2 - |E_r(z)|^2 = \left(\frac{1}{\cosh \kappa L}\right)^2$$

which is a constant independent of z. This means that the net power flowing in the waveguide is the same everywhere. The behavior of $|E_i(z)|^2$ and $|E_r(z)|^2$ is plotted in Fig. 2-6 for two values of κL, $\kappa L = 4.0$ and 1.0. A large κL represents strong coupling and the decay

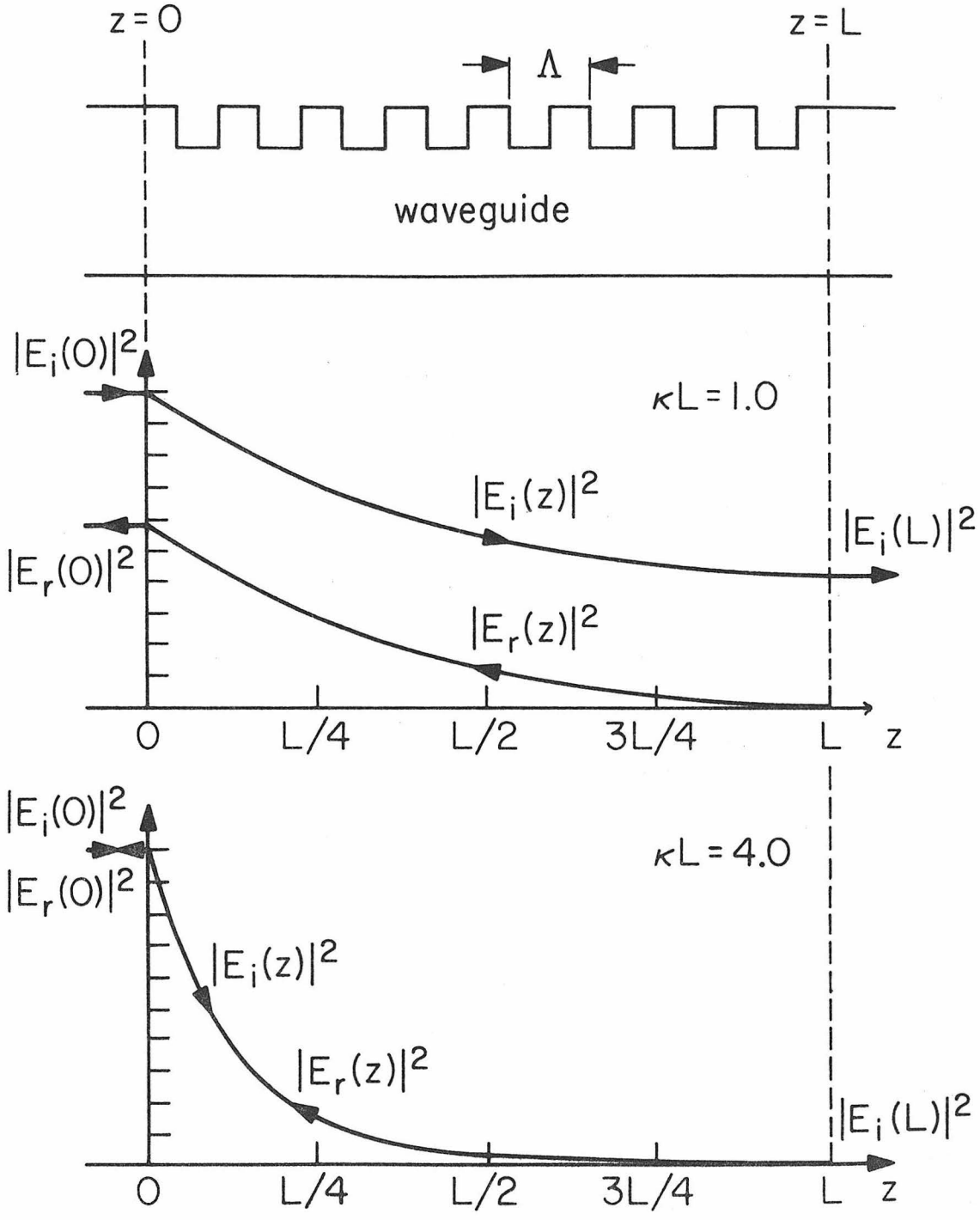

Fig. 2-6 The behavior of $|E_i(z)|^2$ and $|E_r(z)|^2$ in a periodic waveguide with κL = 1.0 and 4.0 ($\Delta\beta$= 0).

rate of the incident wave is fast. This is evident from the figure. We can rewrite $E_i(z)$ as

$$E_i(z) = \frac{\cosh \kappa(L-z)}{\cosh \kappa L} e^{-i\beta z}$$

$$= \frac{e^{-i\beta z}}{2\cosh \kappa L} [e^{\kappa(L-z)} + e^{-\kappa(L-z)}]$$

$$= \frac{e^{\kappa L}}{2\cosh \kappa L} [e^{-\kappa z} e^{-i\beta z} + e^{-2\kappa L} e^{\kappa z} e^{-i\beta z}]$$

Hence the dominant behavior of $|E_i(z)|^2$ is

$$|E_i(z)|^2 \sim \left| \frac{e^{\kappa L}}{2\cosh \kappa L} \right|^2 e^{-2\kappa z}$$

We define L_{eff} as the effective length of the corrugation such that $\kappa L_{eff} = 1$ or $L_{eff} = \frac{1}{\kappa}$. At $z = L_{eff}$ the intensity of the incident wave drops down to $\sim e^{-2}$ of its original value.

The reflectivity of a section of periodic waveguide at the exact Bragg condition ($\Delta\beta = 0$) is given by

$$|R|^2 = \left| \frac{E_r(0)}{E_i(0)} \right|^2 = \tanh^2 \kappa L \qquad (2\text{-}30)$$

It can be shown that $|R|^2_{(\Delta\beta=0)}$ is the maximum reflectivity a periodic waveguide section can provide. Fig. 2-7 is a plot of equation (2-30) which shows that $|r|^2$ rises very fast from zero to unity for κL between 0 and 3.

Suppose $\Delta\beta \neq 0$ we have to solve equation (2-27) with the same boundary condition $A(L) = 0$, $B(0) = 1$ to obtain

$$E_i(z) \equiv B(z) e^{-i\beta z}$$

$$= \frac{[i\Delta\beta \sinh\gamma(L-z) + \gamma \cosh\gamma(L-z)] e^{-i\beta_0 z}}{i\Delta\beta \sinh\gamma L + \gamma \cosh\gamma L} \qquad (2\text{-}31)$$

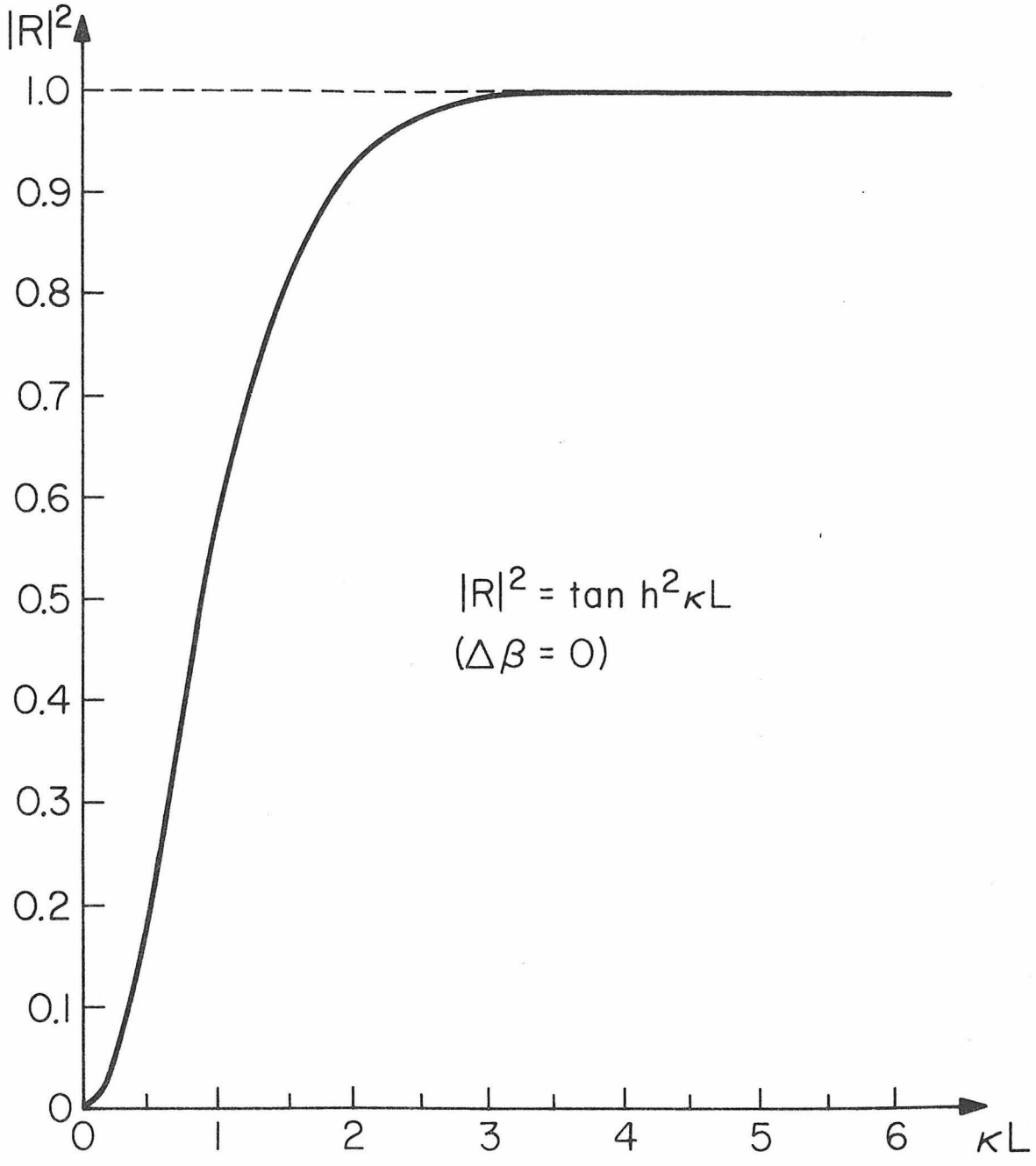

Fig. 2-7 Maximum reflectivity from a periodic waveguide $|R|^2$ plotted as a function of κL.

and

$$E_r(z) \equiv A(z)e^{i\beta z}$$

$$= \frac{-i\kappa \sinh\gamma(L-z)e^{i\beta_o z}}{i\Delta\beta \sinh\gamma L + \gamma\cosh\gamma L} \qquad (2\text{-}32)$$

where

$$\beta_o \equiv \frac{\pi}{\Lambda} \quad , \qquad \Delta\beta = \beta - \beta_o \quad \text{and}$$

$$\gamma^2 = \kappa^2 - \Delta\beta^2$$

Again we can find the reflection coefficient as

$$R = \frac{E_r(0)}{E_i(0)} = \frac{-i\kappa \sinh\gamma L}{i\Delta\beta \sinh\gamma L + \gamma\cosh\gamma L} \qquad (2\text{-}33)$$

and the transmission coefficient

$$T = \frac{E_i(L)}{E_i(0)} = \frac{\gamma e^{-i\beta_o L}}{i\Delta\beta \sinh\gamma L + \gamma\cosh\gamma L} \qquad (2\text{-}34)$$

Since $\Delta\beta \equiv \beta - \beta_o = \frac{\omega}{c} n_{eff} - \frac{\pi}{\Lambda}$, $\Delta\beta$ is directly related to the frequency ω once n_{eff} is known. $n_{eff} \equiv c\beta/\omega$ will be assumed as given since we can always solve the waveguide characteristic equation to determine β. Both R and T are thus frequency dependent complex numbers and can be written as

$$R = r(\omega)e^{-i\phi(\omega)} \qquad (2\text{-}35)$$

$$T = t(\omega)e^{-i\psi(\omega)} \qquad (2\text{-}36)$$

2-5 Reflection and Transmission Characteristics of a Periodic Waveguide

By straightforward calculation one can show that

$$r(\omega) = \left\{ \frac{1}{1 + \frac{\gamma^2}{\kappa^2 \sinh^2 \gamma L}} \right\}^{1/2} \tag{2-37}$$

$$\phi(\omega) = \frac{\pi}{2} + \tan^{-1} \left(\frac{\Delta\beta}{\gamma} \tanh \gamma L \right) + m\pi \tag{2-38}$$

and

$$t(\omega) = \left\{ \frac{1}{1 + \frac{\kappa^2}{\gamma^2} \sinh^2 \gamma L} \right\}^{1/2} \tag{2-39}$$

$$\psi(\omega) = \beta_0 L + \tan^{-1} \left(\frac{\Delta\beta}{\gamma} \tanh \gamma L \right) + m\pi \tag{2-40}$$

where m is an integer

$$m = 0 \qquad |\Delta\beta| \leq \left[\left(\frac{\pi}{2L} \right)^2 + (\kappa)^2 \right]^{1/2}$$

$$m = N \qquad \left\{ \left[\frac{(2N-1)\pi}{2L} \right]^2 + (\kappa)^2 \right\}^{1/2} < |\Delta\beta| \leq \left\{ \left[\frac{(2N+1)\pi}{2L} \right]^2 + (\kappa)^2 \right\}^{1/2}$$

We note first of all that both r and t are even functions of $\Delta\beta$, i.e., $r(\Delta\beta) = r(-\Delta\beta)$, $t(\Delta\beta) = t(-\Delta\beta)$. Also

$$r^2(\omega) + t^2(\omega) = 1$$

for all $\Delta\beta$. This again is a statement of the conservation of energy.

The behavior of $r(\omega)$ can be seen from equation (2-37). When $\Delta\beta < \kappa$, γ is real. So $r(\omega)$ is always larger than zero and approaches unity when κL is large. As a matter of fact $r(\omega)$ reaches a maximum

value of $\tanh\kappa L$ at $\Delta\beta = 0$ as described earlier. When $\Delta\beta > \kappa$, γ is imaginary. We can replace γ by $i\Gamma$ then $r(\omega)$ becomes

$$r(\omega) = \left\{ \frac{1}{1 + \frac{\Gamma^2}{\kappa^2 \sin^2 \Gamma L}} \right\}^{1/2}$$

The denominator of $r(\omega)$ becomes infinite whenever $\sin\Gamma L = 0$. Hence the zeros of $r(\omega)$ appear at

$$\Delta\beta = \pm \left[\kappa^2 + \left(\frac{m\pi}{L}\right)^2\right]^{1/2}$$

The location of local maxima of $r(\omega)$ is determined by finding the minima of

$$f(\Gamma L) = \left(\frac{\Gamma L}{\sin \Gamma L}\right)^2$$

The first few roots of $f'(x) = 0$ are $x = 4.493, 7.725, 10.904, 14.066, 17.221$, etc. The corresponding values of $\Delta\beta$ are calculated from

$$\Delta\beta = \pm \left[\kappa^2 + \left(\frac{x}{L}\right)^2\right]^{1/2}$$

Reflectivity plots are shown in Fig. 2-8, where we plotted $r^2(\omega)$ and $\phi(\omega)$ for $\kappa L = 2.0$ and $\kappa L = 5.0$. It is seen that as κ increases the central high reflectivity band also widens. The curve of $t^2(\omega)$ can be determined by computing $1 - r^2(\omega)$.

Let us go back to equation (2-31) and (2-32) and factor out the z-dependence of $E_i(z)$ and $E_r(z)$. We will find that they consist of waves with propagation constant

$$\beta' = \beta_0 \pm i\sqrt{\kappa^2 - \Delta\beta^2} = \frac{\pi}{\Lambda} \pm i\sqrt{\kappa^2 - \left(\beta - \frac{\pi}{\Lambda}\right)^2} \qquad (2\text{-}41)$$

so that in the case of an incident wave with frequency ω such that

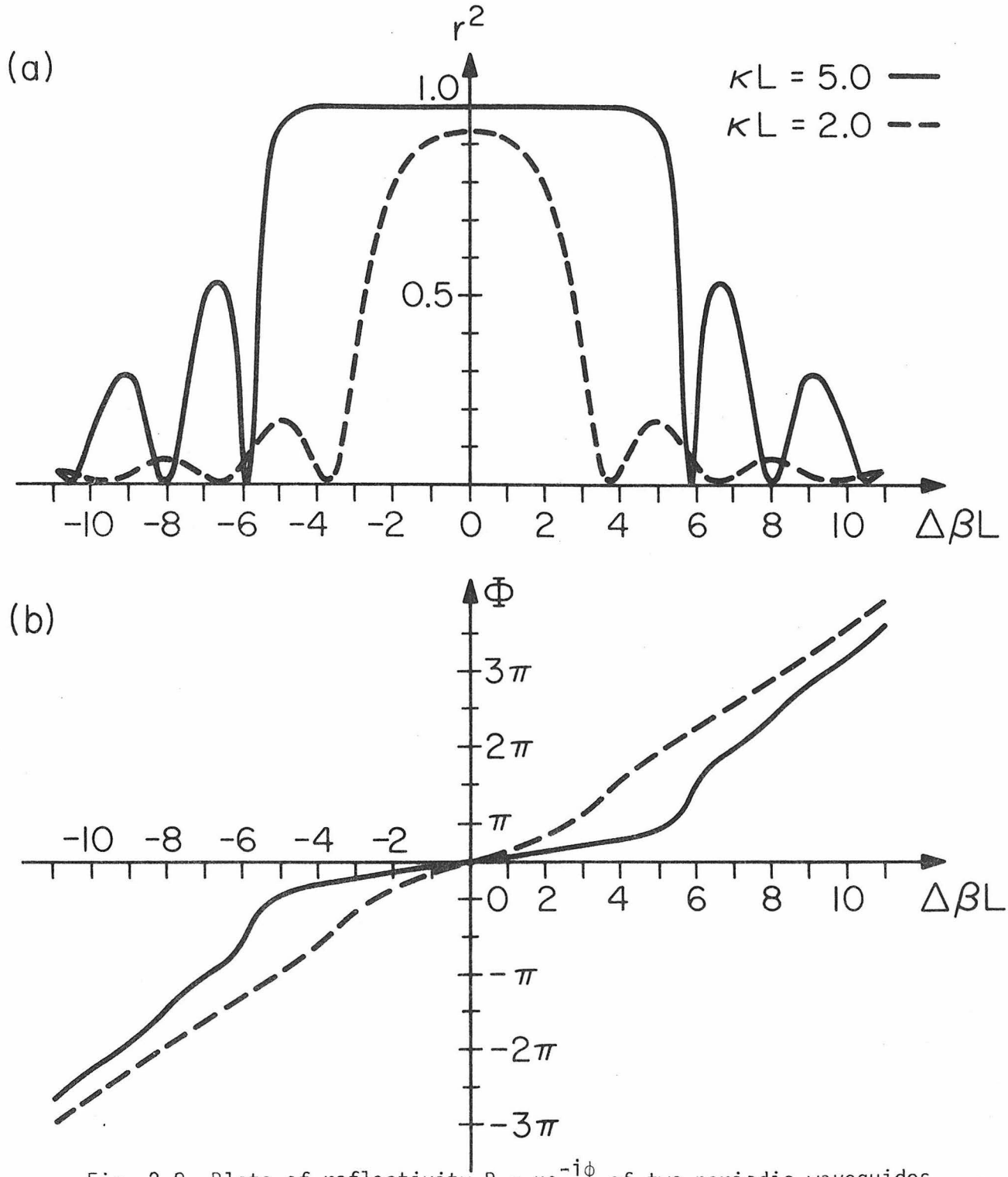

Fig. 2-8 Plots of reflectivity $R = re^{-i\phi}$ of two periodic waveguides with different κL. (a) Intensity reflectivity r^2 as a function of $\Delta\beta L$. (b) Phase ϕ as a function of $\Delta\beta L$.

$$\Delta\beta(\omega) = \frac{\omega}{c} n_{eff} - \frac{\pi}{\Lambda} < \kappa$$

the effective propagation constant is a complex number. The range of frequencies where β' is complex is called the "stop band" or "forbidden region." For frequencies in this region the wave will have evanescent behavior in the periodic waveguide as shown earlier in Fig. 2-6. The stop band will correspond to the high reflectivity part of Fig. 2-8. The width of this stop band is $\Delta\omega = 2\kappa C/n_{eff}$ and the maximum value of the imaginary part of β' is κ as derivable from equation (2-41) directly.

We find that a section of periodic waveguide can be used as a "band rejection" filter or a reflector with frequency sensitive reflectivity. Also, because of the coupling between two opposite traveling waves inside such a structure, if enough gain is provided oscillation can occur. This is the principle of distributed feedback lasers and will be discussed in more detail in Chapter 3. We can also use two sections of periodic waveguide to form a very high Q optical resonator. The laser based on this configuration is called a distributed Bragg reflector laser and will be treated in Chapter 4.

2-6 Periodic Waveguide with External Reflector

So far in solving the coupled-mode equations we have been using the boundary condition $A(L) = 0$. This is true only if the region beyond $z = L$ is of infinite extension and, except for the corrugation, similar to the periodic waveguide. In most real situations we have nonzero reflection at $z = L$. Regardless of the origin of this reflection we can represent it by an equivalent reflection coefficient ρ at the $z = L$ plane looking to the right. The boundary condition instead of using the condition $E_r(L) = 0$ we now have

$$\frac{E_r(L)}{E_i(L)} = \rho$$

If this condition is used together with $E_i(0) = 1$ to solve equation (2-27), one obtains the reflectivity as

$$R' = \frac{E_r(0)}{E_i(0)} = \frac{-i\kappa\sinh\gamma L + \rho e^{-i2\beta_o L}(\gamma\cosh\gamma L - i\Delta\beta\sinh\gamma L)}{(i\Delta\beta\sinh\gamma L + \gamma\cosh\gamma L) + (i\kappa\sinh\gamma L)\rho e^{-i2\beta_o L}}$$

If there are integral number of periods in L, i.e.

$$e^{-i2\beta_o L} = e^{-i2\cdot\frac{\pi}{\Lambda}\cdot N\Lambda} = e^{-i2N\pi} = 1$$

The above expression reduces to

$$R' = \frac{-i\kappa\sinh\gamma L + \rho(\gamma\cosh\gamma L - i\Delta\beta\sinh\gamma L)}{(i\Delta\beta\sinh\gamma L + \gamma\cosh\gamma L) + \rho(i\kappa\sinh\gamma L)} \qquad (2\text{-}42)$$

It may be instructive to solve the same problem by a different approach. As shown in Fig. 2-9, we can treat the whole problem as a periodic waveguide with no external reflector plus a discrete reflector. The periodic waveguide has a reflection coefficient R and a transmission coefficient T as given by equations (2-33) and (2-34), and the

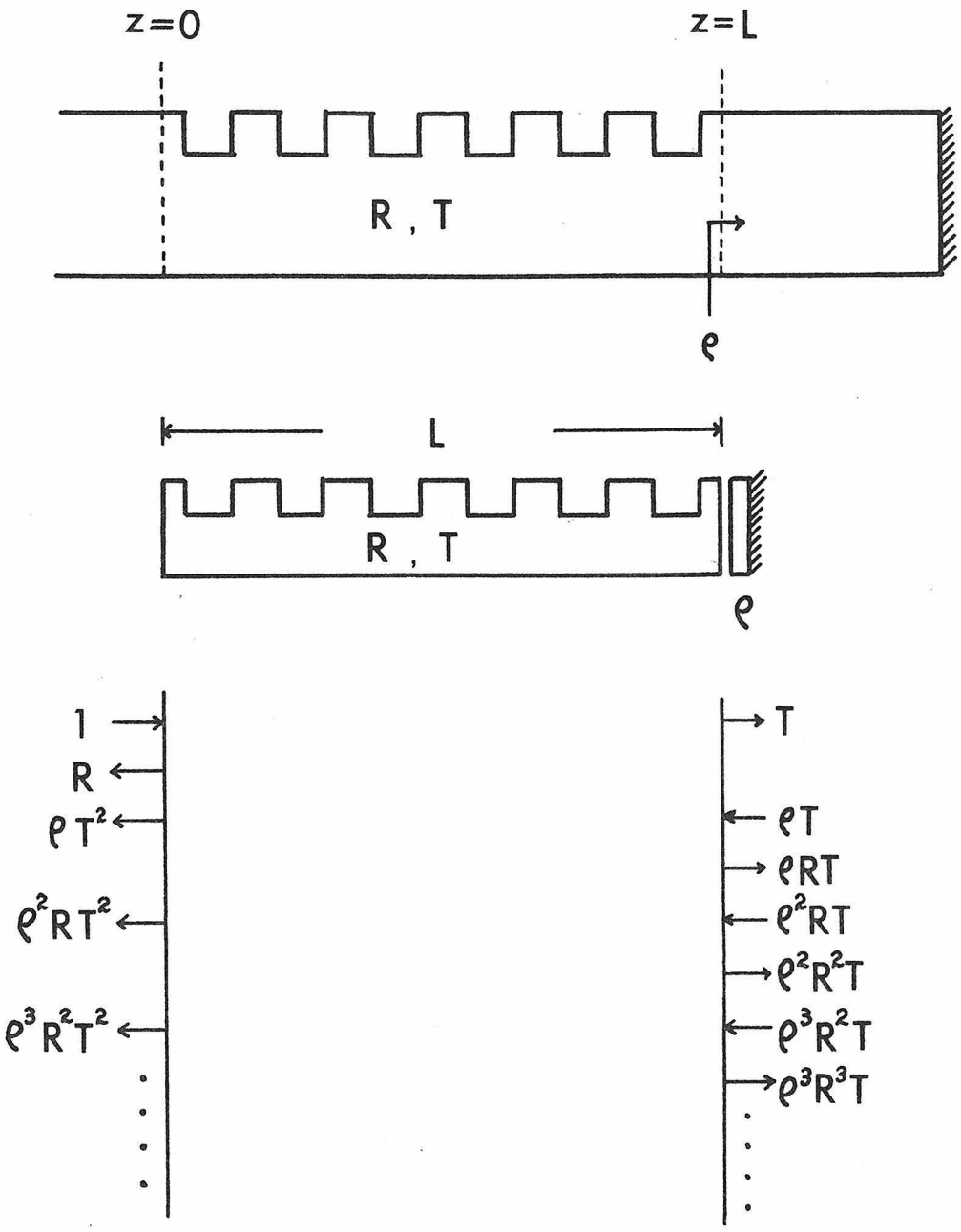

Fig. 2-9 Model used in solving the problem of periodic waveguide with external reflector.

discrete reflector has reflectivity ρ. Assume that the incident wave has unity amplitude, then there will be a reflected wave of amplitude R at z = 0 and a transmitted wave of amplitude T at z = L due to the periodic waveguide. The wave T at z = L is then reflected by the reflector and becomes a left-going incident wave of amplitude ρT at z = L. This wave in turn will have a reflected wave ρRT at z = L and a transmitted wave ρT^2 at z = 0. If we continue this process we will end up with infinite partial waves at z = 0 and z = L. The reflectivity is then found by summing up the amplitude of the partial waves going to the left at z = 0. Hence

$$R' = R + \rho T^2 + \rho^2 RT^2 + \rho^3 R^2 T^2 + \cdots$$

$$= R + \rho T^2 (1 + R + \rho^2 R^2 + \rho^3 R^3 + \cdots)$$

$$= R + \frac{\rho T^2}{1-\rho R} = \frac{R + \rho(T^2 - R^2)}{1 - \rho R} \qquad (2\text{-}43)$$

Substituting the expressions for R and T we have

$$R' = \frac{-i\kappa \sinh\gamma L + \rho\left(\frac{\gamma^2 e^{-i2\beta_o L} + \kappa^2 \sinh^2\gamma L}{i\Delta\beta \sinh\gamma L + \gamma \cosh\gamma L}\right)}{(i\Delta\beta \sinh\gamma L + \gamma\cosh\gamma L) + \rho(i\kappa \sinh\gamma L)}$$

Again if $L = N\Lambda$, $e^{-i2\beta_o L} = 1$ and

$$R' = \frac{-i\kappa \sinh\gamma L + \rho(-i\Delta\beta \sinh\gamma L + \gamma \cosh\gamma L)}{(i\Delta\beta \sinh\gamma L + \gamma\cosh\gamma L) + \rho(i\kappa \sinh\gamma L)}$$

This is identical to equation (2-42) which was obtained by solving the boundary value problem.

When we put $\rho = 0$ in (2-43) i.e. no reflection, R' reduces to R as it should. Also when R = 0 (i.e. $|T| = 1$) $|R'|^2 = |\rho|^2$. In Fig. 2-10 we plotted $|R'|^2$ as a function of $\Delta\beta L$ for $\kappa L = 2.0$ and

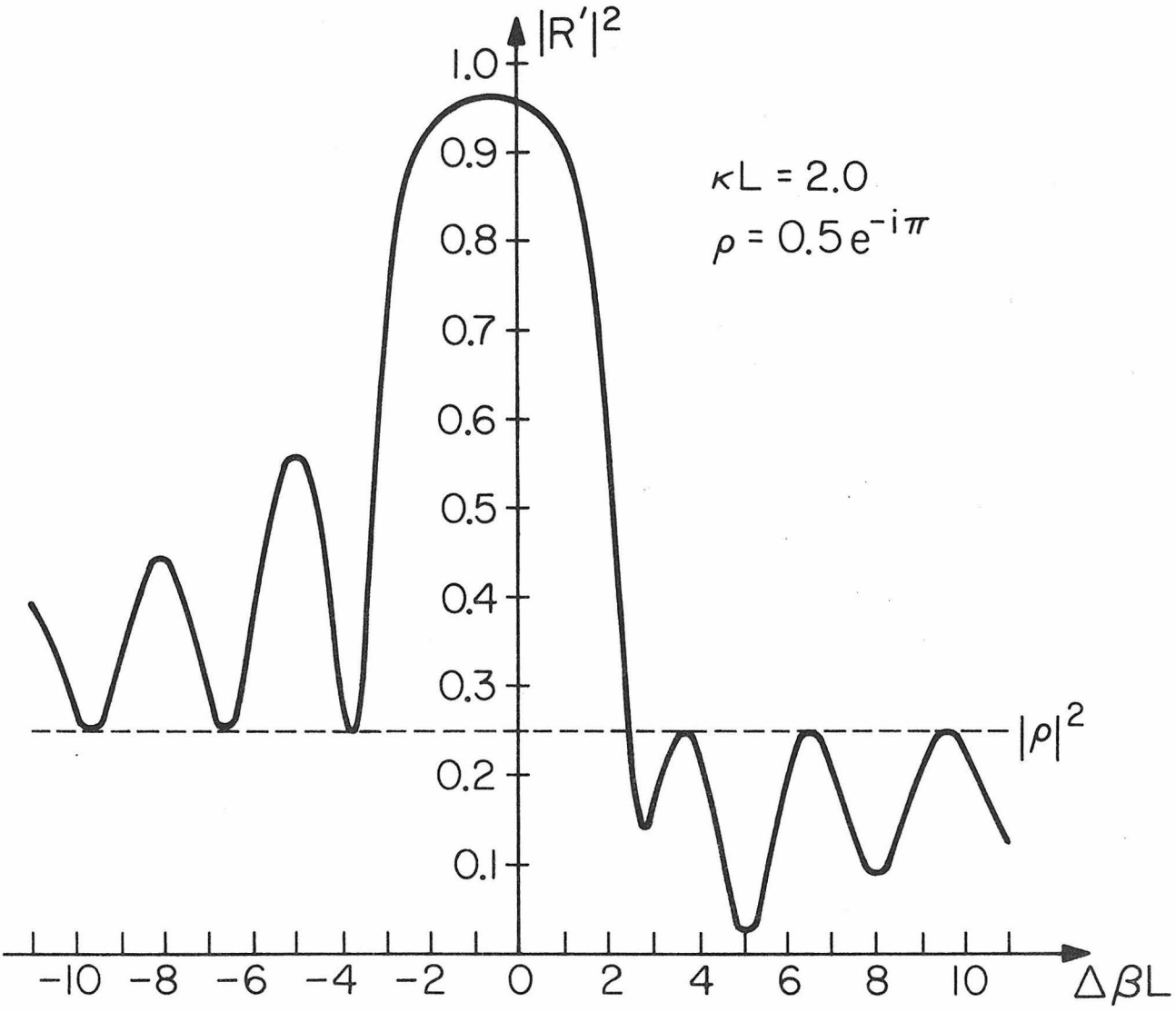

Fig. 2-10 Reflectivity spectrum of a periodic waveguide ($\kappa L = 2.0$) with some external reflector ($\rho = 0.5\ e^{-i\pi}$).

$\rho = 0.5\, e^{-i\pi}$. It is evident that R' is no longer a symmetrical function of frequency. The maximum of $|R'|^2$ is shifted to $\Delta\beta L \approx -0.6$ with a value of ~ 0.962 (as compared to 0.93 at $\Delta\beta L = 0$ for $\rho = 0$). For $\Delta\beta L > 0$ the sidelobes oscillation amplitude is bounded by $|\rho|^2 = 0.25$ while for $\Delta\beta L < 0$, we have a lower bound for $|R'|^2$ at 0.25. This behavior is a direct consequence of the sign of ρ. If we use $\rho = 0.5$ instead, then the side lobe oscillation will have a lower bound for $\Delta\beta > 0$ and an upper bound for $\Delta\beta < 0$.

CHAPTER 2 REFERENCES

(1) D. Marcuse, Theory of Dielectric Optical Waveguide, Academic Press, Inc. New York, 1974.

(2) H. Kogelnik and C. V. Shank, "Coupled-wave theory of distributed feedback lasers," J. Appl. Phys. 43, 2327 (1972).

(3) A. Yariv, "Coupled-mode theory for guided-wave optics," IEEE J. Quantum Electron.9, 919 (1973).

(4) D. Marcuse, "Mode conversion caused by surface imperfections of a dielectric slab waveguide," Bell Syst. Tech. J. 48, 3187 (1969).

(5) M. L. Dakss, L. Kuhn, P. F. Heidrich, and B. A. Scott, "Grating coupler for efficient excitation of optical guided waves in thin films," Appl. Phys. Lett. 16, 523 (1970).

(6) H. Kogelnik and T. Sosnowski, "Holographic thin film couplers," Bell Syst. Tech. J. 49, 1602 (1970).

(7) See for example L. Brillouin, Wave Propagation in Periodic Structures, McGraw-Hill, New York (1946).

(8) See for example, A. Yariv, Quantum Electronics, 2nd edition, John Wiley & Sons, Inc. New York, p. 512 (1975).

(9) W. Streifer, D. R. Scifres and R. D. Burnham, "Coupling coefficients for distributed feedback single- and double-heterostructure diode lasers," IEEE J. Quantum Electron. 11, 867 (1975).

(10) W. Streifer, D. R. Scifres, and R. D.Burnham, "TM-mode coupling coefficients in guided-wave distributed feedback lasers," IEEE J. Quantum Electron. 12, 74 (1976).

CHAPTER 3

DISTRIBUTED FEEDBACK LASERS

3-1 Introduction

A conventional laser oscillator, as shown in Fig. 3-1(a), consists of two major parts: the optical resonator and the laser medium. The laser medium which is pumped by some external agent provides the gain. The resonator is usually formed by two (or more) mirrors, outside the gain medium, which provide the necessary feedback. This type of feedback is localized at the two mirrors and is completely separated from the gain medium.

In 1971 Kogelnik and Shank[1] suggested and demonstrated a new type of laser structure called the "distributed feedback" laser in which the feedback mechanism is distributed along the length of the laser and integrated with the gain medium as illustrated in Fig. 3-1(b). It utilizes the backward Bragg scattering of the optical waves in a periodic structure as the feedback mechanism. A simplified picture of this phenomena is illustrated in Fig. 3-2. In Fig. 3-2(a) we show an incident wave which travels at an angle θ to the normal of the periodic planes. When the "Bragg condition" $2\Lambda\cos\theta = m\lambda$ ($m = 1,2,3...$) is satisfied there will be a constructive reflection of the incident wave. λ is the wavelength and Λ is the period of the spatial modulation. Fig. 3-2(b) shows the special case when $\theta = 0$, i.e., normal incidence. The Bragg condition now becomes $\Lambda = m\lambda/2$ and constructive backward scattering or reflection results without the benefit of external reflectors. If we introduce a periodic modulation of the parameters of the lasing medium and provide sufficient gain, laser oscillation

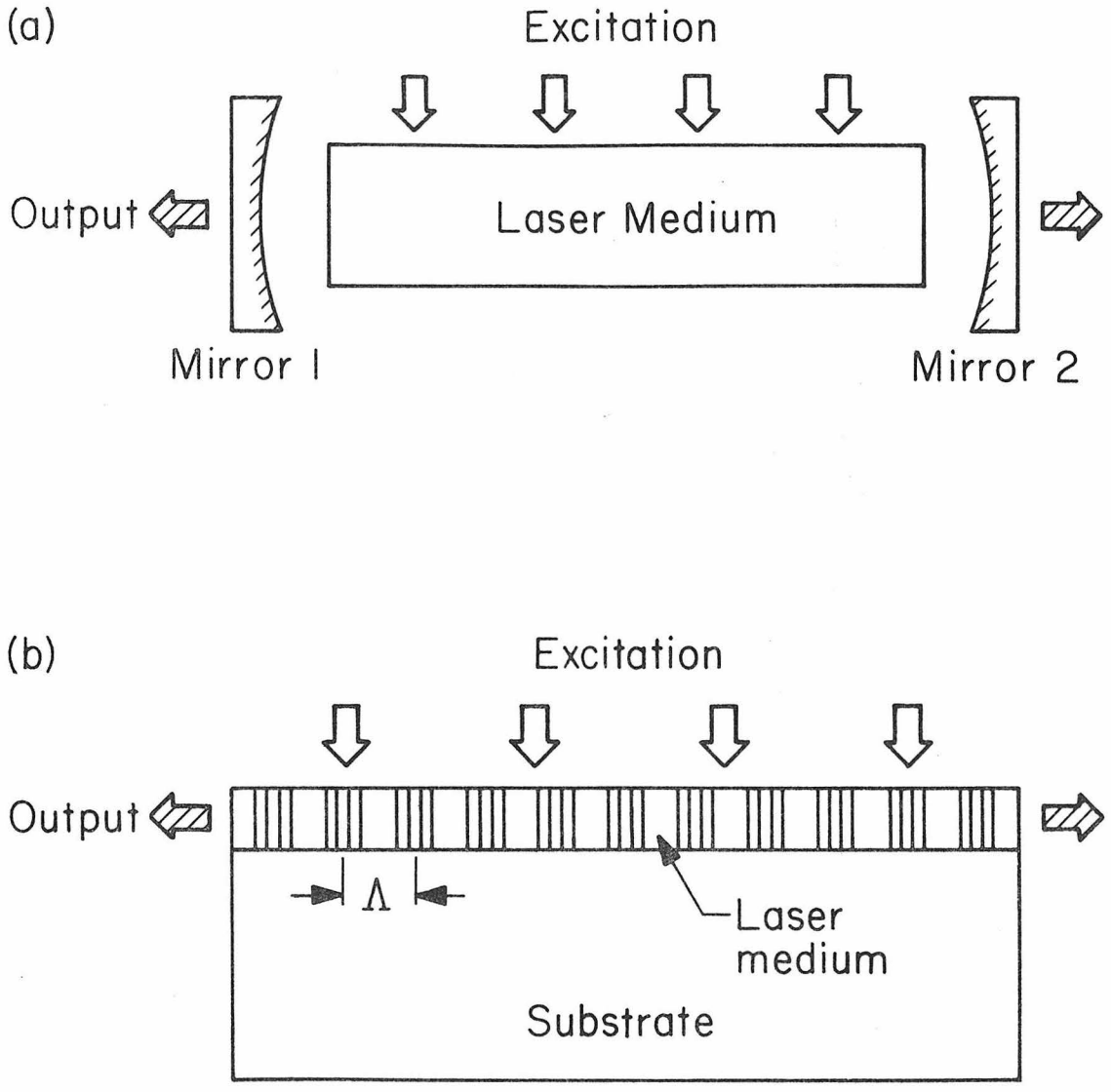

Fig. 3-1 Schematic diagrams of (a) a conventional laser (b) a distributed feedback laser.

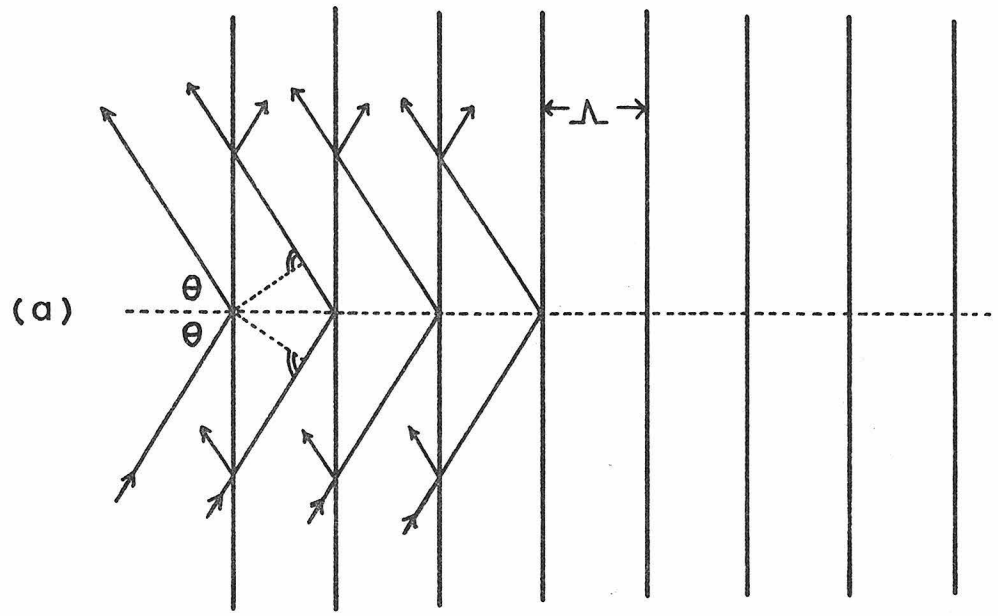

Bragg Condition : $2\Lambda\cos\theta = m\lambda$

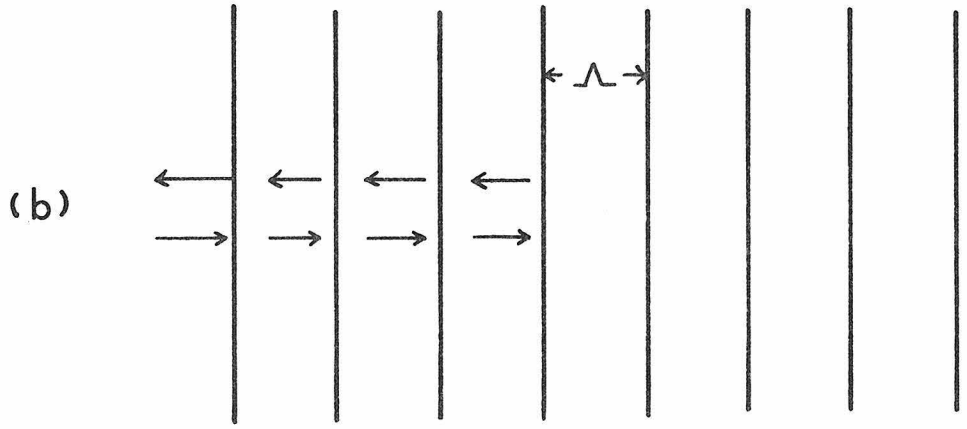

Bragg Condition : $2\Lambda = m\lambda$

Fig. 3-2 A simplified picture showing the Bragg reflection for (a) incident with an angle θ (b) normal incidence.

is possible in this kind of structure. But because of the frequency sensitivity of the Bragg reflection process, laser oscillation is limited to a very narrow spectral range centered around $\omega_o = m\pi c/\Lambda n_{eff}$ ($m = 1,2,3,\ldots$).

A coupled-wave analysis of one dimensional distributed feedback lasers was first given by Kogelnik and Shank[2]. They derived the oscillation condition and determined the mode structure. Their results were later extended to multi-layer dielectric waveguide configurations by several researchers[3-5]. Also the effect of external reflectors on the longitudinal mode structure was discussed[6,7]. And schemes of transverse mode control in this kind of laser were suggested[8].

Because of the possibility of longitudinal and transverse mode control, the lasing frequency stabilization by the period of modulation, and the compatibility of fabrication process with planar technology, the distributed feedback laser has attracted a great deal of interest in the field of integrated optics. Researchers are striving to realize a practical distributed feedback laser as the light source for integrated optical circuits.

Distributed feedback laser oscillation was first observed in organic thin films doped with Rhodamine 6G dye where a periodic spatial gain modulation was created by pumping the film by the interference pattern produced by two laser beams[1]. It is possible to change the angle of the two incident beams and vary the period of the modulation to achieve tuning in this kind of laser[9-11].

It was pointed out that a periodic corrugation of a waveguide surface is in effect a periodic modulation of the effective refractive

index of the waveguide modes. Laser oscillation was demonstrated in both liquid dye[12] and organic thin films doped with dye[13] on corrugated substrates. Similarly one can also corrugate the surface of a GaAs waveguide and achieve distributed feedback oscillation. A series of experiments[14-16] were carried out at Caltech which clearly demonstrated the feasibility of GaAs distributed feedback laser for the first time. A theoretical analysis by Nakamura and Yariv[18] indicated that GaAs heterostructure injection lasers with corrugation feedback can be fabricated with thresholds comparable to those in ordinary injection lasers. Since then GaAs distributed feedback injection lasers of various structure have been demonstrated at low temperatures[19-21]. It is not until the adoption of separate confinement double heterostructure that room temperature cw operation was possible[22,23]. There remain, however, additional problems to be solved before these lasers can be used as practical devices. Among them is the reliability (operating lifetime) problem.

In this chapter we will apply the coupled-mode formalism established in the previous chapter to study the characteristics of an amplifying periodic waveguide. The distributed feedback laser oscillation condition is derived by two different approaches. The general properties of distributed feedback lasers and Fabry Perot lasers are compared. Also we describe the design of GaAs distributed feedback lasers. Finally experimental results on GaAs lasers are given and compared with theory.

3-2 Amplification and Oscillation in Periodic Waveguides

The propagation properties of a periodically corrugated passive optical waveguide were considered in Chapter 2. We found that in the Bragg regime ($\Lambda \approx \lambda/2$) the behavior of the waveguide is characterized by strong evanescence of the incident wave due to backward coherent scattering (reflection). In this section we shall consider the propagation of waves in an amplifying periodic waveguide.

Assume that the total field inside the guide is given by

$$E(z) = E_i(z) + E_r(z) = A(z)e^{i\beta z-\alpha z} + B(z)e^{-i\beta z+\alpha z}$$

where α is the amplitude gain coefficient of the uniform waveguide. If we follow a procedure similar to that leading to equation (2-11) we obtain the coupled-mode equations

$$\begin{aligned} \frac{dA}{dz} &= i\kappa B e^{-i2(\Delta\beta+i\alpha)z} \\ \frac{dB}{dz} &= -i\kappa A e^{i2(\Delta\beta+i\alpha)z} \end{aligned} \tag{3-1}$$

These equations are of a form identical to that of equation (2-27) provided we perform the substitution

$$\Delta\beta \rightarrow \Delta\beta + i\alpha$$

With this substitution we can then use (2-31) and (2-32) to obtain the solutions for the incident wave $E_i(z) = B(z)e^{-i\beta z+\alpha z}$ and the reflected wave $E_r(z) = A(z)e^{i\beta z-\alpha z}$ within a section of waveguide of length L as

$$E_i(z) = B(z)e^{-i\beta z+\alpha z}$$

$$= E_i(0)\,\frac{[(\alpha-i\Delta\beta)\sinh\gamma(L-z) - \gamma\cosh\gamma(L-z)]e^{-i\beta_o z}}{(\alpha-i\Delta\beta)\sinh\gamma L - \gamma\cosh\gamma L} \tag{3-2}$$

$$E_r(z) = A(z)e^{i\beta z-\alpha z}$$

$$= E_i(0)\,\frac{i\kappa\sinh\gamma(L-z)e^{i\beta_o z}}{(\alpha-i\Delta\beta)\sinh\gamma L - \gamma\cosh\gamma L} \tag{3-3}$$

where

$$\gamma^2 = \kappa^2 + (\alpha-i\Delta\beta)^2$$

Fig. 3-3 shows the behavior of $|E_i(z)|^2$ and $|E_r(z)|^2$ for $\kappa L = 1.0$, $\alpha L = 1.0$ and $\Delta\beta L = 0$. We see that the incident wave no longer decays along the whole length but after a certain distance it starts to grow exponentially. Also the reflected wave grows more rapidly and exceeds the incident wave at $z = 0$ so that the device acts as an amplifier. This is fundamentally different from that of a passive waveguide which is also shown for comparison.

We can define, as before, the amplitude reflection and transmission coefficient as

$$R = \frac{E_r(0)}{E_i(0)} = \frac{i\kappa\sinh\gamma L}{(\alpha-i\Delta\beta)\sinh\gamma L - \gamma\cosh\gamma L} \tag{3-4}$$

$$T = \frac{E_i(L)}{E_i(0)} = \frac{-\gamma e^{-i\beta_o L}}{(\alpha-i\Delta\beta)\sinh\gamma L - \gamma\cosh\gamma L} \tag{3-5}$$

If the condition

$$(\alpha-i\Delta\beta)\sinh\gamma L = \gamma\cosh\gamma L \tag{3-6}$$

is satisfied, it follows from equation (3-4) and (3-5) that both R and T become infinite. The device acts as an oscillator since it yields finite output fields $E_r(0)$ and $E_i(L)$ with no input field

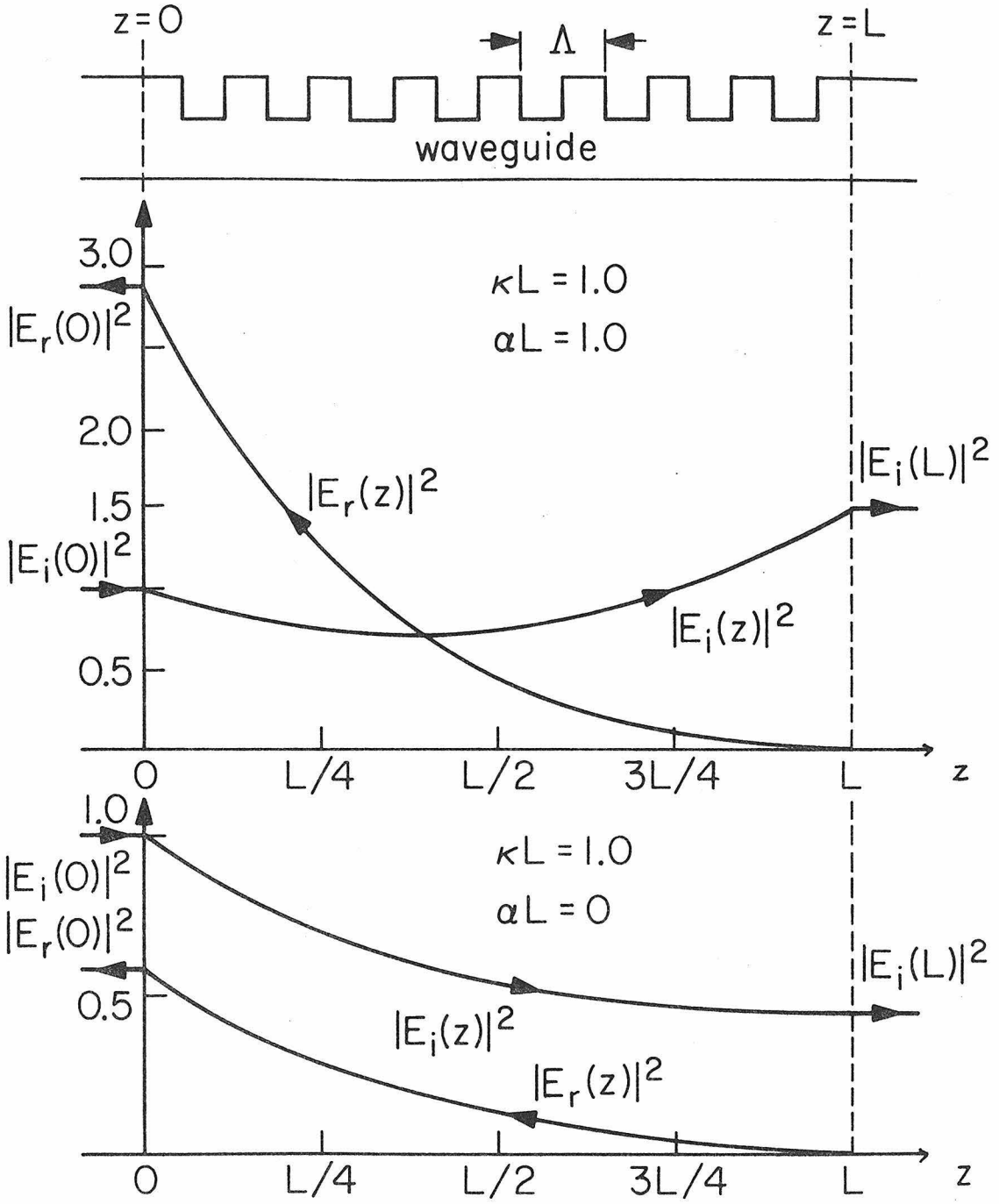

Fig. 3-3 The behavior of $|E_i(z)|^2$ and $|E_r(z)|^2$ in a periodic waveguide (a) with gain $\alpha L = 1.0$ (b) without gain $\alpha L = 0$.

($E_i(0) = 0$). Hence equation (3-6) is the oscillation condition of a distributed feedback laser.

For frequencies very near the Bragg frequency ($\omega_o = \pi c/\Lambda n_{eff}$), where condition (3-6) can be nearly satisfied with small gain coefficient α, the device acts as a high gain amplifier. The amplified output is available either in reflection with amplitude gain R or in transmission with amplitude gain T. In Fig. 3-4 and 3-5 we plot the intensity reflection gain $|E_r(0)/E_i(0)|^2$ and the transmission gain $|E_i(L)/E_i(0)|^2$ as functions of $\Delta\beta L$ and αL for $\kappa L = 0.4$. Each plot contains four infinite gain singularities at which the condition (3-6) is satisfied. The plots are symmetrical with respect to $\Delta\beta L$.

The coordinates of the singularities correspond to the oscillation frequency and threshold for different longitudinal modes of the laser as will be discussed in more detail in Section 3-4.

It should be noted that Fig. 3-4 and 3-5 were plotted using linear analysis which means that saturation effects were not taken into consideration. In a real device the maximum amplification is always limited by saturation. It can be treated by a nonlinear analysis with numerical computation as was done by Hill and Watanabe[24].

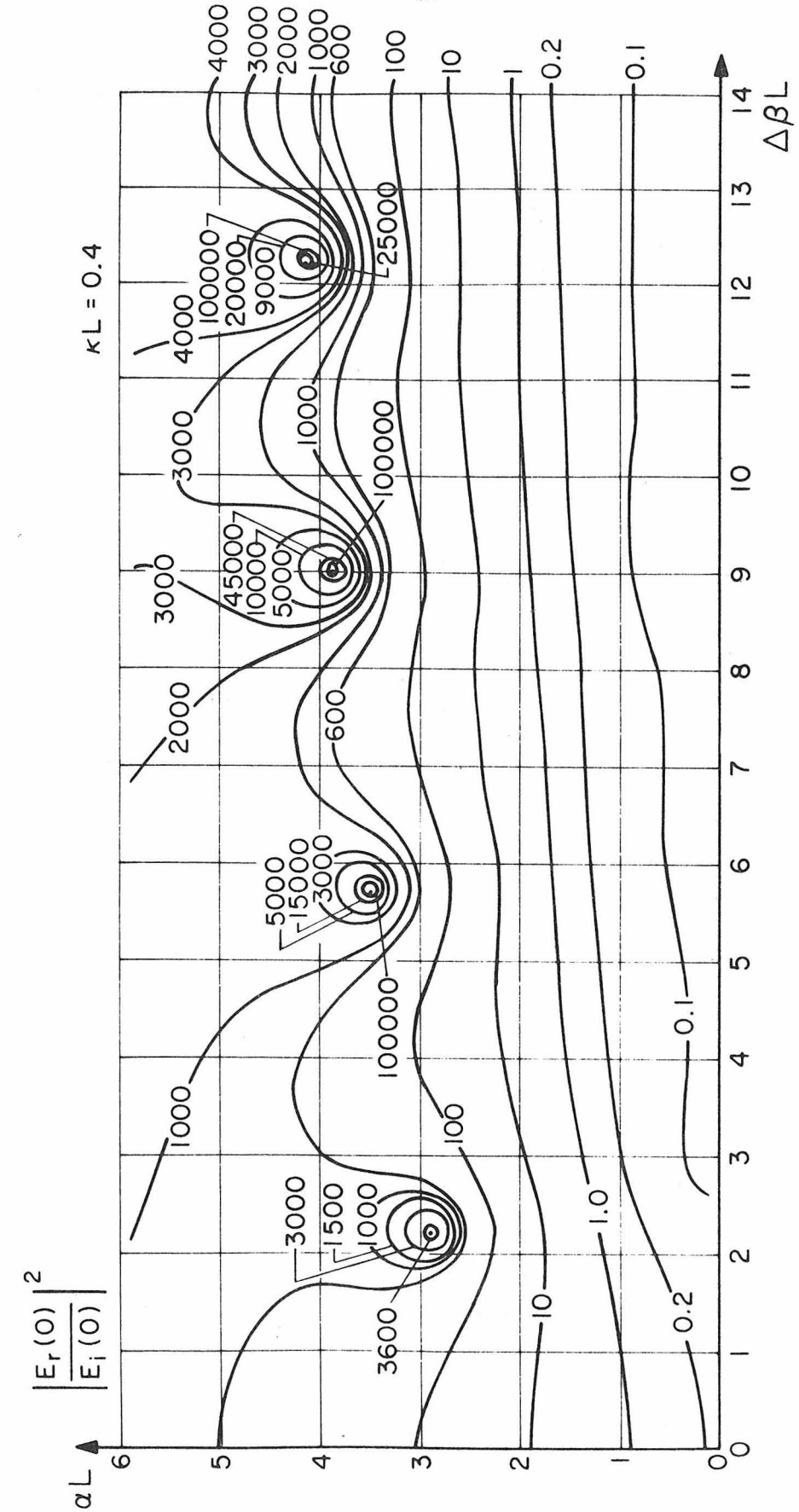

Fig. 3-4 The reflection gain as a function of $\Delta\beta L$ and αL for $\kappa L = 0.4$.

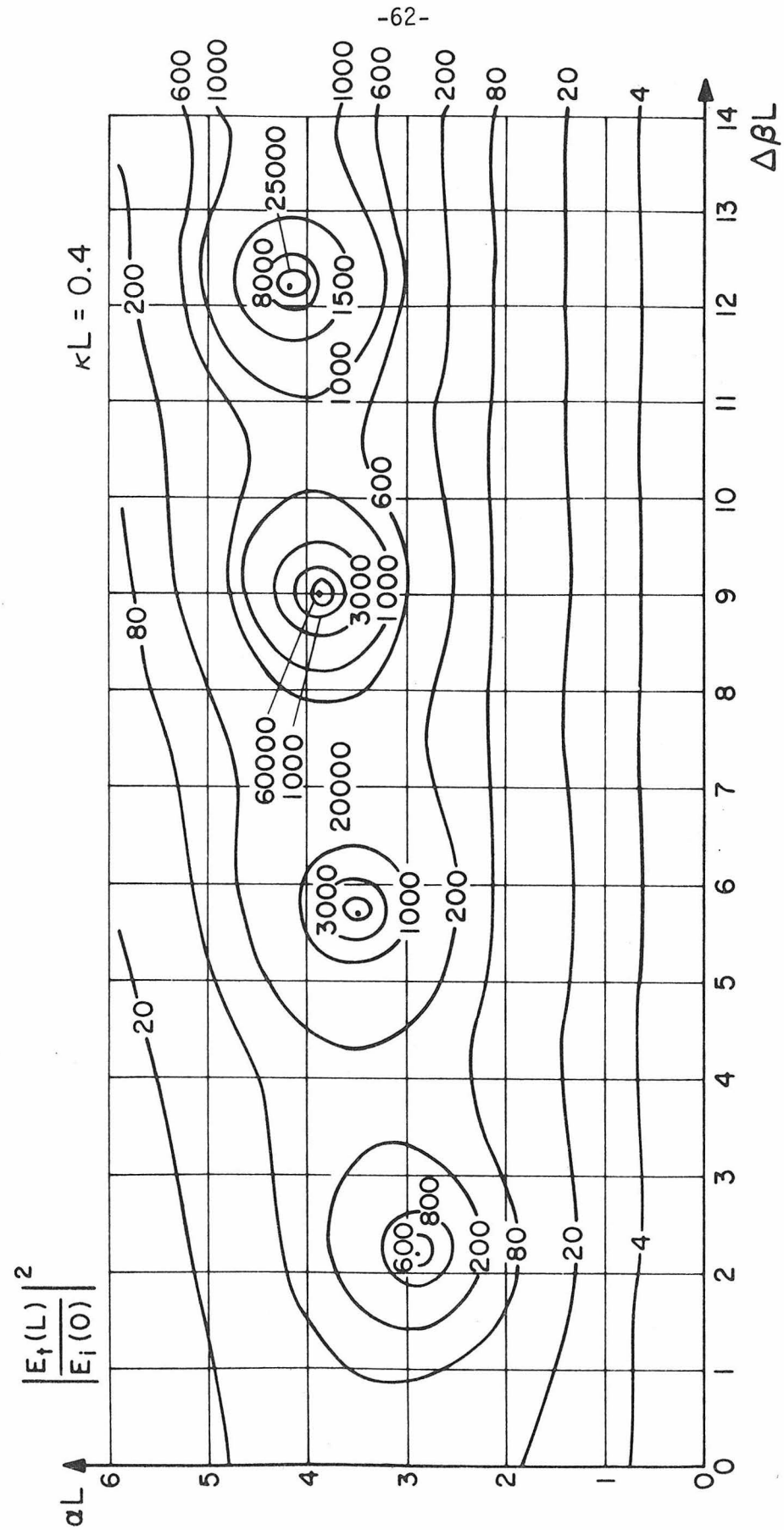

Fig. 3-5 The transmission gain as a function of $\Delta\beta L$ and αL for $\kappa L = 0.4$.

3-3 Alternative Derivation of the Oscillation Condition

In an ordinary laser oscillator the oscillation condition is determined by following a wave generated inside the cavity for one complete round trip. By setting this round trip gain equal to unity one can obtain the condition for oscillation. In this section we shall use this recipe in a distributed feedback laser. As shown in Fig. 3-6 the periodic waveguide section with gain α extending from $z = 0$ to $z = L$. Let us pick a random reference plane, say $z = \ell$, and find the reflection coefficients at this plane looking into the two divided waveguide sections. Denote them by $R(\ell)$ and $R(L-\ell)$ respectively. Using equation (3-4) we can write $R(\ell)$ and $R(L-\ell)$ directly as

$$R(\ell) = \frac{i\kappa \sinh\gamma\ell}{(\alpha - i\Delta\beta)\sinh\gamma\ell - \gamma\cosh\gamma\ell}$$

and

$$R(L-\ell) = \frac{i\kappa \sinh\gamma(L-\ell)}{(\alpha - i\Delta\beta)\sinh\gamma(L-\ell) - \gamma\cosh\gamma(L-\ell)}$$

And the round trip gain in the periodic waveguide is

$$R(\ell)R(L-\ell) = 1$$

Substituting the expressions for $R(\ell)$ and $R(L-\ell)$ we have

$$\left[\frac{i\kappa \sinh\gamma\ell}{(\alpha - i\Delta\beta)\sinh\gamma\ell - \gamma\cosh\gamma\ell}\right]\left[\frac{i\kappa \sinh\gamma(L-\ell)}{(\alpha - i\Delta\beta)\sinh\gamma(L-\ell) - \gamma\cosh\gamma(L-\ell)}\right] = 1$$

After simplification it becomes

$$(\alpha - i\Delta\beta)\sinh\gamma L - \gamma\cosh\gamma L = 0$$

This is the same as relation (3-6) obtained earlier. Note that the oscillation condition is independent of the choice of ℓ as it should be. As a matter of fact we can take ℓ to be infinitesimally small,

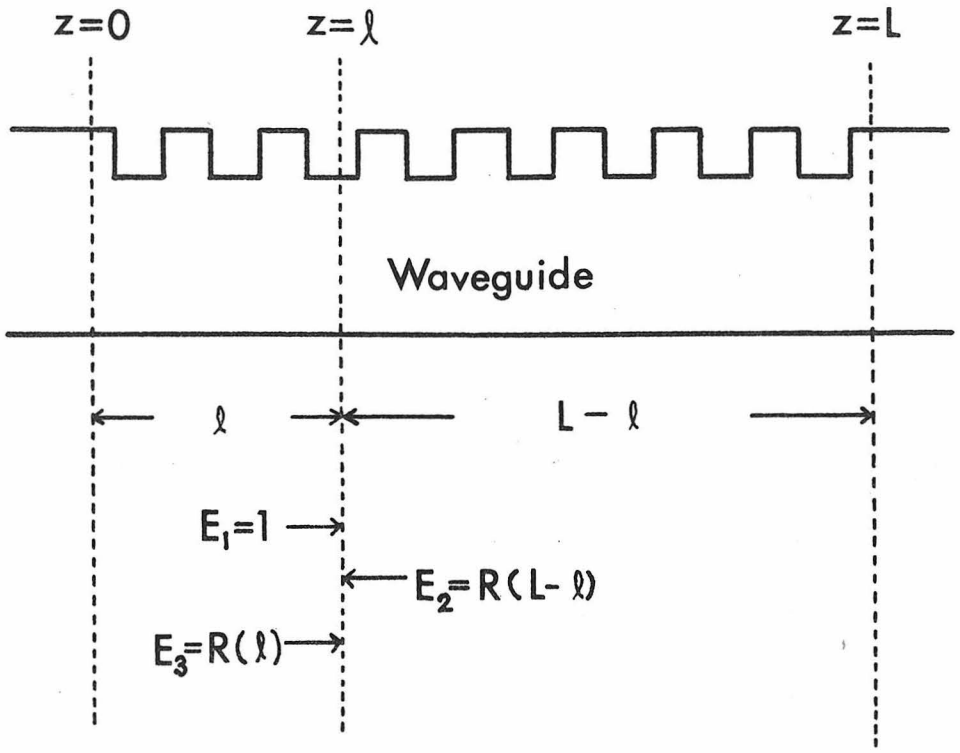

Oscillation Condition : $R(\ell)R(L-\ell)=1$

Fig. 3-6 Schematic drawing shows the derivation of the distributed feedback laser oscillation condition.

$\ell=\varepsilon$, and write

$$\lim_{\varepsilon\to 0} R(\varepsilon)R(L-\varepsilon) = 1$$

Since $\lim_{\varepsilon\to 0} R(\varepsilon) \to 0$ and $\lim_{\varepsilon\to 0} R(L-\varepsilon) \to R(L)$ we must have $R(L) = \infty$. This is the condition used to derive equation (3-6). As a special case, let us take $\ell = L/2$, then the oscillation condition can be expressed as

$$R(\tfrac{L}{2}) = r(\tfrac{L}{2})e^{-i\phi(\frac{L}{2})} = \pm 1 \qquad (3\text{-}7)$$

where

$$r(\tfrac{L}{2}) = \left\{ \frac{\kappa^2[\cosh\gamma_r L - \cos\gamma_i L]}{(\alpha^2+\Delta\beta^2+\gamma_r^2+\gamma_i^2)\cosh\gamma_r L+(\Delta\beta\gamma_i-\alpha\gamma_r)\sinh\gamma_r L-(\alpha^2+\Delta\beta^2-\gamma_r^2-\gamma_i^2)\cos\gamma_i L} \right\}^{1/2}$$

$$-(\gamma_r\Delta\beta+\alpha\gamma_i)\sin\gamma_i L$$

and

$$\phi(\tfrac{L}{2}) = \frac{\pi}{2} + \tan^{-1}\frac{\sinh\frac{\gamma_r L}{2}\left[\Delta\beta\cos\frac{\gamma_i L}{2}+\gamma_r\sin\frac{\gamma_i L}{2}\right]+\cosh\frac{\gamma_r L}{2}\left[\gamma_i\cos\frac{\gamma_i L}{2}-\alpha\sin\frac{\gamma_i L}{2}\right]}{-\sinh\frac{\gamma_r L}{2}\left[\alpha\cos\frac{\gamma_i L}{2}+\gamma_i\sin\frac{\gamma_i L}{2}\right]+\cosh\frac{\gamma_r L}{2}\left[\gamma_r\cos\frac{\gamma_i L}{2}-\Delta\beta\sin\frac{\gamma_i L}{2}\right]}$$

$$- \tan^{-1}(\coth\gamma_r L\tan\gamma_i L) + m\pi$$

where

$$\gamma = [\kappa^2+(\alpha-i\Delta\beta)^2]^{1/2} = \gamma_r + i\gamma_i$$

When $\Delta\beta = 0$, $\gamma_i = 0$ and $\phi(L/2)$ reduces to $\pi/2$ so equation (3-7) cannot be satisfied. This means no laser oscillation is possible at the exact Bragg frequency.

If the laser is connected to other circuit components there will be some external effect that cannot be neglected. But we can always represent these outside effects as an external reflector and calculate the composite reflectivity as was done in section 2-6. Then the oscillation condition is derived with the new reflection coefficients.

Let us assume that the external reflectivity at z = 0 is ρ_1 and at z = L is ρ_2. (Refer to Fig. 3-6.) Then the composite reflectivities are

$$R'(\ell) = \frac{-[\rho_1(\alpha-i\Delta\beta)-i\kappa]\sinh\gamma\ell - \rho_1\gamma\cosh\gamma\ell}{[(\alpha-i\Delta\beta)-i\rho_1\kappa]\sinh\gamma\ell - \gamma\cosh\gamma\ell}$$

and

$$R'(L-\ell) = \frac{-[\rho_2(\alpha-i\Delta\beta)-i\kappa]\sinh\gamma(L-\ell) - \rho_2\gamma\cosh\gamma(L-\ell)}{[(\alpha-i\Delta\beta)-i\rho_2\kappa]\sinh\gamma(L-\ell) - \gamma\cosh\gamma(L-\ell)}$$

Then the oscillation condition

$$R'(\ell)R'(L-\ell) = 1$$

becomes

$$(1-\rho_1\rho_2)\gamma\cosh\gamma L = [(1+\rho_1\rho_2)(\alpha-i\Delta\beta) - i\kappa(\rho_1+\rho_2)]\sinh\gamma L \qquad (3\text{-}8)$$

Again this condition is independent of ℓ and it reduces to equation (3-6) when both ρ_1 and ρ_2 vanish. Note that if either ρ_1 or ρ_2 is zero the equation can be greatly simplified. The effect of external reflectors on the dsitributed feedback laser mode structure is very complicated and we must resort to numerical examples to see what is going on. A special case of $\rho_1 = \rho_2$ was treated by Chinn[6] and the more general case $\rho_1 \neq \rho_2$ was calculated by Streifer et al[7].

3-4 Determination of the Lasing Frequency and the Threshold Gain

The oscillation condition of a uniform distributed feedback laser with no external reflectors was found to be

$$(\alpha-i\Delta\beta)\sinh\gamma L = \gamma\cosh\gamma L$$

where $\gamma^2 = \kappa^2 + (\alpha - i\Delta\beta)^2$. In general γ is a complex number $\gamma = \gamma_r + i\gamma_i$ where

$$\gamma_r = \sqrt{\frac{1}{2}} \{(\kappa^2+\alpha^2-\Delta\beta^2) + [(\kappa^2+\alpha^2-\Delta\beta^2)^2+4\alpha^2\Delta\beta^2]^{1/2}\}^{1/2} \qquad (3\text{-}9)$$

and

$$\gamma_i = -\frac{2\alpha\Delta\beta}{\gamma_r}$$

So the oscillation condition

$$(\alpha - i\Delta\beta)\sinh(\gamma_r+i\gamma_i)L = (\gamma_r+i\gamma_i)\cosh(\gamma_r+i\gamma_i)L$$

becomes

$$F(\alpha,\Delta\beta) = (\alpha^2+\Delta\beta^2+\gamma_r{}^2+\gamma_i{}^2)\cosh 2\gamma_r L - (\alpha^2+\Delta\beta^2-\gamma_r{}^2-\gamma_i{}^2)\cos 2\gamma_i L$$

$$+ 2(\Delta\beta\gamma_i-\alpha\gamma_r)\sinh 2\gamma_r L - 2(\gamma_r\Delta\beta+\alpha\gamma_i)\sin 2\gamma_i L$$

$$= 0 \qquad (3\text{-}10)$$

This is the eigenvalue equation of the distributed feedback laser which can be solved numerically or graphically to obtain an infinite set of eigenvalue pairs $(\Delta\beta_n, g_n)$. Each such pair determines the oscillation frequency $\Delta\beta_n$ and the threshold gain g_n of the n-th longitudinal mode of the laser. It can be shown easily that $F(\alpha,\Delta\beta) = F(\alpha,-\Delta\beta)$ which means that the location of the longitudinal modes are symmetric about the Bragg frequency ($\Delta\beta=0$). Also simple physical reasoning requires that α be positive. In Fig. 3-7 we plot the solutions of $F(\alpha,\Delta\beta) = 0$ for various values of κL. It is evident from the figure that the laser always oscillates outside the stop band, i.e., $|\Delta\beta_n| > \kappa$ for all n. The dependence of αL on κL can be seen

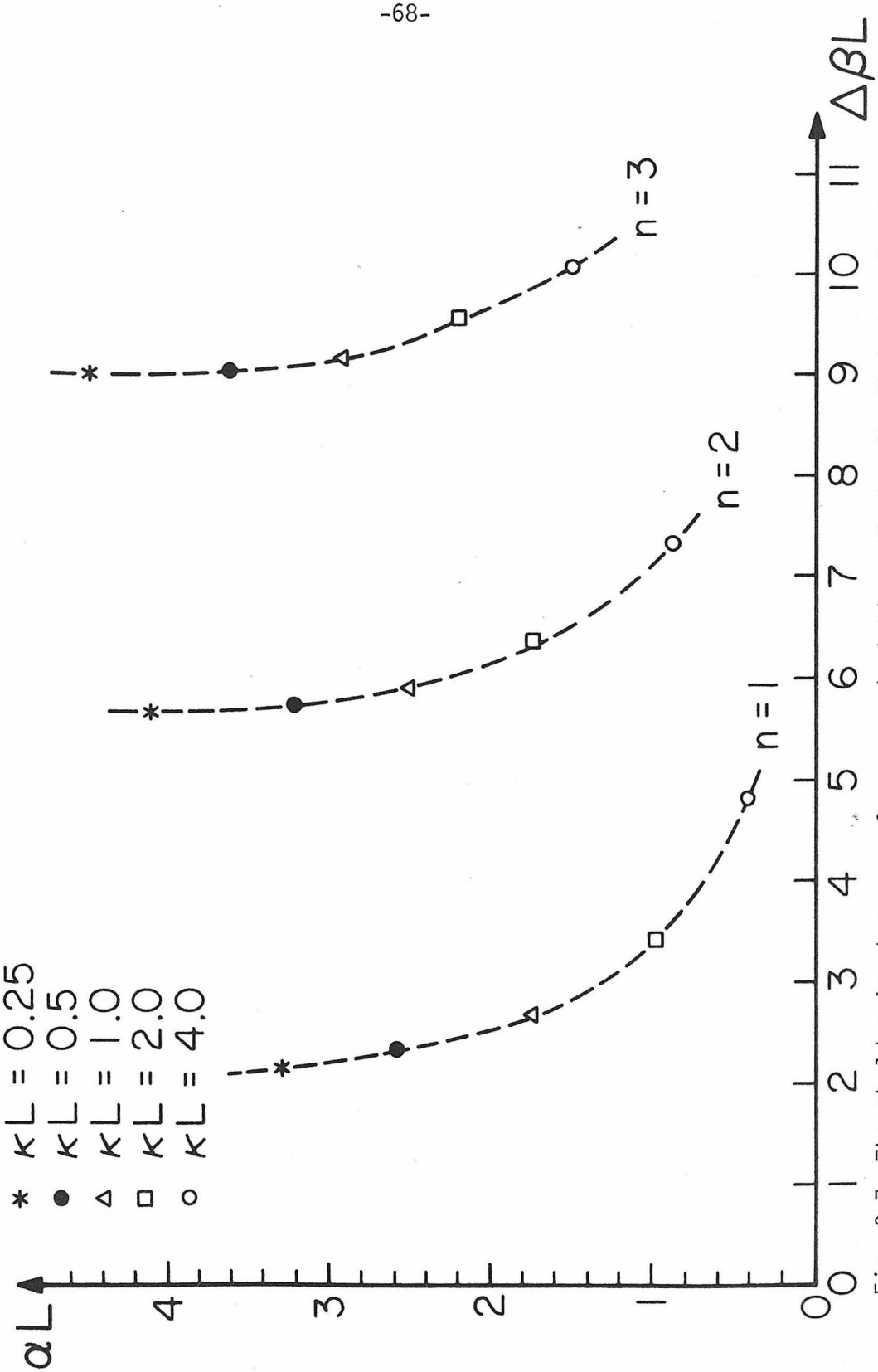

Fig. 3-7 Threshold gain αL versus frequency deviation ΔβL for disributed feedback lasers with different values of κL.

from the dotted curves in Fig. 3-7 for different longitudinal modes. We can also derive the dependence of threshold gain α on the laser length L for a fixed κL. This result is shown in Fig. 3-8.

In general the process of solving for the eigenvalues is tedious. It is desirable to obtain some approximate analytic solutions instead. Let us look into the case when κ is small and $\Delta\beta$ is large. Recall the expression for γ_r (3-9)

$$\gamma_r = \left\{ \frac{(\kappa^2+\alpha^2-\Delta\beta^2) + [(\kappa^2+\alpha^2-\Delta\beta^2)^2 + 4\alpha^2\Delta\beta^2]^{1/2}}{2} \right\}^{1/2}$$

If κ is small and $\Delta\beta$ is large, the laser will need a large gain to oscillate. Under these conditions γ_r becomes

$$\gamma_r \approx \alpha\left[1 + \frac{\kappa^2(\alpha^2-\Delta\beta^2)}{4\alpha^2(\alpha^2+\Delta\beta^2)}\right] \equiv \alpha(1+\delta) \tag{3-11}$$

and consequently

$$\gamma_i = -\frac{\alpha\Delta\beta}{\gamma_r} \approx -\Delta\beta\left[1 - \frac{\kappa^2(\alpha^2-\Delta\beta^2)}{4\alpha^2(\alpha^2+\Delta\beta^2)}\right] = -\Delta\beta(1-\delta) \tag{3-12}$$

where

$$\delta = \frac{\kappa^2(\alpha^2-\Delta\beta^2)}{4\alpha^2(\alpha^2+\Delta\beta^2)} \ll 1$$

The oscillation condition (3-6) can be written as

$$\frac{\gamma - (\alpha-i\Delta\beta)}{\gamma + (\alpha-i\Delta\beta)} e^{2\gamma L} = -1 \tag{3-13}$$

Use (3-11) and (3-12) in (3-13), we have

$$\frac{\delta(\alpha+i\Delta\beta)}{2(\alpha-i\Delta\beta)} e^{2[\alpha(1+\delta)]L} e^{-i2\Delta\beta(1-\delta)L} = -1 \tag{3-14}$$

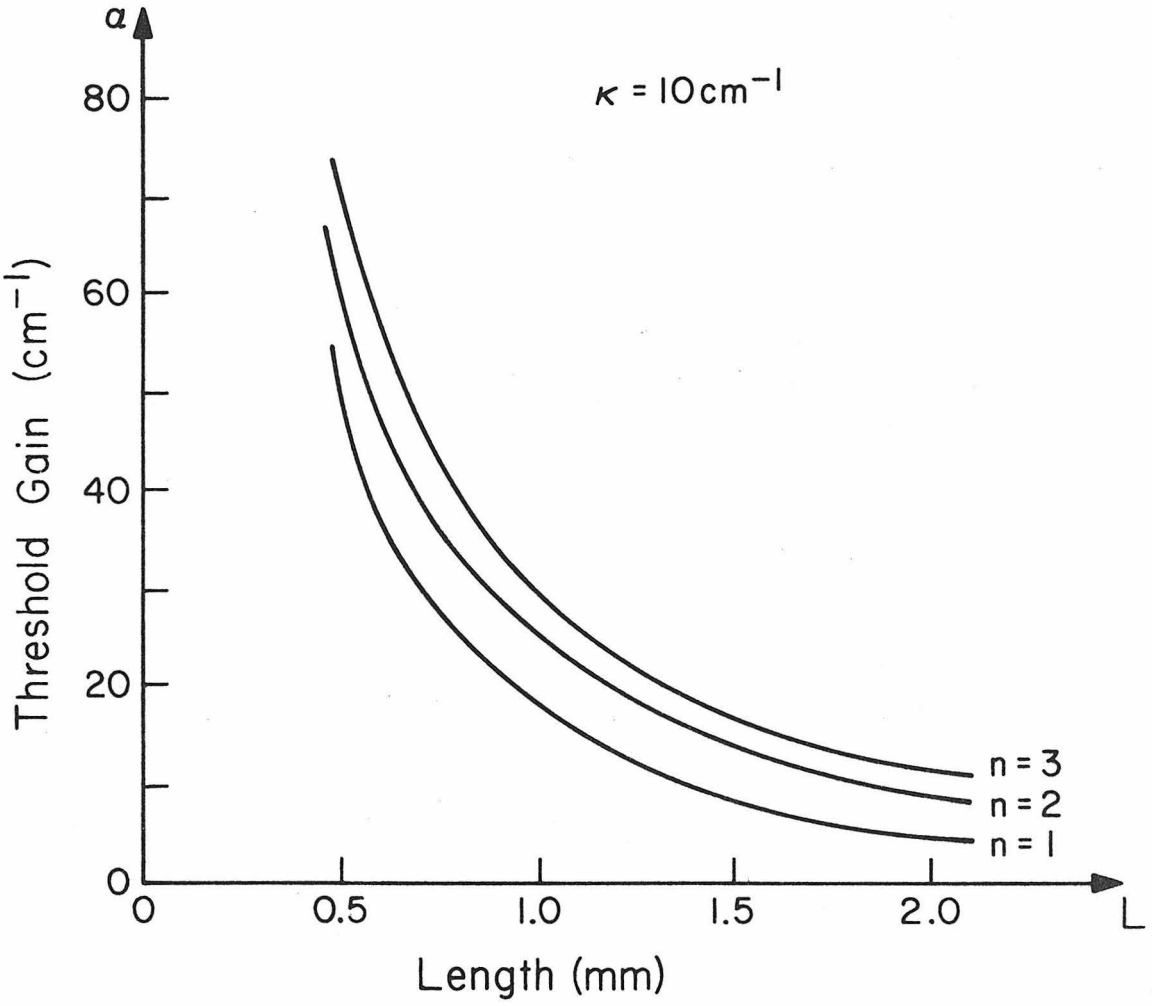

Fig. 3-8 A plot of threshold gain α vs. length of the laser L for different longitudinal modes.

Equating the phases of both sides of (3-14) we have

$$2\tan^{-1}\frac{\Delta\beta_n}{\alpha_n} - 2\Delta\beta_n L + \frac{\kappa^2\Delta\beta_n L(\alpha_n^2-\Delta\beta_n^2)}{2\alpha_n^2(\alpha_n^2+\Delta\beta_n^2)} = (2n+1)\pi$$

where $n = 0,\pm1,\pm2,\pm3,\ldots$

If $\alpha_n >> \Delta\beta_n$ the oscillation frequencies will be given approximately by

$$\Delta\beta_n L = (n + \tfrac{1}{2})\pi$$

and the frequency

$$\omega_n = \frac{\beta_n c}{n_{eff}} = \left(\frac{\beta_o+\Delta\beta_n}{n_{eff}}\right) c = \omega_o + (n + \tfrac{1}{2})\frac{\pi c}{n_{eff}L} \qquad (3\text{-}15)$$

Once again we see that no laser oscillation can exist at $\omega = \omega_o$ ($\Delta\beta_n = 0$). The longitudinal mode spacing in this limiting case is

$$\Delta\omega = \omega_{n+1} - \omega_n = \frac{\pi c}{n_{eff}L}$$

This result is identical to that of a Fabry-Perot laser with a length L.

Once $\Delta\beta_n$ is found we can write

$$\beta_n = \beta_o + \Delta\beta_n = \frac{\pi}{\Lambda} + \Delta\beta_n$$

or

$$\frac{2\pi}{\lambda} n_{eff} = \frac{\pi}{\Lambda} + \Delta\beta_n$$

Hence

$$n_{eff} = \frac{\lambda}{2}\left(\frac{1}{\Lambda} + \frac{\Delta\beta_n}{\pi}\right) \equiv \frac{\lambda}{2\Lambda_n} \qquad (3\text{-}16)$$

where

$$\frac{1}{\Lambda_n} \equiv \frac{1}{\Lambda} + \frac{\Delta\beta_n}{\pi}$$

Thus each longitudinal mode is represented by a straight line with slope $1/2\Lambda_n$ in the n_{eff}-λ plane. We can also plot the waveguide dispersion curve

$$n_{eff}(\lambda) = \frac{\lambda\beta(\lambda)}{2\pi}$$

on the same plane as shown in Fig. 3-9. The intersections of this curve with the family of lines represented by equation (3-16) give the lasing wavelengths of the different longitudinal modes.

If the waveguide can support several transverse modes the sitaution is more complicated. As discussed in Chapter 2, different transverse modes experience different coupling constants so that for each transverse mode we have a different dispersion curve and a different set of lines like equation (3-16) to determine the lasing wavelengths.

3-5 The Effect of Distributed Feedback on Spontaneous Emission Spectrum

In this section we study the spectral properties of a distributed feedback laser operating below threshold. This problem is treated by using multi-reflection approach to calculate the output of spontaneous emission from a section of amplifying periodic waveguide. As depicted in Fig. 3-10 the waveguide has a length L with amplitude gain coefficient α. We pick an arbitrary plane z_o and consider a small volume of the medium. Because of the spontaneous emission process this small volume emits electromagnetic wave of amplitude E isotropically. We are interested in the direction perpendicular to the periodic planes (parallel to the z-axis).

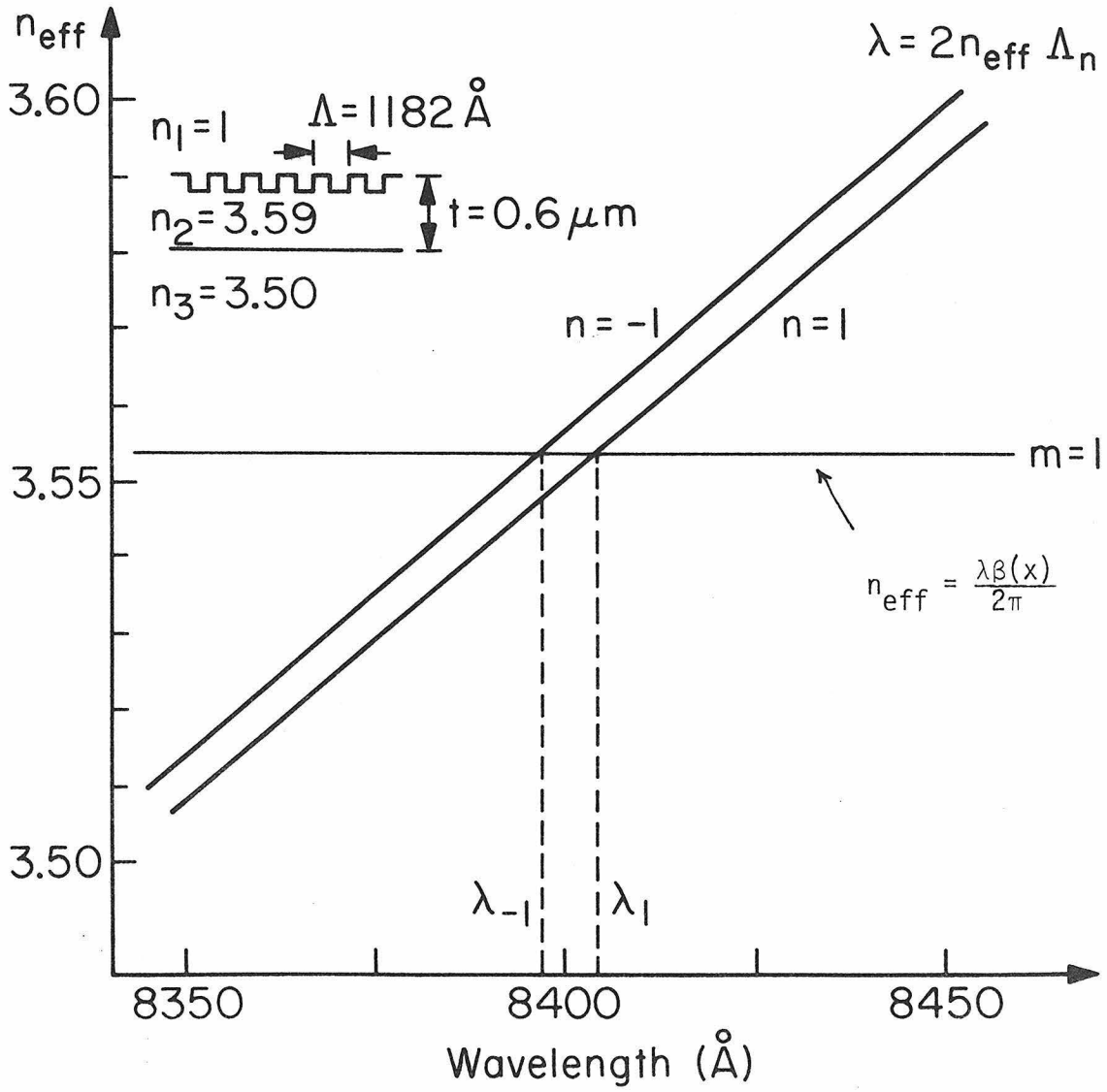

Fig. 3-9 Graphical method for determining the lasing wavelength of a distributed feedback laser.

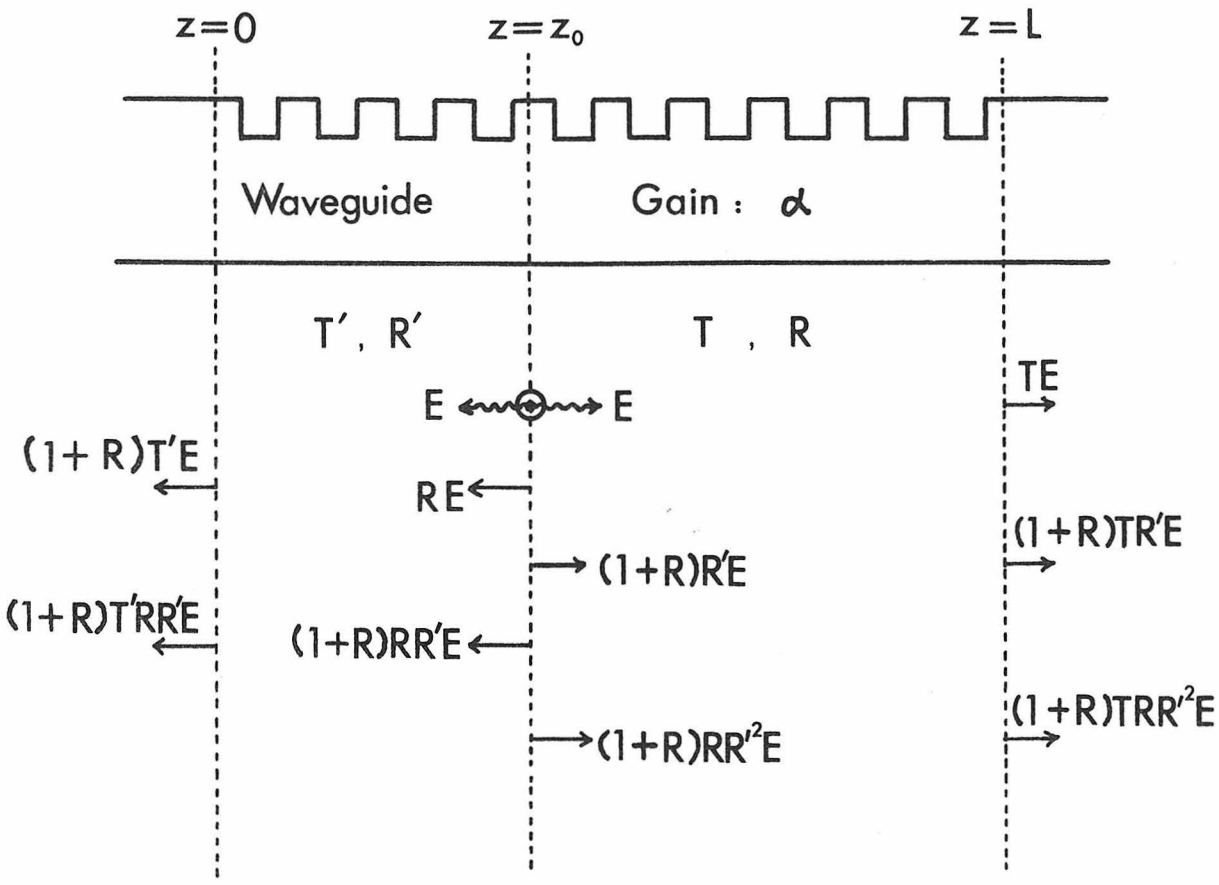

Fig. 3-10 A schematic drawing shows the processes of amplified spontaneous emission in an amplifying periodic waveguide.

We could follow the radiation emitted from the differential volume to the output and then sum the contributions from the rest of the volume to find the total output at z = L.

The section of the waveguide to the right of the $z = z_o$ plane with length $L - z_o$ is characterized by the transmission and reflection parameters T and R. And the other section with length z_o is characterized by T' and R'. We sum up the partial waves due to the repeated reflections and obtain

$$E_{out} = TE + \frac{(1+R)R'TE}{1-RR'} = \frac{(1+R')TE}{1-RR'}$$

Expressions for R,R',T,T' can be obtained by slight modification of equation (3-4) and (3-5). It can be shown by direct substitution that

$$|E_{out}|^2 = |E|^2 \left| \frac{\gamma \cosh\gamma z_o - [\alpha - i(\Delta\beta - \kappa)]\sinh\gamma z_o}{\gamma\cosh\gamma L - (\alpha - i\Delta\beta)\sinh\gamma L} \right|^2$$

The intensity output at z = L is obtained by integrating $|E_{out}|^2$ over z_o (we sum the intensities since spontaneous emissions from different sections are assumed to be incoherent).

$$I(z=L) = \int_0^L |E_{out}|^2 dz_o \qquad (3\text{-}17)$$

Equation (3-17) is plotted in Fig. 3-11 as a function of frequency for various values of αL and $\kappa L = 0.4$. Spectral narrowing is evident from the curves. For $\kappa L = 0.4$ the lowest order longitudinal mode of this device will oscillate at $\Delta\beta L = \pm 2.2$ when $\alpha L = 2.9$. The absolute output powers at $\Delta\beta L = 2.2$ and $\Delta\beta L = -2.2$ are plotted as a function of the gain coefficient αL in Fig. 3-12(a). At each of

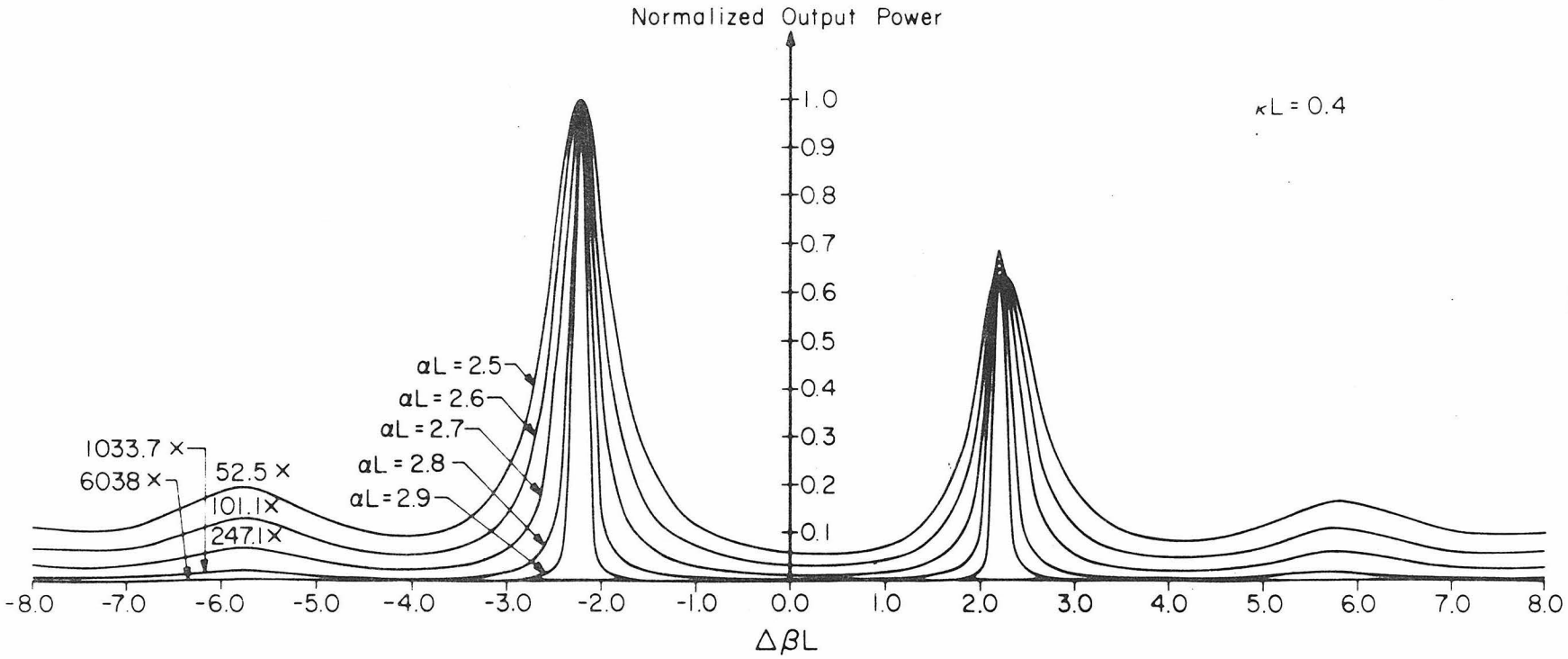

Fig. 3-11 The emission spectrum of amplified spontaneous emission from a periodic waveguide with $\kappa L = 0.4$. The amplitude gain coefficient αL is used as a parameter.

these two $\Delta\beta L$ values the output power increases rapidly as the threshold ($\alpha L = 2.9$) is approached. Although these two modes have equal threshold gains their output powers are not identical. A plot of the spectral width of the peak ($\Delta\beta = -2.2$) below threshold as a function of $1/P_{out}$ is shown in Fig. 3-12(b). It is almost a straight line, implying

$$\delta(\Delta\beta) \propto \frac{1}{P_{out}}$$

a relation common to all amplified spontaneous emission processes. Similar results were also obtained by Chinn and Kelley[25].

If the waveguide gain coefficient exceeds the threshold of oscillation the above analysis is not valid. A nonlinear analysis should be used to include saturation effects.

3-6 Comparison of GaAs Distributed Feedback Lasers and Fabry-Perot Lasers

As discussed in section 3-4 the lowest order longitudinal mode of distributed feedback lasers with large κL lase at $\Delta\beta \sim \pm\kappa$. And since $\beta_o = \pi/\Lambda$ is of the order of 30 μm^{-1} in GaAs, while typical value of κ is $\sim 10^{-2}\,\mu m^{-1}$, so generally speaking a distributed feedback laser oscillates at a frequency

$$\omega \approx \omega_o = \frac{\beta_o c}{n_{eff}} = \frac{\pi c}{n_{eff}\Lambda}$$

or

$$\lambda \approx 2n_{eff}\Lambda \qquad (3\text{-}18)$$

where n_{eff} is the effective index of refraction of the laser mode in the waveguide. If the ℓ-th order corrugation is used for the feedback equation (3-18) is modified to

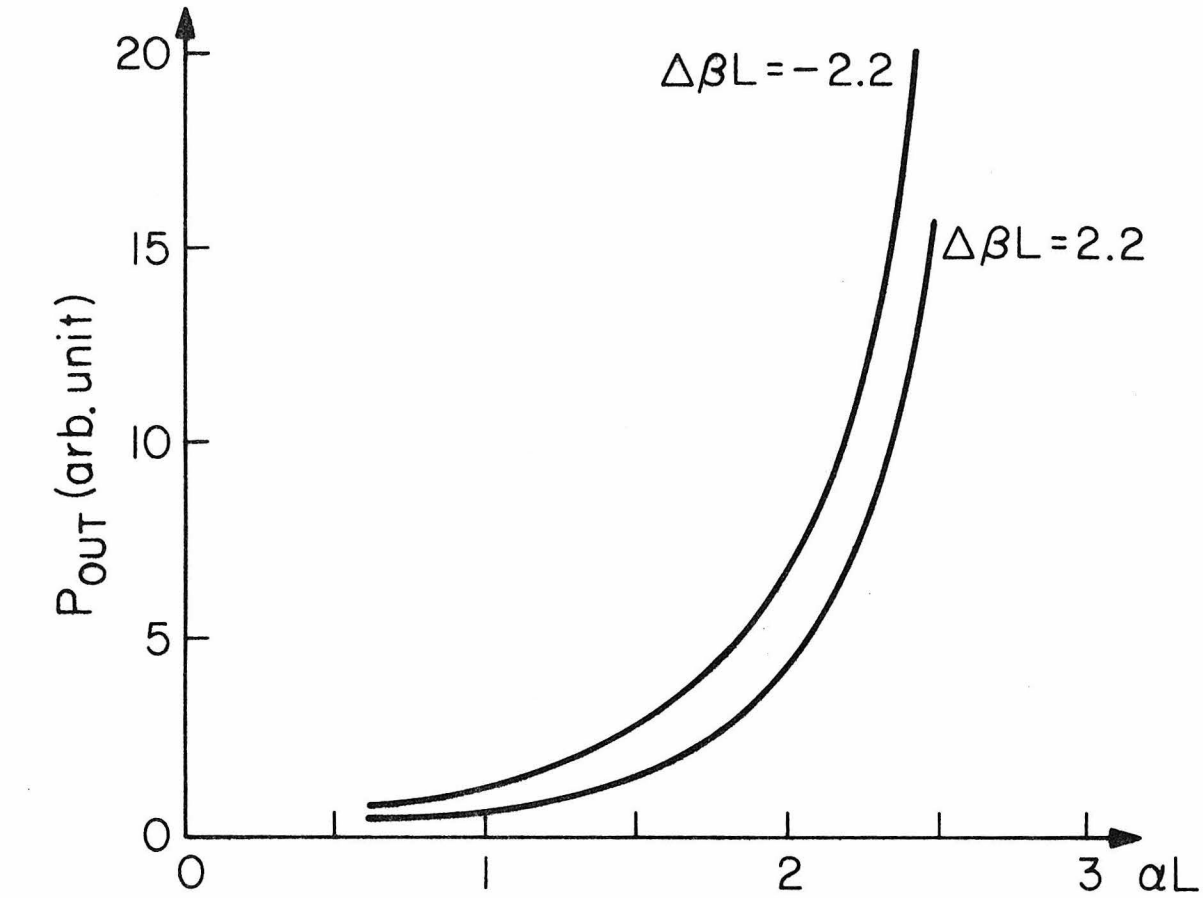

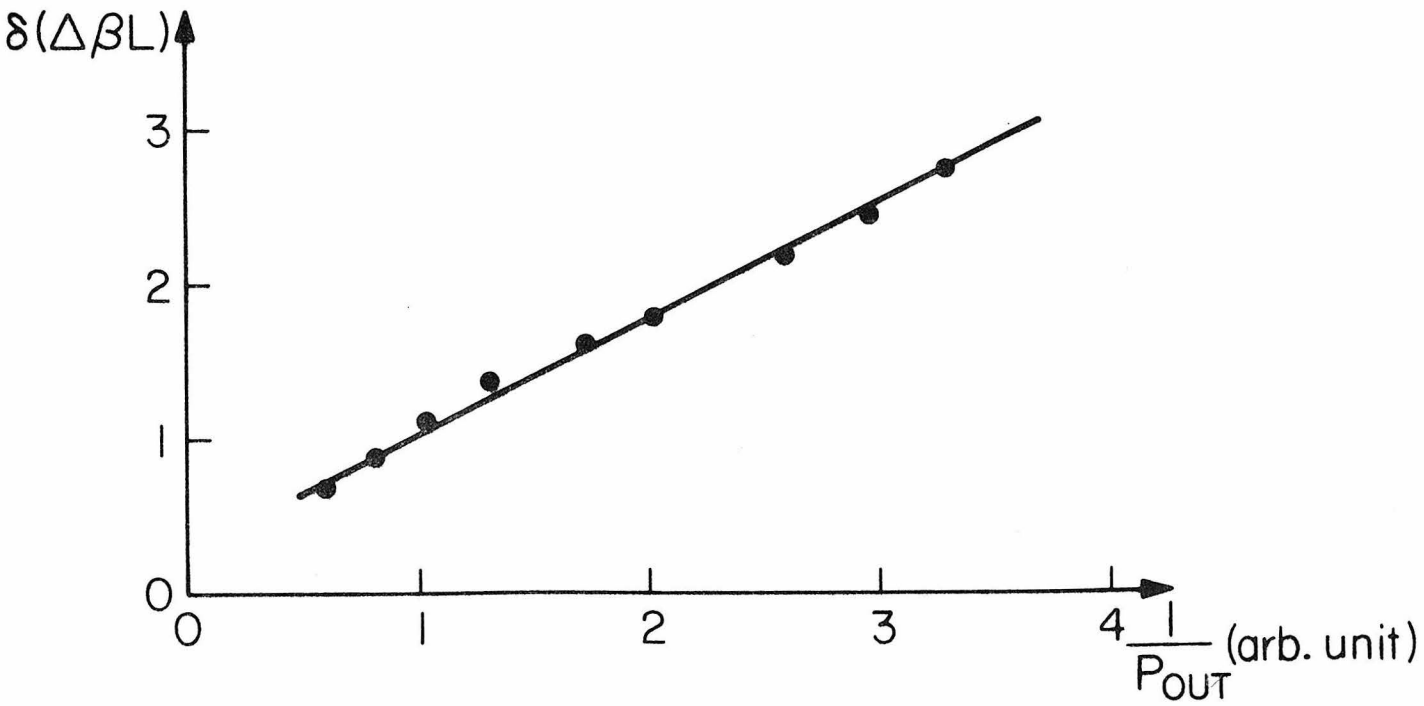

Fig. 3-12 Plots of (a) The dependence of output power on gain
(b) The relation between spectral width and the reciprocal of the output power.

$$\lambda \approx 2n_{eff} \frac{\Lambda}{\ell} \tag{3-19}$$

This is a very simple expression which determines roughly the lasing wavelength once n_{eff} and Λ are known. And it is obvious that one can design a waveguide structure with known n_{eff}, and select a proper Λ for a desired wavelength λ. This is not true in general for ordinary injection lasers. The gain spectrum of GaAs usually spans several hundred angstroms, the cavity is formed by two parallel cleaved crystal planes which provide almost uniform reflectivity over a large frequency range. Hence there is no strong mechanism to provide longitudinal mode discrimination. Usually several modes oscillate simultaneously with comparable thresholds and span typically a spectral region of $\sim$30Å or more. This nonmonochromatic radiation presents a problem in fiber communication systems. In distributed feedback lasers we have a built-in longitudinal mode discrimination so it is not difficult to obtain single mode operation with linewidths less than one angstrom.

Another advantage of distributed feedback lasers over Fabry-Perot GaAs lasers is that the temperature stability of lasing wavelength is improved. The temperature variation of lasing wavelength in distributed feedback lasers is due to the change of the effective index of refraction (n_{eff}) with temperature as evident from equation (3-18). Hence

$$\frac{d\lambda}{dT} = \frac{\lambda}{\left(n_{eff} - \lambda \frac{\partial n_{eff}}{\partial \lambda}\right)} \frac{\partial n_{eff}}{\partial T} \tag{3-20}$$

If we use $\frac{\partial n_{eff}}{\partial T} \approx 3 \times 10^{-4}/\text{deg}$ [26] and $n_{eff} - \lambda \frac{\partial n_{eff}}{\partial \lambda} \approx 4.5$, $\frac{d\lambda}{dT}$ turns out to be ~ 0.58Å/deg. In ordinary GaAs lasers the band gap energy varies with temperature thus causing both the spontaneous emission spectrum and the laser wavelength to shift with temperature. This shift has a rate of ~ 2Å/deg which is about 4 times that of distributed feedback lasers. There is, however, a penalty which accompanies this improved wavelength stability. An ordinary laser can operate at any temperature if threshold is attainable. But in distributed feedback lasers the choice of Λ "clamps" the lasing wavelength for a certain temperature and since the temperature coefficients of λ_{DFB} and the center of gain spectrum are different at some temperatures λ_{DFB} falls outside the gain spectrum completely and no oscillation is possible.

3-7 Design Factors in GaAs Distributed Feedback Lasers

In this section we address ourselves to the problem of designing a GaAs distributed feedback laser. We treat the problem in a general way without going into details of specific structures. First of all we have to specify the desired lasing wavelength λ and the operating temperature T. Next we choose a proper waveguide structure which can be either a homojunction structure, or single heterostructure, or double heterostructure, etc. From the given structure we can calculate the number of guided transverse modes and their respective effective indices of refraction. In order to obtain single mode operation, however, it is desirable to use a single mode waveguide with definite

n_{eff} at λ. The necessary corrugation period Λ is calculated through the equation $\Lambda = \lambda/2n_{eff}$ for fundamental Bragg coupling and $\Lambda = \ell\lambda/2n_{eff}$ for the ℓ-th order coupling. The choice of λ has to be such that at the particular operating temperature the medium can provide sufficiently large gain at that wavelength. The typical photoluminescence spectrum of GaAs is about 150-200Å wide. At 77°K the peak occurs at ∿8450Å and at 300°K it shifts to 8900Å. For temperatures in between, the luminescence peak can be estimated roughly by the formula

$$\lambda(T) \sim [8450 + 2x(T-77)]\text{Å}$$

The luminescence spectrum will change slightly by varying carrier concentrations and dopants. It can also be varied by incorporating into the active region a small amount of Al. As a matter of fact checking the luminescence spectrum is one of the methods of obtaining a rough estimate of the amount of Al in a GaAlAs layer.

For example in GaAs typical numbers at 77°K are λ = 8450Å, $n \sim 3.59$, then Λ = 1177Å is required for ℓ = 1 fundamental operation. This small period is difficult to fabricate and ℓ = 3 is used in most of our experiments, which results in Λ = 3531Å. The corrugation height can be measured by using SEM (scanning electron microscope) pictures. This quantity is then used to calculate the coupling coefficient. From a curve similar to those in Fig. 3-8 we can obtain, given κ, an optimal length for our laser. The laser oscillation threshold can be estimated from

$$\alpha_{th} = \alpha^{o}_{th}(\kappa,L) + \alpha_{bulk}$$

where $\alpha_{th}^{o}(\kappa,L)$ is that found by solving the eigenvalue equation (3-10) $F(\alpha,\Delta\beta) = 0$ and α_{bulk} is the bulk material loss coefficient at the lasing wavelength.

If a third order corrugation is used there exist losses due to the coupling of the guided laser mode to the unguided radiation modes through the first and the second order Bragg scattering processes. These losses can be represented by a distributed loss coefficient α_{rad}[27,28] which must be added to the other losses in the medium. The laser threshold condition in this case becomes

$$\alpha_{th} = \alpha_{th}^{o}(\kappa,L) + \alpha_{bulk} + \alpha_{rad} \qquad (3\text{-}21)$$

Typical value of α_{rad} for a third order corrugation with tooth height 500Å is $\sim 10 cm^{-1}$.

In most of our optical pumping experiments we start out with slabs of GaAs-GaAlAs waveguides. Through photoluminescence measurements we determine the peak of the gain spectrum. By making Fabry-Perot lasers from part of the sample and measuring the longitudinal mode spacings we obtain a good estimate of n_{eff}. The corrugation period Λ is then determined from the condition

$$\Lambda = \frac{\lambda}{2n_{eff}}$$

where λ corresponds to the central wavelength of the luminescence spectrum.

3-8 Optically Pumped GaAs Distributed Feedback Lasers

Optical excitation is a very convenient way and a very powerful tool for studying the spontaneous and stimulated emission processes in semiconductors. This method of pumping obviates the need for electrical contacts which greatly simplifies the sample preparation and makes it possible to explore new materials and structures without first solving the contact problem. Furthermore, it is nondestructive in the sense that sample surface will not be damaged unless excessive optical power density is used. In this section we shall describe some of the experiments on optically pumped GaAs distributed feedback lasers.

The first attempt to demonstrate distributed feedback lasing action in GaAs was done by optically pumping a slab of a GaAs crystal with periodic surface corrugation. A schematic drawing of the laser is shown in Fig. 3-13. The GaAs wafer was n-type (Si doped) with a carrier concentration of about $10^{18}cm^{-3}$. The top surface (100 plane) was polished and chemically etched. The corrugation was produced by ion milling through a photoresist mask generated by holographic photolithography as will be described in Chapter 5. The height of the grooves was estimated from the SEM picture to be around 500Å. The period Λ was 0.35 μm which corresponds to $\ell = 3$ in the Bragg condition $2\beta = \ell \frac{2\pi}{\Lambda}$ where β is the propagation constant of the guided mode.

The experimental set-up is shown in Fig. 3-14. The gain was provided by optical pumping using a Q-switched ruby laser ($\lambda \sim 0.6943$ μm). Each individual pumping pulse had a duration of ∿20 nsec and the peak power was attenuated to ∿10 KW. A cylindrical lens was used to pump a

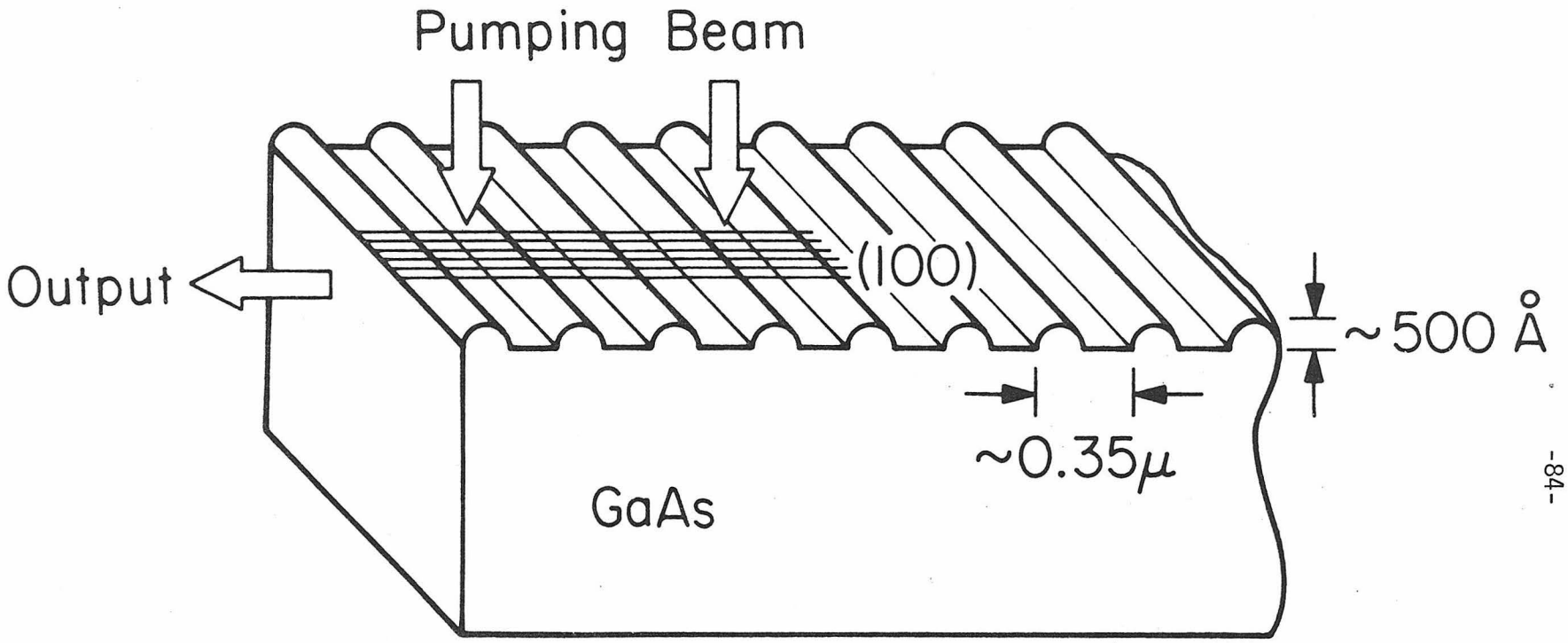

Fig. 3-13 Schematic structure of a GaAs distributed feedback laser.

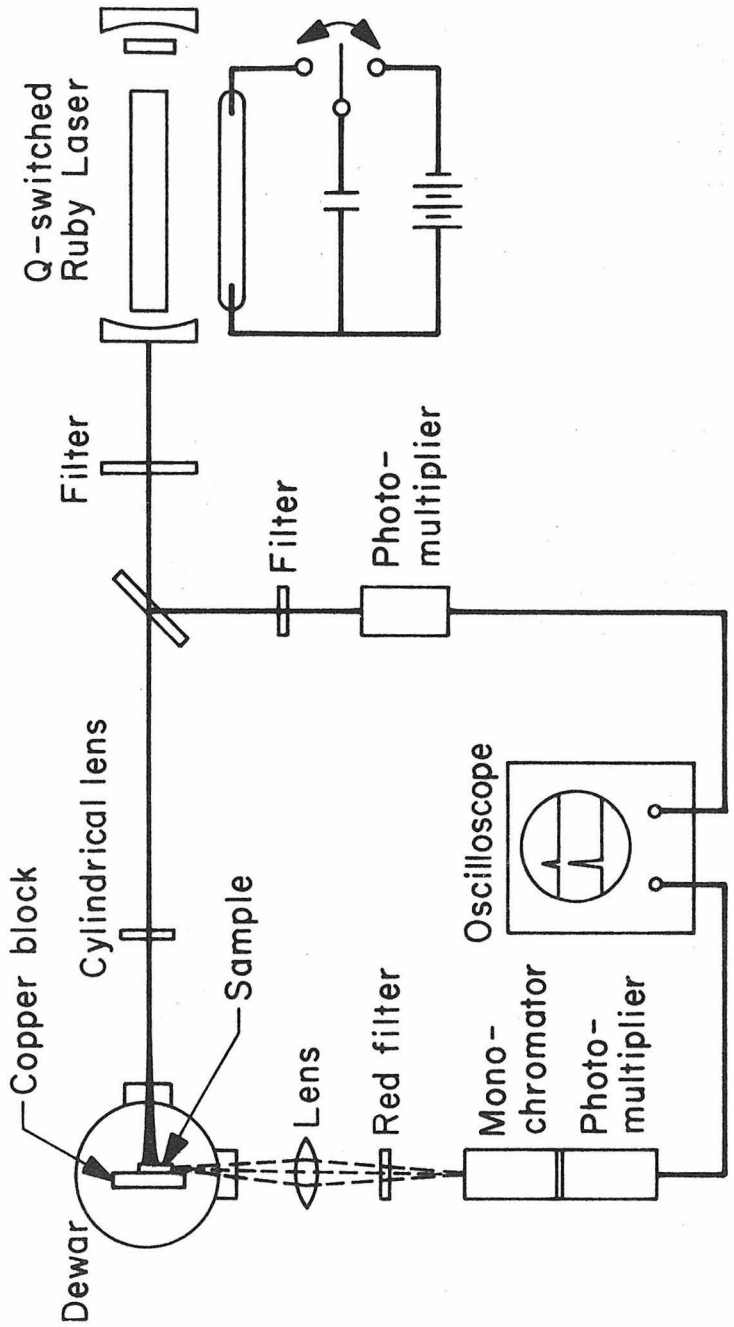

Fig. 3-14 Experimental set-up for optical excitation of GaAs distributed feedback surface lasers.

rectangular strip of 3 x 0.5 mm. Samples were attached to a copper block heat sink with vacuum grease and mounted inside a liquid nitrogen dewar. Special care was taken to make sure that the pumping beam did not fall across the whole length of the sample. Also the output face of the crystal was lapped so that it was not parallel to the grooves and to the other end face. This was done to minimize the reflection feedback. The system was carefully aligned with a He-Ne laser. The pumping beam passed through the front window of the dewar and struck the sample surface perpendicularly. The output from the GaAs sample passed through the side window and was collected by a lens and fed into a monochromator. The signal was subsequently amplified by a photomultiplier (S-1) and displayed on a memory scope. The pumping pulse was also monitored on the scope.

The oscillation threshold of such lasers at 77°K was found to be $\sim 2 \times 10^5 W/cm^2$. A typical emission spectrum of a sample excited above threshold is shown in Fig. 3-15. Stimulated emission is indicated by the narrow resolution limited peak. Also shown in the same figure is the spectrum of a sample without corrugation under similar pumping conditions. This sample displays only the broad ($\sim 180\text{Å}$) spontaneous emission feature. The stimulated emission peak at $\lambda = 0.832\ \mu m$ corresponds, using equation (3-19), to an index of refraction $n = 3.6$ at 77°K for GaAs.

Figure 3-16 shows plots of the emission power as a function of the pumping intensity for a corrugated and an uncorrugated sample. The "break" in the curve of the corrugated sample near $2.5 \times 10^5 W/cm^2$ coincides well with the first appearance of the narrow spectral peak in

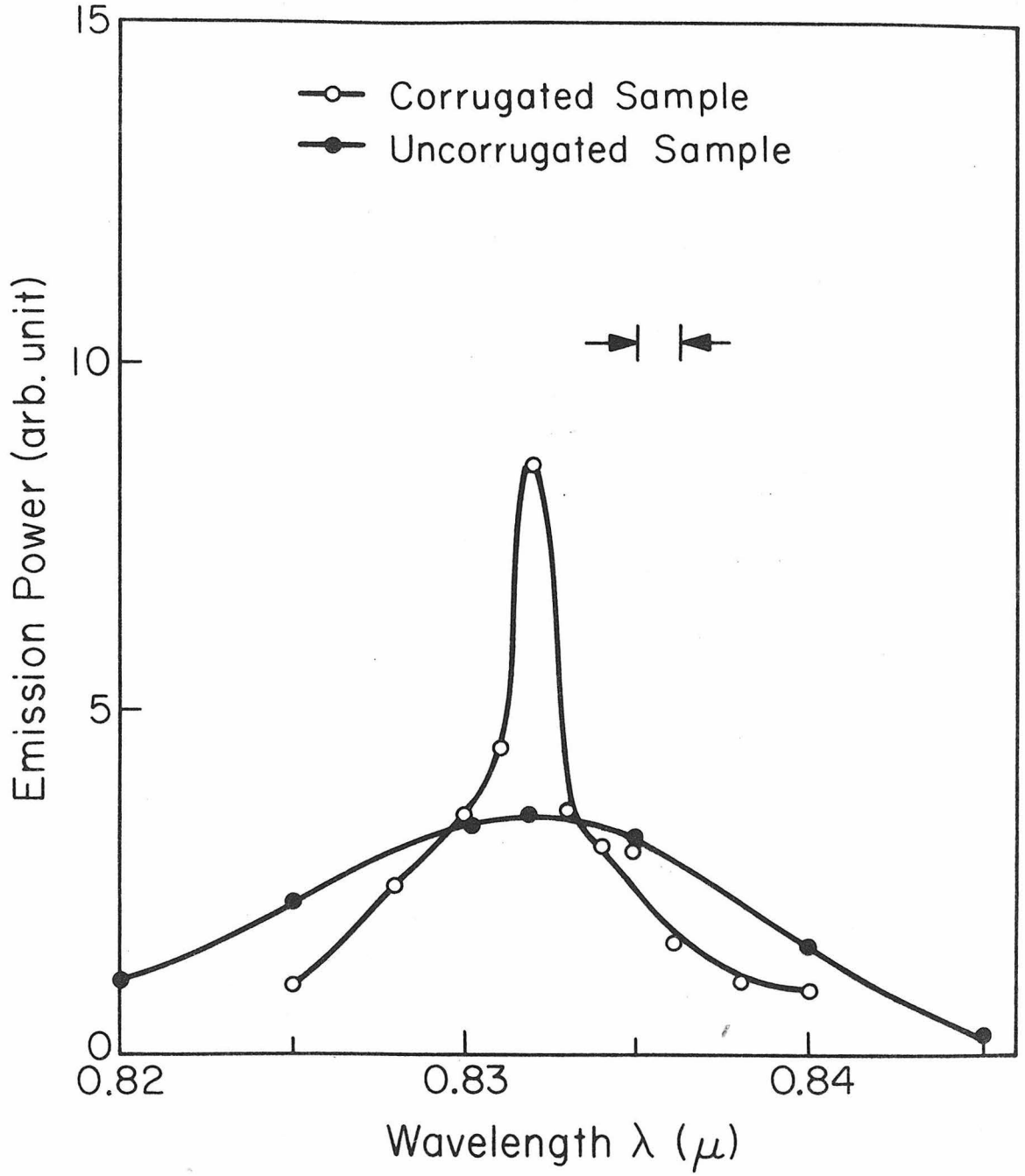

Fig. 3-15 The emission spectrum of a corrugated and an uncorrugated sample. Pumping intensity is 5×10^5 W/cm^2.

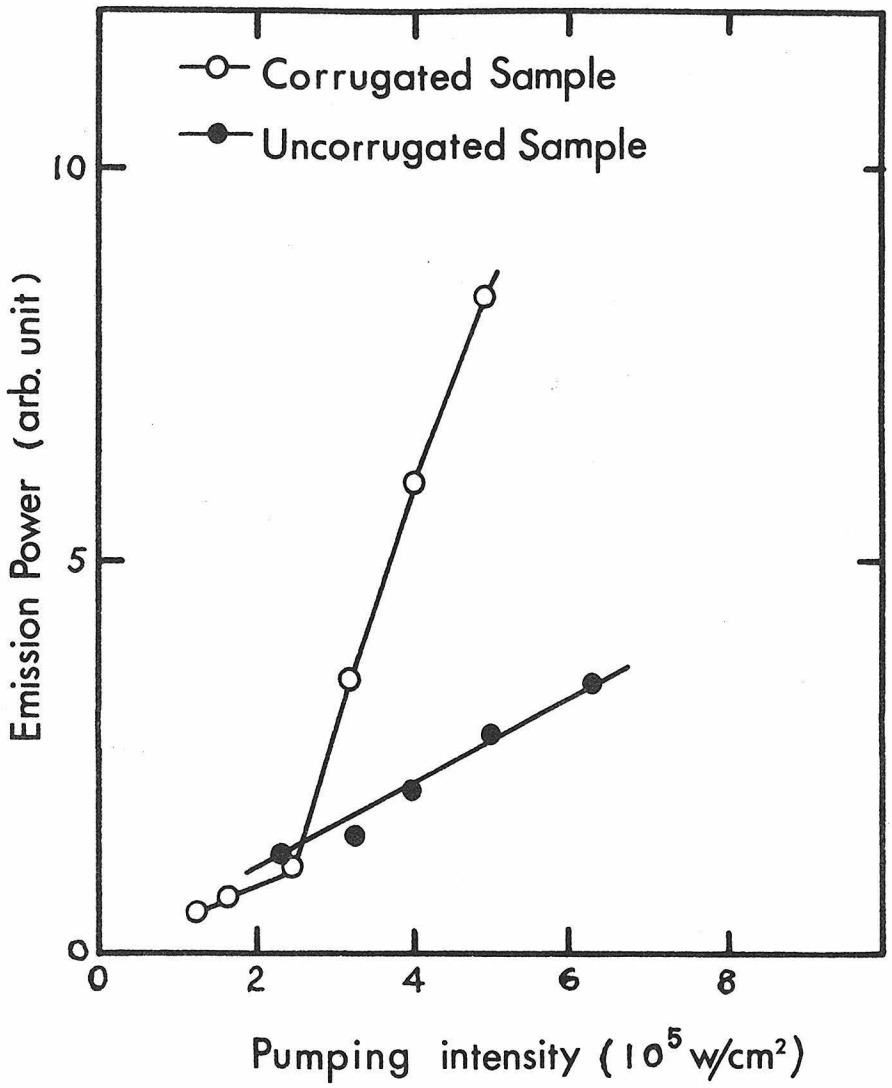

Fig. 3-16 Emission power as a function of pumping intensity at λ = 0.832 μm.

Fig. 3-15. The characteristics of the uncorrugated sample, however, remain linear up to the highest pumping power employed. For pumping power exceeding $10^6 W/cm^2$ surface damage was found on both corrugated and uncorrugated samples.

This very first experiment demonstrated that a GaAs crystal with surface corrugation can be made to lase if enough gain is provided. The threshold, however, was very high. This is largely due to poor optical confinement. In a bulk crystal the optical confinement comes from the "inverted layer" which is not a strong effect. The threshold pumping level is expected, as in the case of injection lasers, to depend strongly on the optical confinement. Realizing this we repeated the experiment with epitaxial GaAs dielectric waveguides. Two different types of dielectric waveguides, illustrated by Fig. 3-17, were used in the experiment. The first structure consisted of an epitaxial GaAs layer which in different experiments varied between 1 and 3 μm in thickness with a carrier concentration of $n \sim 6 \times 10^{16} cm^{-3}$. The substrate was a GaAs crystal with $n \sim 2 \times 10^{18} cm^{-3}$. Due to the carrier concentration difference the epitaxial layer has a larger index of refraction than the substrate and the condition for dielectric waveguiding are thus satisfied. The second structure consisted of GaAs and $Ga_{0.7}Al_{0.3}As$ double layers on a GaAs substrate. The larger the Al concentration, the smaller the index of refraction of the layer. The surface corrugations were produced as described above. Due to the improved confinement, the pumping threshold intensity was reduced by 10X and a different pumping source could be used. This is shown in Fig. 3-18. A repetitively pulsed

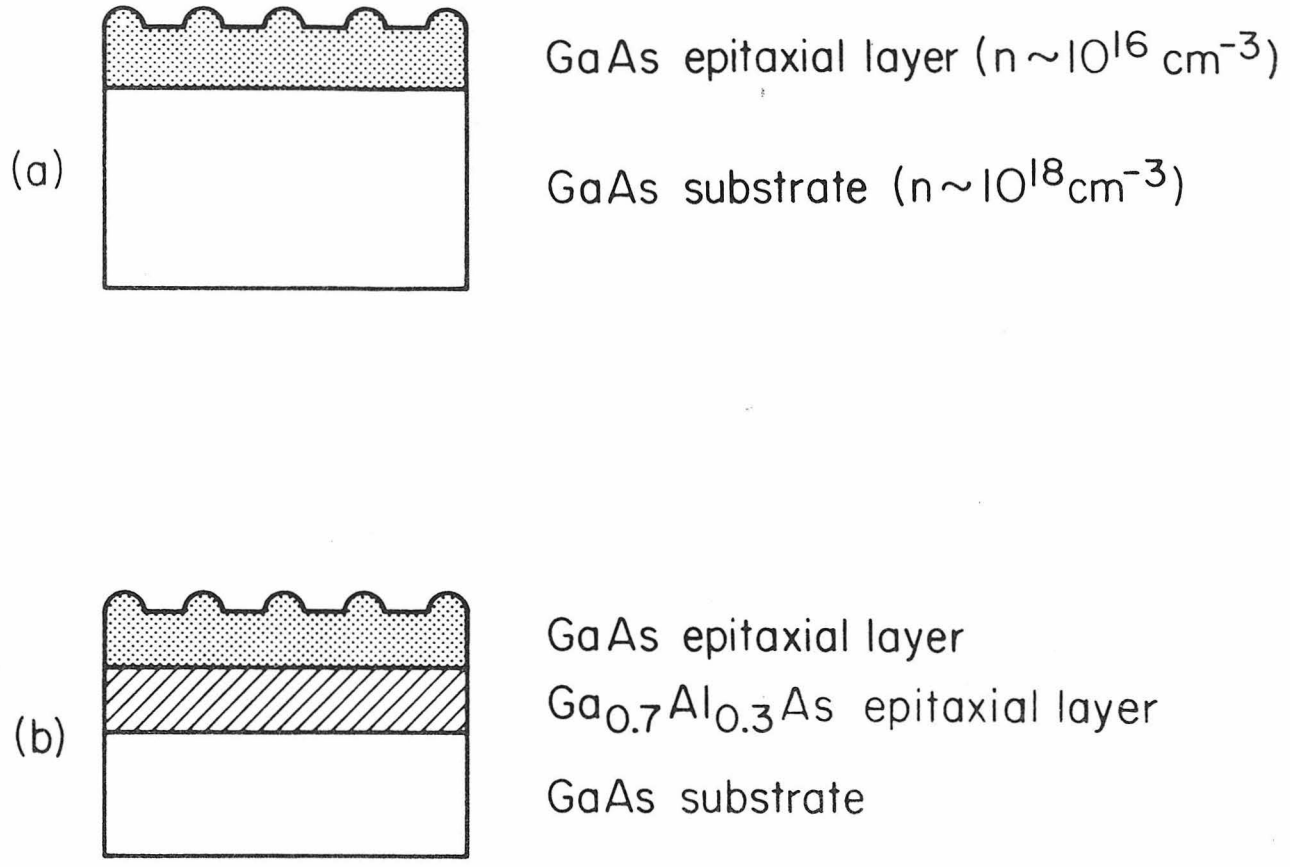

Fig. 3-17 Cross sections of GaAs waveguide structure distributed feedback lasers.

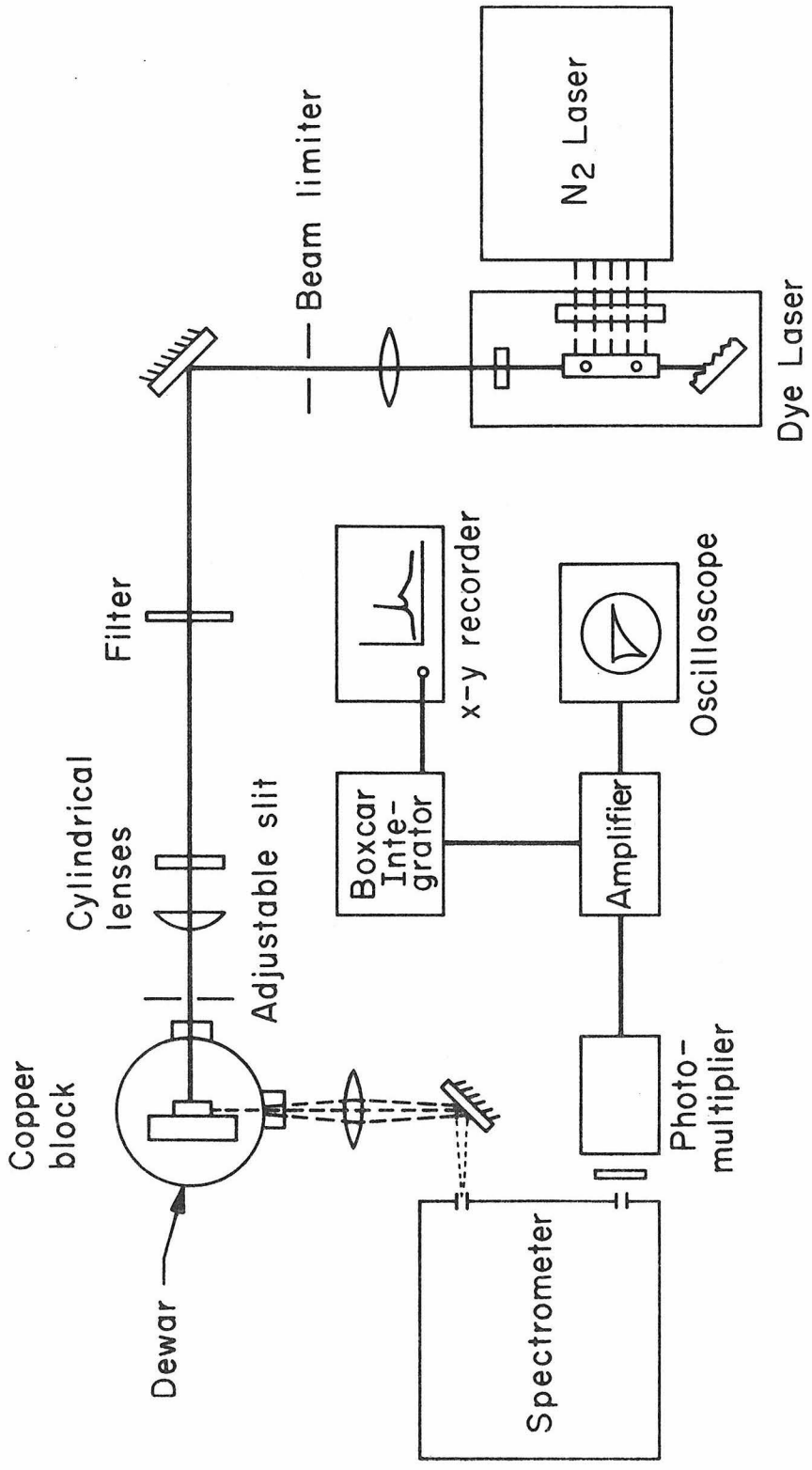

Fig. 3-18 The optical pumping set-up using an N_2-laser pumped dye laser.

nitrogen laser pumped a dye laser (Rhodamine B) whose output tuned to $\sim$0.63 μm was used to pump the GaAs dielectric waveguide. Each individual pumping pulse had a duration of $\sim$7 nsec and a peak power of up to 2 KW. Cylindrical lenses and an adjustable slit were used to pump a rectangular strip 0.3 mm wide and of a variable length. The output was collected by a lens and guided into a spectrometer whose acceptance wavelength was scanned to record the emission spectrum.

When the first sample was pumped the output power from the corrugated region was about two orders of magnitude smaller than that from the uncorrugated region of the same wafer. It was found that ion milling introduced defects in the GaAs layer which reduces the carrier recombination efficiency drastically. Since the laser emission was restricted by dielectric waveguiding to the vicinity of the surface the effect of this damage on threshold was severe. Annealing in a hydrogen atmosphere at 450°C for $\sim$30 min removed most of the defects and made lasing possible at threshold pumping intensity $\sim 10^4 W/cm^2$. A typical output spectrum from these waveguide lasers is shown in Fig. 3-19 displaying both the spontaneous and the stimulated emission peaks. The stimulated emission peak was found to be stable against excitation level while the spontaneous emission peak moved toward longer wavelength as the excitation level was increased.

A number of waveguides were prepared with different corrugation periods. The measured oscillation wavelengths were plotted against the corrugation period Λ in Fig. 3-20. The straight line is a theoretical plot of the equation

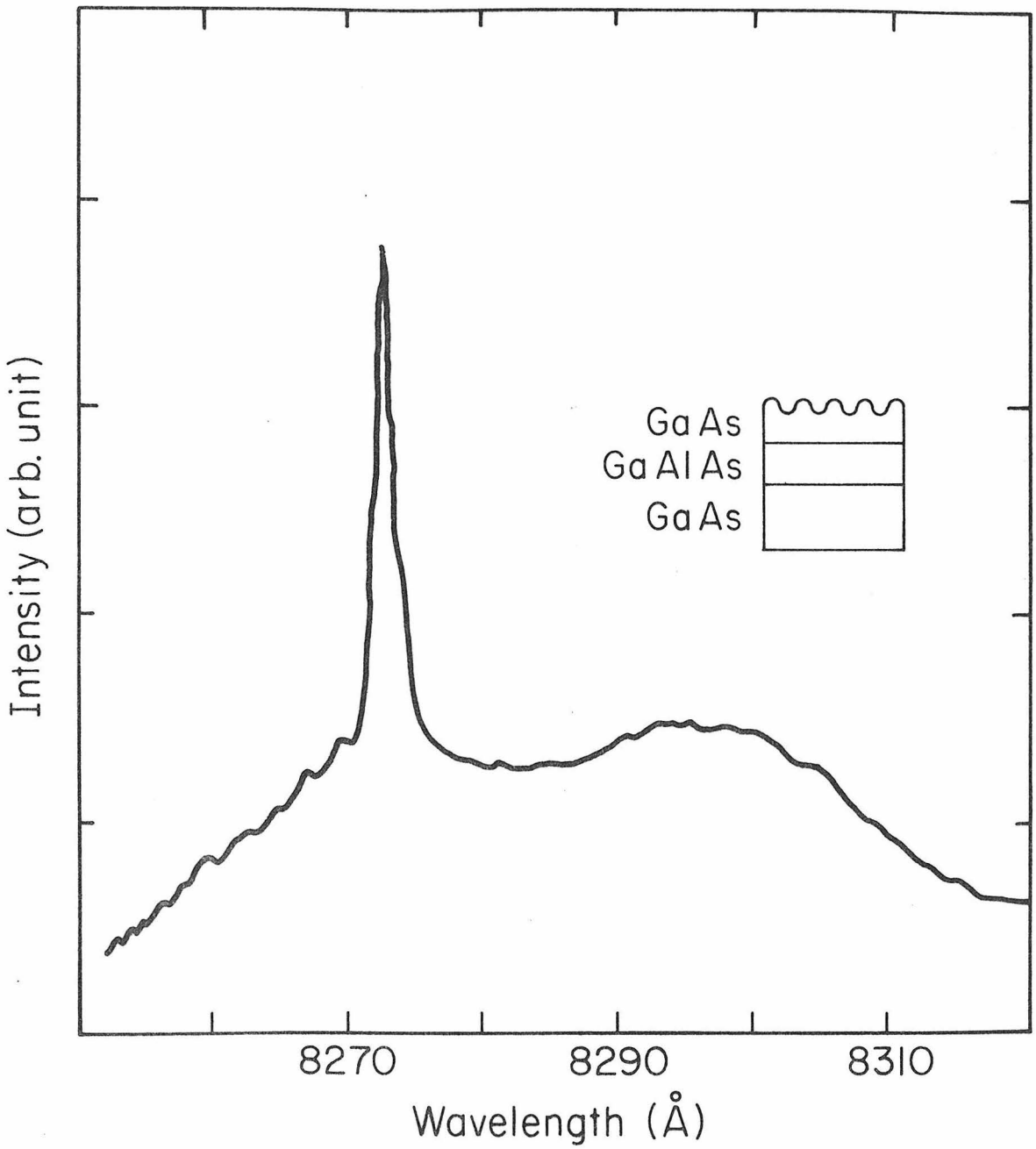

Fig. 3-19 Emission spectrum of an optically pumped waveguide laser with surface corrugation.

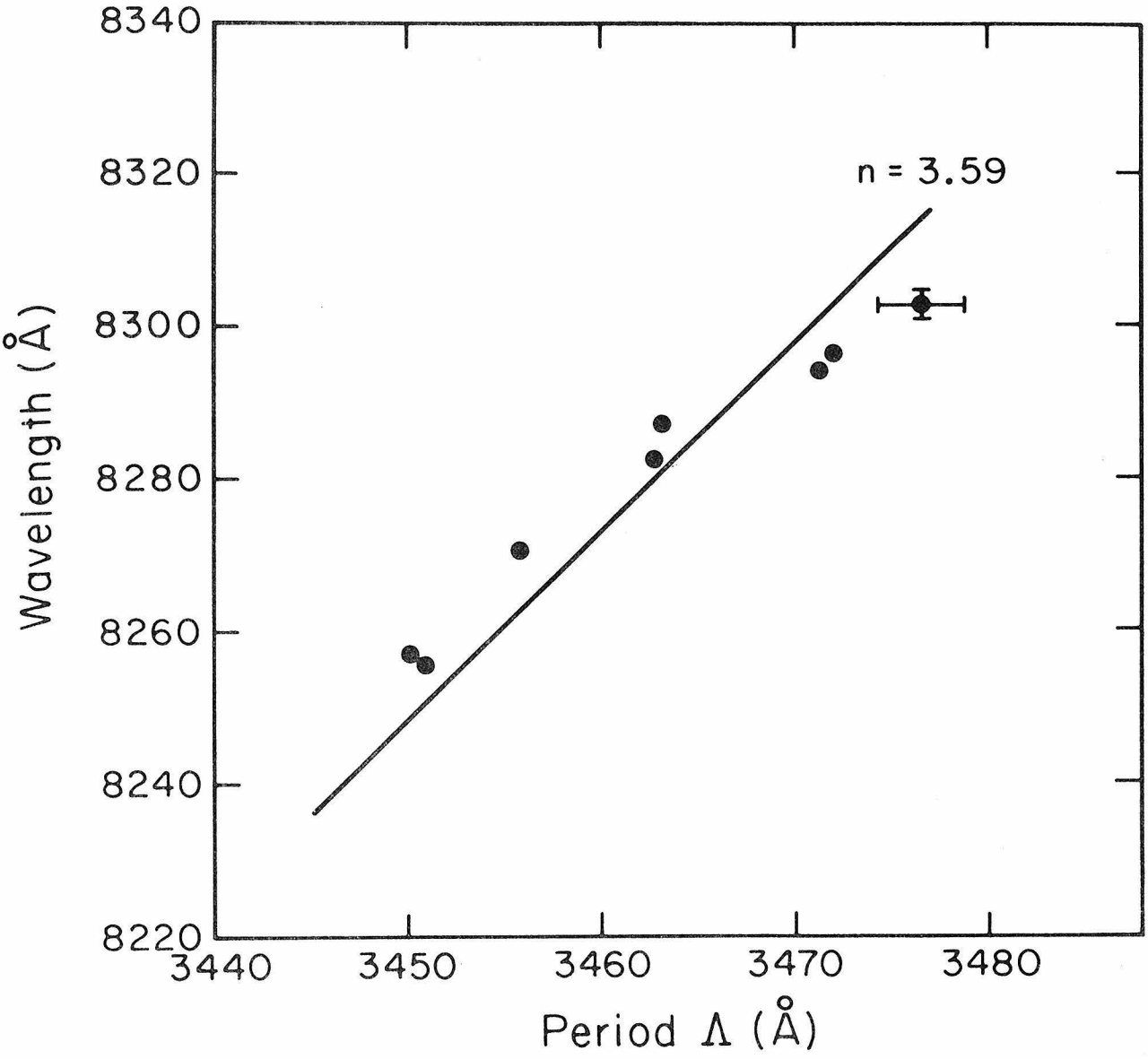

Fig. 3-20 Oscillation wavelength vs. period of corrugation.

$$\lambda = \frac{2}{3} n_{eff} \Lambda$$

with $n_{eff} = 3.59$. It is seen that a tuning range of 45Å was spanned by varying the corrugation period from 3450Å to 3476Å. This is a clear indication that the laser feedback is indeed caused by the corrugation. And the corrugation acts as a built-in grating filter leading to a stabilization of the output wavelength.

As a check on the theory we calculated the coupling constant κ for one of the samples and determined it to be $\sim 1.93\ cm^{-1}$. The laser threshold was measured for various pumping lengths of the same waveguide. The result is shown in Fig. 3-21. The solid curve is a plot of equation (3-21) using the data of this sample with $\alpha_{bulk} + \alpha_{rad} \sim 15\ cm^{-1}$ as determined by experiments. This aspect of the experiment is described in Chapter 5. The fair agreement between the experimental results and the theoretical curve in Fig. 3-21 lends support to the existence of distributed feedback action in this sample.

GaAs waveguides with a corrugation period of 0.115 μm were fabricated and pumped optically. This period corresponds to the fundamental ($\ell = 1$) Bragg reflection in equation (3-19). Single mode as well as multi-longitudinal mode oscillation were observed at different pumping levels and pumping lengths as shown in Fig. 3-22. In (b) the measured longitudinal mode spacing $\Delta\lambda$ is ~ 1Å which agrees with the theoretical value calculated from

$$\Delta\lambda \simeq \frac{\lambda}{2L(n - \lambda \frac{\partial n}{\partial \lambda})}$$

where λ is the vacuum oscillation wavelength and L is the laser

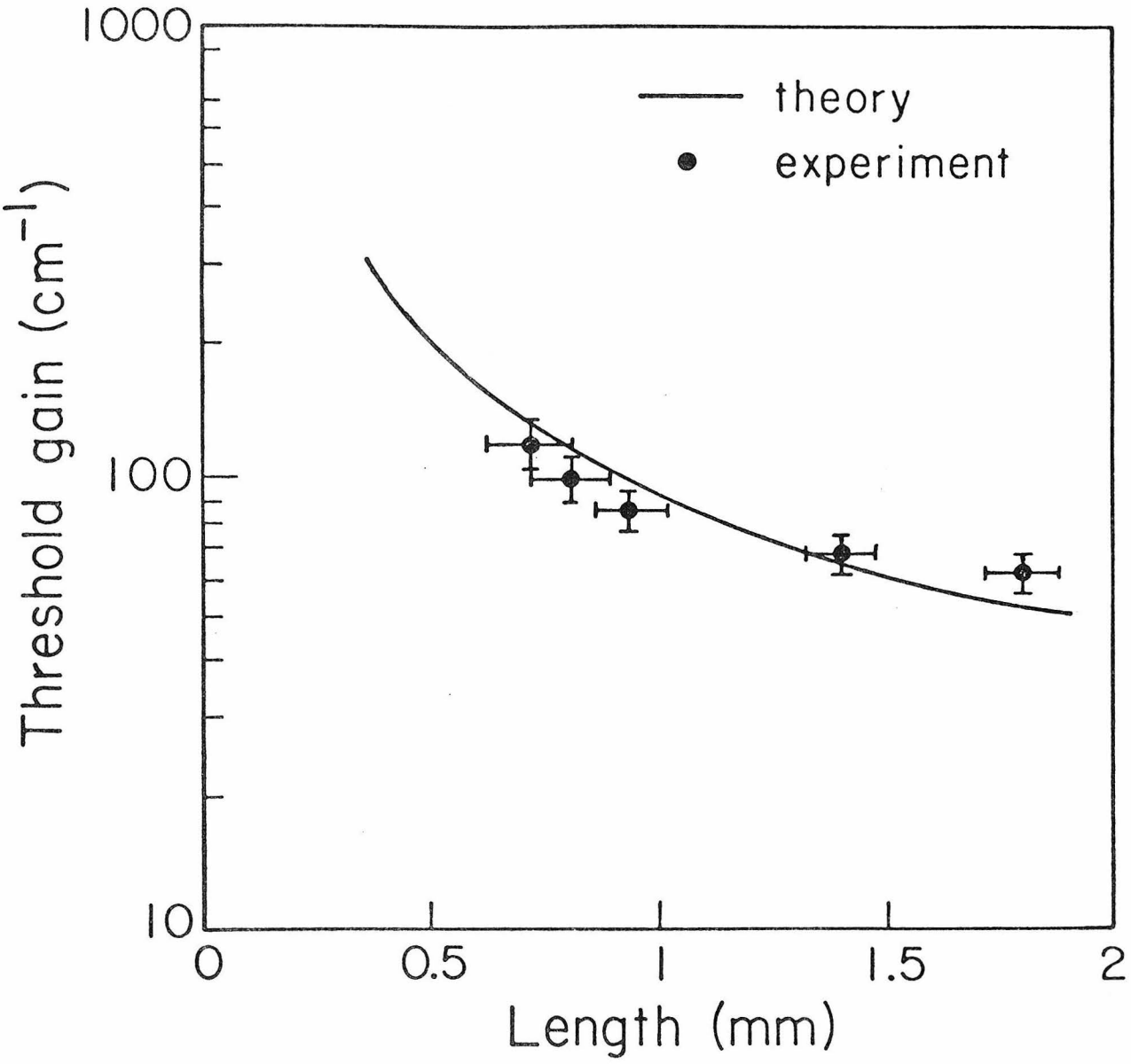

Fig. 3-21 Threshold gain of a distributed feedback laser plotted against the laser length.

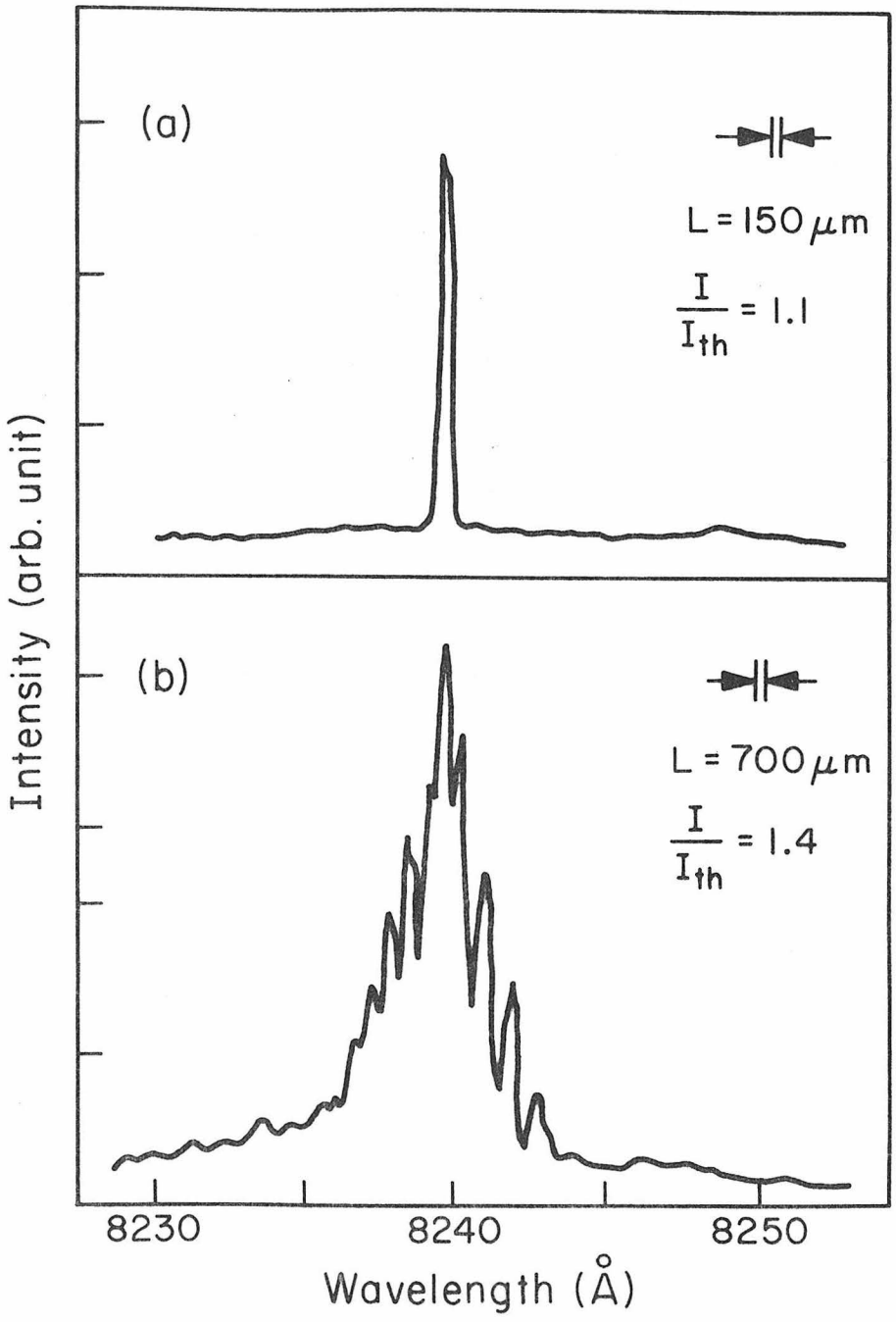

Fig. 3-22 Oscillation spectrum of GaAs distributed feedback laser with fundamental corrugation $\Lambda \sim 0.115$ μm.

length $\sim$ 700 μm in our example. The use of fundamental corrugation was expected to reduce the radiation loss and to increase the magnitude of coupling constant (as compared to the 3rd order corrugation with the same corrugation height). The expected reduction in threshold was not realized, however, in our experiment. The threshold pumping intensity was comparable to that obtained with a 3rd order grating. This is believed to be due to the fact that the quality of the 0.115 μm corrugation was not as good as that of the 0.35 μm corrugation. In fact it was found difficult to produce a 0.115 μm corrugation with tooth height larger than 700Å while for 0.35 μm corrugation we can easily fabricate tooth heights larger than 1500Å. This point will be considered further in Chapter 5.

3-9 GaAs-GaAlAs Distributed Feedback Injection Lasers

Although optical pumping is convenient in laboratory studies, it is not practical in actual applications. Since the technology of ordinary GaAs injection lasers has been very successful it was felt that GaAs distributed feedback lasers with electrical injection could also be fabricated. A theoretical analysis by Nakamura and Yariv[18] of GaAs injection lasers with a corrugated interface indicated the possibility of a large reduction of the threshold current density as well as of frequency and mode discrimination. We thus started experimenting with the fabrication of a double heterostructure distributed feedback laser diode.

Figure 3-23 shows a schematic drawing of a double-heterostructure GaAs laser with internal corrugations. The fabrication process went as

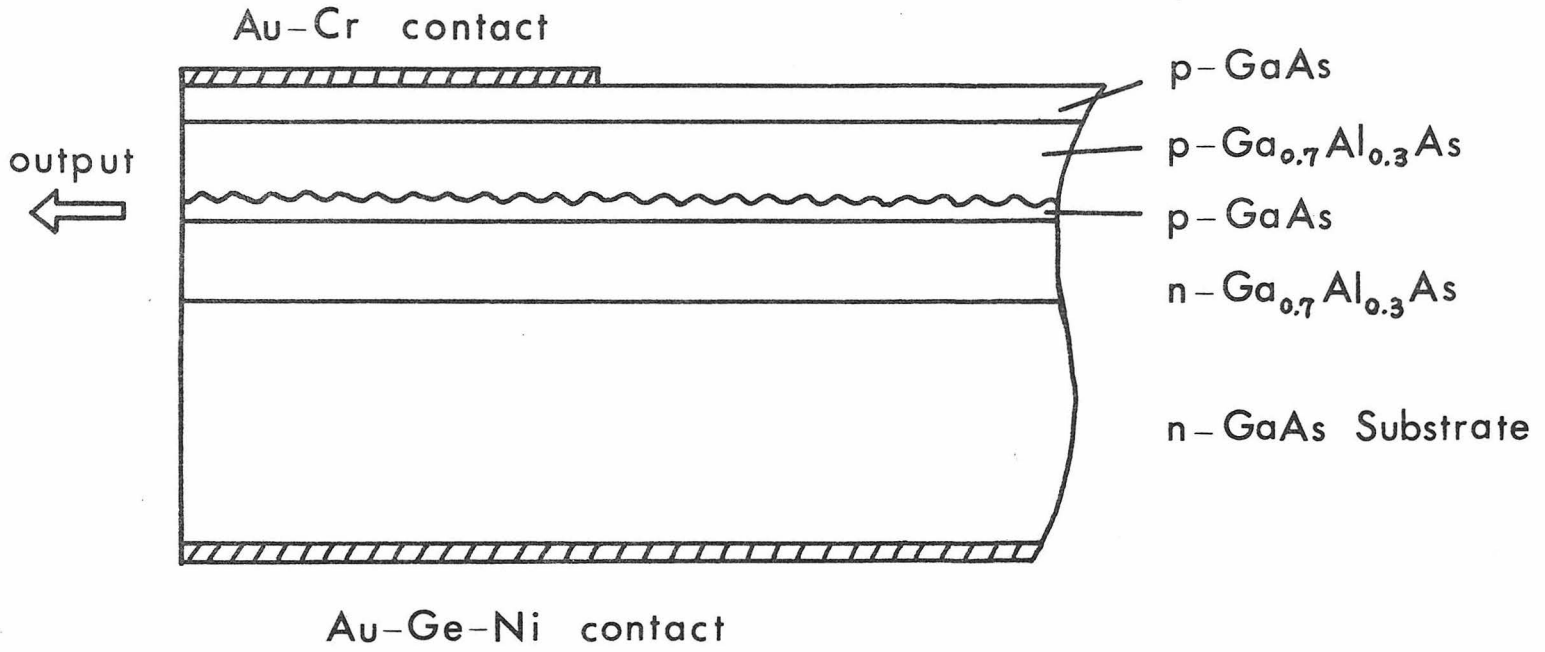

Fig. 3-23 Cross section of a GaAs-GaAlAs double-heterostructure distributed feedback laser diode.

follows. An n-$Ga_{0.7}Al_{0.3}As$ layer ($\sim$ 4 μm) doped with Sn and a p-GaAs active layer ($\sim$ 1.5 μm) doped with Ge were grown on an n-GaAs substrate by liquid phase epitaxy. The process is then interrupted for the fabrication of corrugations. The thickness of the active layer was etched down to 0.5-1.3 μm before fabricating corrugations with a period of $\sim$0.34 μm and a depth of $\sim$900Å. Next a p-$Ga_{0.7}Al_{0.3}As$ layer ($\sim$ 3 μm) and a p-GaAs layer ($\sim$ 1 μm), both doped with Ge, were grown on the corrugated surface of the p-GaAs layer by liquid phase epitaxy. Special care was taken in this step to prevent the meltback of the corrugated surface during the epitaxial growth to be described in Chapter 5. The laser had a mesa-stripe geometry so that the current injection was limited to a rectangular region. The width of the stripe was $\sim$50 μm. Metallic contacts to the diodes were made by evaporating Cr and Au on the p-side and Au-Ge-Ni on the n-side. The length of the Au-Cr contact was varied from 150 to 700 μm. A lossy unpumped waveguide with a length 2.5-3 mm was contiguous to the current injecting area. This was done in order to minimize the optical feedback from the end face. The output was taken from the front face as indicated in Fig. 3-23.

A pulser which provided current pulses of $\sim$50 nsec duration with variable repetition rates was used. The diode characteristics were measured under various temperatures. A typical spectrum from these lasers is shown in Fig. 3-24. The corrugation period is 3416Å and the threshold current density is 9 KA/cm^2. The output spectrum consists of two main components . The spontaneous emission, which has a broad peak centered around 8135Å and, at injection current above threshold (2.6A),

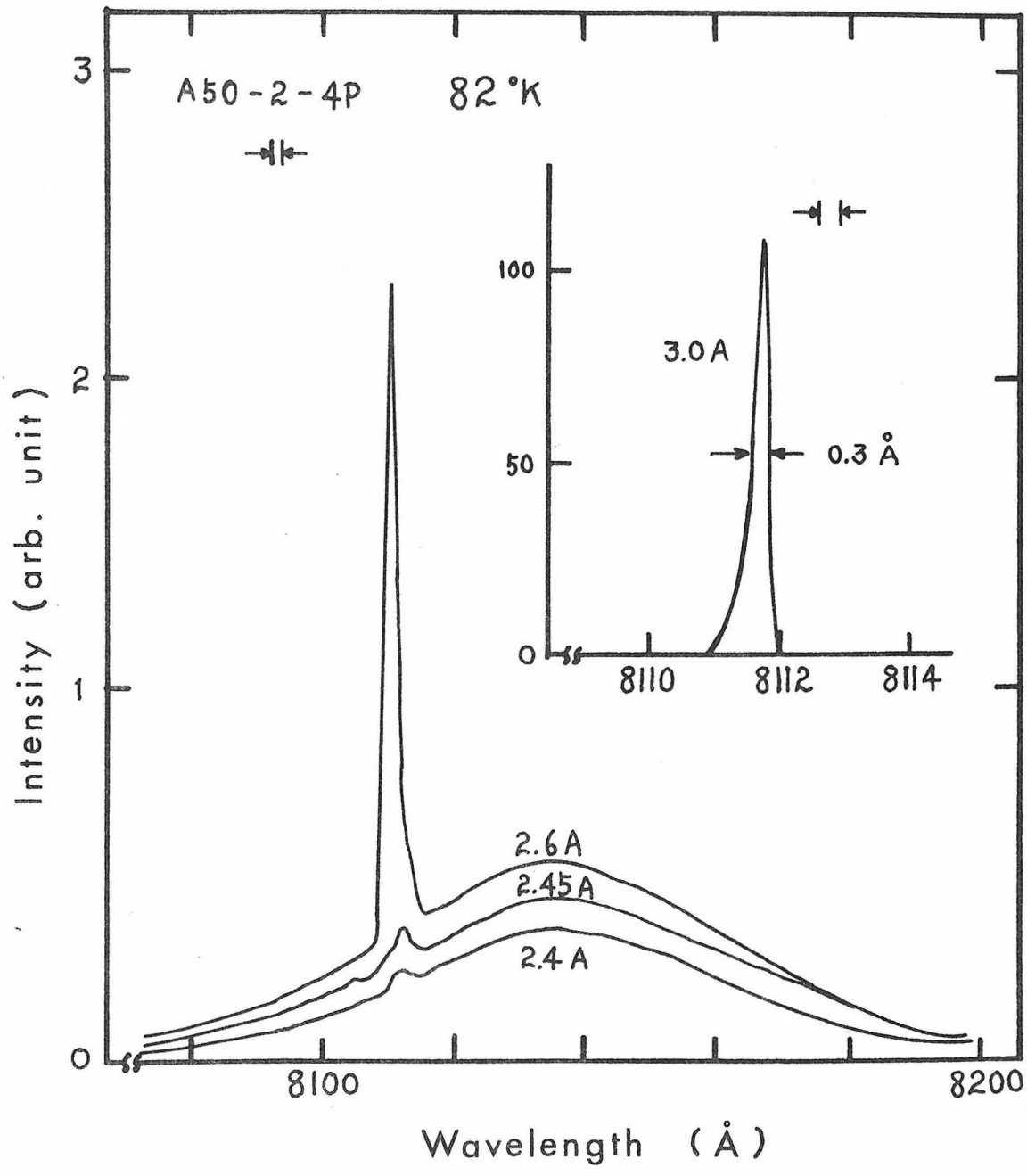

Fig. 3-24 The emission spectra of a typical laser with a corrugation period of 3416Å and a corrugation height of 900Å.

a narrow peak at 8112Å due to stimulated emission. The line width of the stimulated emission is usually less than 1Å. From the lasing wavelength and the period we calculated the effective index of refraction for the lasing mode in our diode structure to be ∿3.56. The inset of Fig. 3-24 shows the detail of the stimulated emission peak. It shows that the diode lased in a single longitudinal mode whose wavelength was stable against the change of excitation level. The laser output was polarized with the electric field parallel to the junction plane.

Lasers in which the length of the unexcited waveguide section was less than 1 mm long exhibited the coexistence of two types of laser oscillation. In one of these, the feedback was due to the corrugation. In the other the feedback was due to the two end faces. These two oscillation spectra are separable by their temperature dependence as was discussed in section 3-6. When the unexcited waveguide length exceeded 2 mm no effect of the end face was observed and the laser spectrum became very simple.

The lowest threshold obtained in this kind of laser was ∿ 2.5 kA/cm^2 at 80°K. It was found that the surface damage caused by ion-milling severely reduced the radiative recombination efficiency of the carriers in the active region. This caused the threshold of this type of laser to become too high for oscillation at the higher temperatures. This problem was alleviated somewhat by using chemical etching for fabricating rather than ion etching the corrugations. We were then able to operate lasers at lower thresholds and at temperatures up to

$\sim$ 145°K. Figure 3-25 shows the lasing wavelength as a function of temperature for both distributed feedback and Fabry-Perot lasers. It is seen that the distributed feedback lasing wavelength shifts at a rate of 0.5Å/degree and that of the Fabry-Perot lasers shifts $\sim$ 2Å/degree which agrees well with the results given in section 3-6.

The improvements in laser performance which resulted from chemical etching were not sufficient to obtain room temperature operation. This is believed due to the large number of nonradiative recombination centers introduced by the etching. This problem was solved, partially, by adopting a separate-confinement heterostructure (SCH). A schematic drawing of the cross section of a laser diode is shown in Fig. 3-26. The first two layers were grown in a manner similar to that of double-heterostructure. The gratings were not fabricated on the p-GaAs layer, instead two additional layers were grown directly, one was a p-$Ga_{0.83}Al_{0.07}As$ layer ($\sim$ 0.1 μm) and the other is a p-$Ga_{0.93}Al_{0.07}As$ layer ($\sim$ 0.2 μm). The corrugation was fabricated on the last mentioned layer. This was followed by a layer of p-$Ga_{0.7}Al_{0.3}As$ layer ($\sim$ 2 μm) and a layer of p-GaAs ($\sim$ 1 μm). In this structure the electrons injected from the n-$Ga_{0.7}Al_{0.3}As$ layer "see" a potential barrier presented by the p-$Ga_{0.83}Al_{0.17}As$ layer and thus are prevented from reaching the corrugated region where nonradiative recombination centers exist. The thickness ($\sim$ 0.1 μm) of this layer is too small, however, to affect the confinement so that the wave extends and "sees" the corrugation. The optical mode confinement is sketched on the left side of Fig. 3-26. The need for the p-$Ga_{0.93}Al_{0.07}As$ layer is due to the fact that the p-$Ga_{0.83}Al_{0.17}As$ layer oxidizes when exposed to air

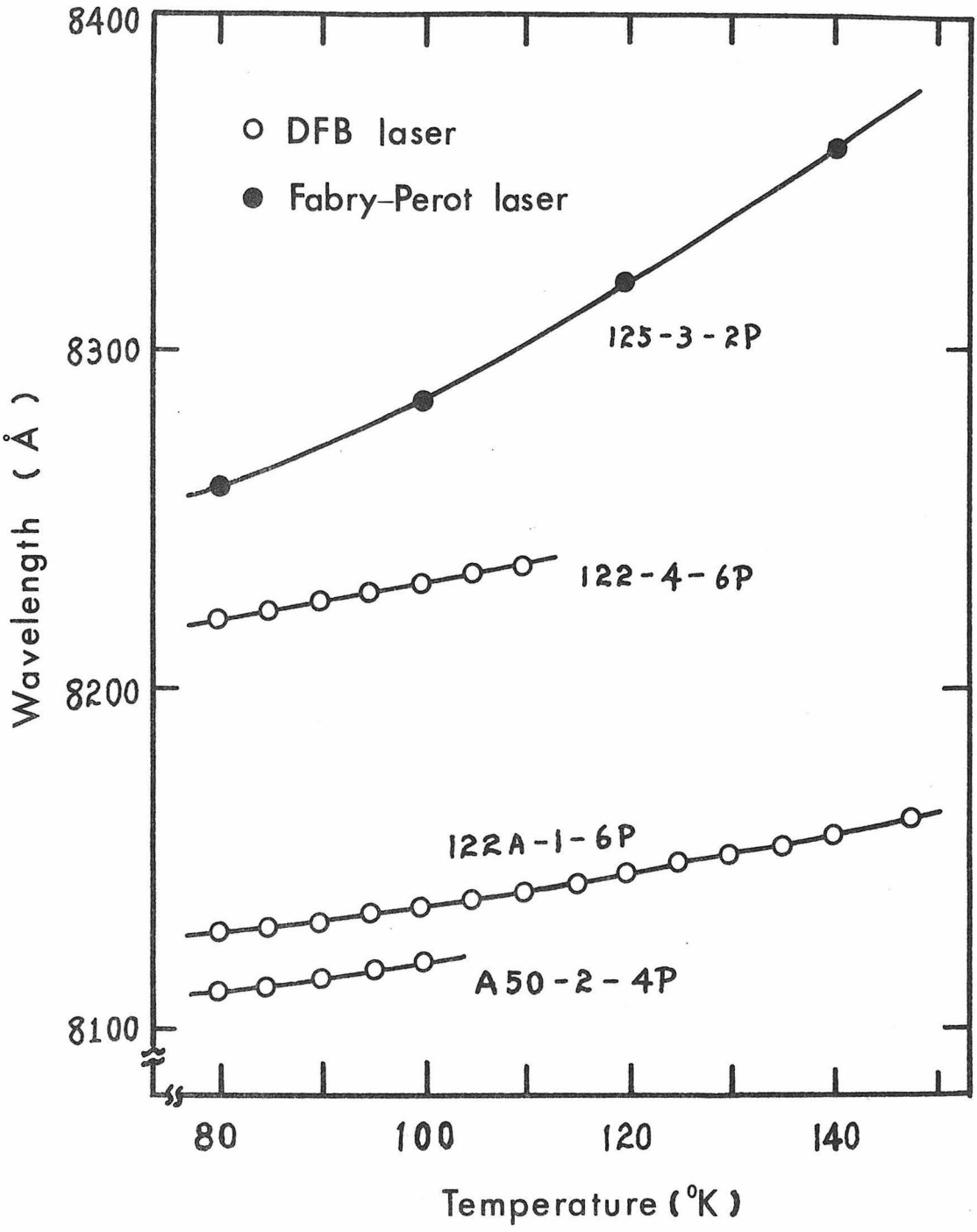

Fig. 3-25 The lasing wavelength as a function of temperature.

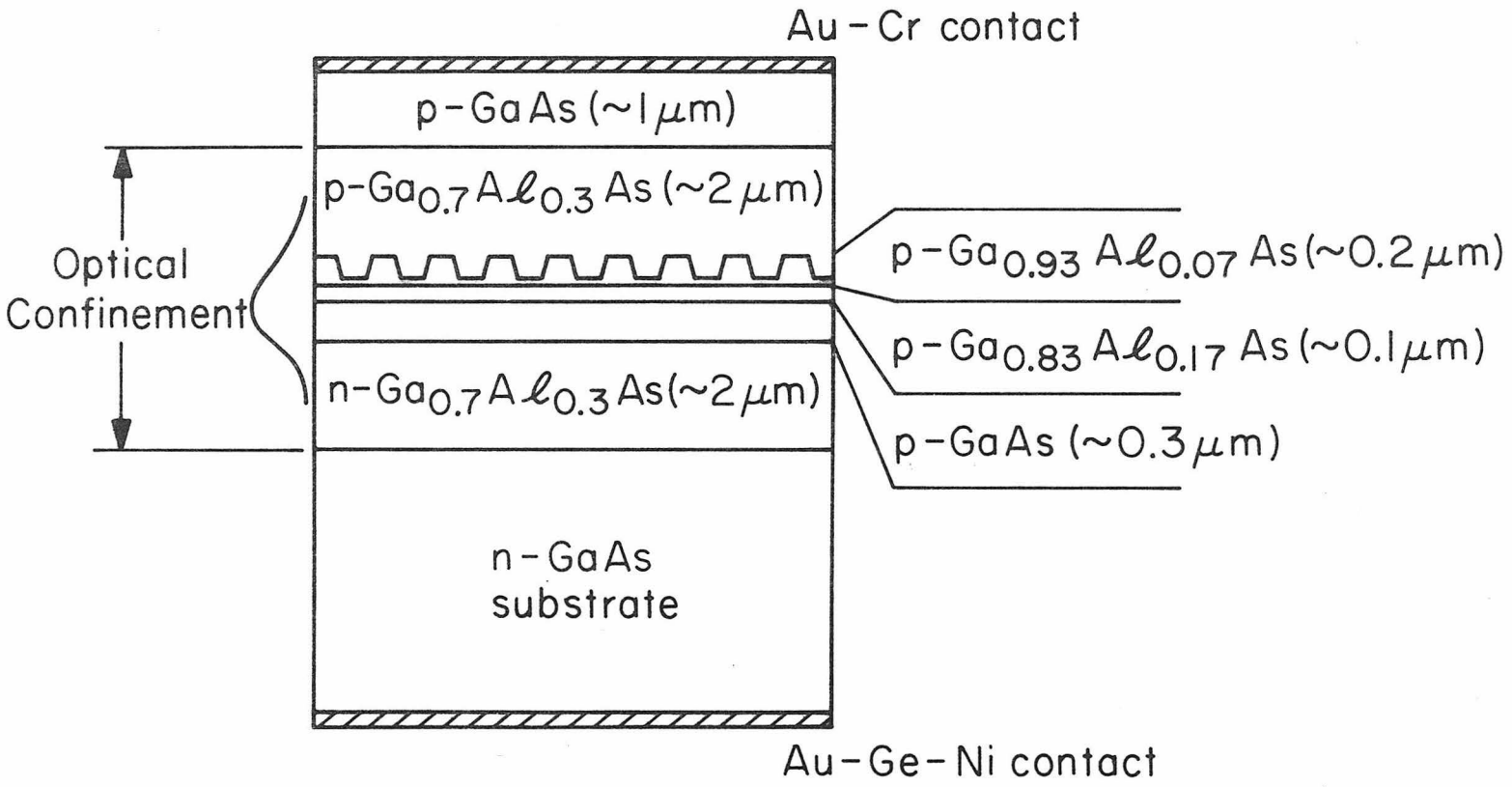

Fig. 3-26 Cross section of a separate confinement heterostructure GaAs distributed feedback injection laser.

and subsequent epitaxial growth is impossible. The corrugations are thus fabricated on the oxidation resistant p-$Ga_{0.93}Al_{0.07}As$ layer.

Diodes with this structure were found to lase with extremely low thresholds. For example, one of the lasers with length $L = 500$ μm, $\Lambda = 3600\text{Å}$ lased with threshold current density $J_{th} = 500 A/cm^2$ at 80°K. Another laser with $L = 500$ μm, $\Lambda = 3770\text{Å}$ has $J_{th} \sim 3$ KA/cm^2 at 300°K. This value is low enough for CW operation if proper heat sinking is provided as reported by Nakamura et al.[23]

So far most of the experiments in GaAs distributed feedback lasers have been limited to third order corrugations for which the radiation loss is not negligible. Hopefully some day we will have convenient CW UV source with wavelength less than 2000Å so that corrugations with period around 0.1 μm can easily be made and used in GaAs lasers to further reduce the threshold. With the room temperature GaAs distributed feedback lasers available the next question is how to incorporate the laser with other optical circuit components. This is an interesting current research area because the result could lead to the first monolithic integrated optical circuit. Meanwhile an equally important problem that has to be solved is the laser lifetime. The lifetime of the laboratory GaAs distributed feedback lasers ranged from ten minutes to twenty or thirty hours. In order to be a practical device, lifetime on the order of 10^6 hours is necessary. So there remains a lot of research to be done in this area.

Chapter 3 - References

(1) H. Kogelnik and C. V. Shank, "Stimulated emission in a periodic structure," Appl. Phys. Lett. 18, 152 (1971).

(2) H. Kogelnik and C. V. Shank, "Coupled-wave theory of distributed feedback lasers," J. Appl. Phys. 43, 2327 (1972).

(3) S. Wang, "Proposal of periodic layered waveguide structures for distributed lasers," J. Appl. Phys. 44, 767 (1972).

(4) A. Yariv, "Coupled mode theory for guided wave optics," IEEE J. Quantum Electron. 9, 919 (1973).

(5) R. Shubert, "Theory of optical-waveguide distributed feedback lasers with non-uniform gain and coupling," J. Appl. Phys. 45, 209 (1974).

(6) S. Chinn, "Effects of mirror reflectivity in a distributed feedback laser," IEEE J. Quantum Electron. 9, 574 (1973).

(7) W. Streifer, R. D. Burnham, and D. R. Scifres, "Effect of external reflectors on longitudinal modes of distributed feedback lasers," IEEE J. Quantum Electron. 11, 154 (1975).

(8) S. Somekh, "Transverse mode control in a distributed feedback semiconductor laser," Proc. IEEE (Lett.) 62, 277 (1974).

(9) C. V. Shank, J. E. Bjorkholm, and H. Kogelnik, "Tunable distributed feedback dye laser," Appl. Phys. Lett. 18, 395 (1971).

(10) R. L. Fork, K. R. German, and E. A. Chandross, "Photo-dimer distributed feedback laser," Appl. Phys. Lett. 20, 139 (1971).

(11) J. E. Bjorkholm and C. V. Shank, "Higher-order distributed feedback oscillators," Appl. Phys. Lett. 20, 306 (1972).

(12) P. Zory, "Laser oscillation in leaky corrugated optical waveguides," Appl. Phys. Lett. 22, 125 (1973).

(13) D. P. Schinke, R. G. Smith, E. G. Spencer, and M. F. Galvin, "Thin film distributed feedback laser fabricated by ion milling," Appl. Phys. Lett. 21, 494 (1972).

(14) M. Nakamura, A. Yariv, H. W. Yen, S. Somekh, and H. L. Garvin, "Optically pumped GaAs surface laser with corrugation feedback," Appl. Phys. Lett. 22, 515 (1973).

(15) M. Nakamura, H. W. Yen, A. Yariv, E. Garmire, S. Somekh, and H. L. Garvin, "Laser oscillation in epitaxial GaAs waveguides with corrugation feedback," Appl. Phys. Lett. 23, 224 (1973).

(16) H. W. Yen, M. Nakamura, E. Garmire, S. Somekh, A. Yariv, and H. L. Garvin, "Optically pumped GaAs waveguide lasers with a fundamental 0.11μ corrugation feedback," Optics Commun. 9, 35 (1973).

(17) C. V. Shank, R. V. Schmidt, and B. I. Miller, "Double-heterostructure GaAs distributed-feedback laser," Appl. Phys. Lett. 25, 200 (1974).

(18) M. Nakamura and A. Yariv, "Analysis of the threshold of double hetero-junction GaAs-GaAlAs lasers with a corrugated interface," Optics Commun. 11, 18 (1974).

(19) R. D. Burnham, D. R. Scifres, and W. Streifer, "Single-heterostructure distributed feedback GaAs diode lasers," IEEE J. Quantum Electron. 11, 439 (1975).

(20) M. Nakamura, K. Aiki, J. Umeda, A. Katzir, A. Yariv, and H. W. Yen, "GaAs-GaAlAs double-heterostructure injection lasers with distributed feedback," IEEE J. Quantum Electron. 11, 436 (1975).

(21) H. M. Stoll and D. H. Seib, "Distributed feedback GaAs homojunction injection laser," Appl. Opt. 13, 1981 (1974).

(22) K. Aiki, M. Nakamura, J. Umeda, A. Yariv, A. Katzir, and H. W. Yen, "GaAs-GaAlAs distributed feedback diode lasers with separate optical and carrier confinement," Appl. Phys. Lett. 27, 145 (1975).

(23) M. Nakamura, K. Aiki, J. Umeda, and A. Yariv, "CW operation of distributed feedback GaAs-GaAlAs diode lasers at temperatures up to 300°K," Appl. Phys. Lett. 27, 403 (1975).

(24) K. O. Hill and A. Watanabe, "Envelope gain saturation in distributed feedback lasers," Appl. Opt. 14, 950 (1975).

(25) S. R. Chinn and P. L. Kelley, "Analysis of the transmission, reflection and noise properties of distributed feedback laser amplifiers," Optics Commun. 10, 123 (1974).

(26) J. Zoroofchi and J. K. Butler, "Refractive index of n-type gallium arsenide," J. Appl. Phys. 44, 3697 (1973).

(27) D. Marcuse, "Radiation losses of tapered dielectric slab waveguide," Bell Syst. Tech. J. 49, 273 (1970).

(28) P. Zory, "Corrugated grating coupled devices and coupling coefficients," Integrated Optics Conference--Technical Digest, Salt Lake City, Utah, January 1976.

Chapter 4

Distributed Bragg Reflector Lasers

4-1 Introduction

As described in Chapter 3 the GaAs-GaAlAs distributed feedback laser has attracted a great deal of interest in the field of integrated optics. This is due, in part, to the frequency selective nature of the feedback which makes possible longitudinal and transverse mode control. Another important advantage is the compatibility of the fabrication process with planar technology.

One disadvantage revealed in the course of experiments on such lasers[1] is the degradation of the recombination efficiency in the active region by the steps used to obtain the corrugation. Another unresolved problem is the effect of the corrugation on the laser operating lifetime. These problems can be alleviated somewhat by schemes such as separate optical and carrier confinement in which the recombining carriers are kept away from the corrugation as described in the previous chapter.

An alternative to the distributed feedback laser is one where the Bragg coupling between the laser forward and backward waves is achieved in two corrugated waveguide sections which are contiguous with the active (amplifying) region. It has been suggested theoretically[2,3] and demonstrated experimentally[4-6] that such sections can act as high reflectance "mirrors" for waveguide modes at frequencies within the "stop band" where the Bragg condition is nearly satisfied. Such Bragg reflector lasers are expected to possess the main advantages of the

distributed feedback lasers, i.e., frequency and mode selectivity while avoiding the problem of degradation of the recombination efficiency.

The theoretical analyses of distributed Bragg reflector (DBR) lasers to date[2,3] employ a generalization of the analysis of the distributed feedback laser[7] and are consequently complicated and not easily amenable to intuitive physical interpretation. In addition, a variation of the basic configuration from that of the original model requires that the complicated boundary value problems be solved anew.

In this chapter we present a formally equivalent solution of the distributed Bragg reflector laser. In this approach we replace, in the analysis, the Bragg reflectors; i.e., the physically corrugated sections of the waveguide adjacent to the amplifying region, by fictitious reflectors with complex reflectances $r_{1,2}(\omega)\exp[-i\phi_{1,2}(\omega)]$. The complex reflectance of each reflector (denoted by subscript 1 or 2) is obtained from the solutions of Bragg reflectors and is assumed known. The derivation of the laser oscillation condition now becomes identical to that of a conventional two-reflector laser. It is obtained by requiring that the round-trip complex gain of the laser field amplitude including two reflections be equal to unity.

The oscillation condition can then be solved numerically or graphically to determine the lasing frequency and threshold. It is shown that distributed Bragg reflector lasers have similar frequency and modal control as the distributed feedback lasers. The effect of

reflector losses, which include bulk absorption loss and radiation loss, on the lasing characteristics is also treated. The losses in the periodic section are found to have little effect on the lasing frequency but can cause the threshold to go up considerably. Experimental results on optically pumped GaAs waveguide distributed Bragg reflector lasers were given at the end of the chapter. Lasing characteristics were determined and compared with theory. Also some potential applications of this kind of laser in fiber communication systems are discussed.

4-2 Distributed Bragg Reflector Laser with Lossless Reflectors

We have shown in Chapter 2 that a section of lossless periodic waveguide behaves as a band rejection filter or reflector. In general, the reflectivity of such a device can be expressed as a complex quantity

$$R(\omega) = r(\omega)\, e^{-i\phi(\omega)} \tag{4-1}$$

The spectral behavior of $r^2(\omega)$ for a lossless waveguide has been shown in Fig. 2-8(a). When $\Delta\beta < \kappa$, $r^2(\omega)$ is large, and for $\kappa L > 3.0$ is close to unity. When $\Delta\beta > \kappa$, $r^2(\omega)$ has several side lobes with progressively decreasing reflectivities.

Figure 4-1(a) shows a schematic drawing of a distributed Bragg reflector waveguide laser. It consists of an amplifying region of length L_2 flanked on each side by corrugated sections of length L_1 and L_3. We use the equivalent reflectors method described in the last two chapters to obtain the equivalent laser shown in Fig. 4-1(b). The corrugations are replaced, at their respective input planes, by two conventional mirrors with properly assigned complex reflectivities. The laser

(a)

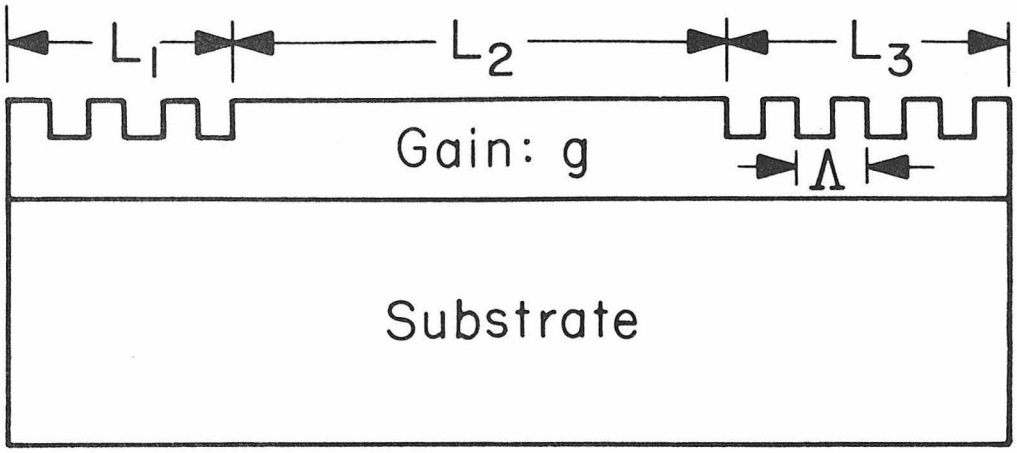

(b)

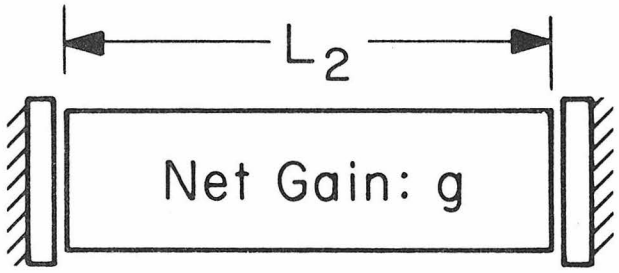

$$R_1 = r_1(\omega)e^{-i\phi_1(\omega)} \qquad R_2 = r_2(\omega)e^{-i\phi_2(\omega)}$$

Fig. 4-1 (a) Schematic diagram of a distributed Bragg reflector laser.

(b) Equivalent cavity of a distributed Bragg reflector laser.

cavity is of length L_2 and consists of a medium with net gain g at the wavelength region of interest. The oscillation condition is then obtained by setting the round trip complex gain equal to unity, i.e.,

$$r_1(\omega)\, r_2(\omega)\, e^{-i[\phi_1(\omega) + \phi_2(\omega)]}\, e^{2[g(\omega) - i\beta(\omega)]L_2} = 1 \qquad (4\text{-}2)$$

After using equations (2-33) and (4-1) the last equation becomes

$$-\kappa^2 e^{2(g-i\beta)L_2} = (i\Delta\beta + \gamma \coth\gamma L_1)(i\Delta\beta + \gamma\coth\gamma L_3) \qquad (4\text{-}3)$$

where $\gamma^2 = \kappa^2 - \Delta\beta^2$, β is the propagation constant of the laser mode and $\Delta\beta \equiv \beta - \frac{\pi}{\Lambda}$. Equation (4-3) is the eigenvalue equation of a distributed Bragg reflector laser and it can be solved numerically or graphically to obtain an infinite set of eigenvalues $(\Delta\beta_n, g_n)$. Each such set gives the oscillation "frequency" $\Delta\beta_n$ and the threshold gain g_n of the n^{th} longitudinal mode of the laser. The extension of equation (4-3) to the case of two different corrugated sections (i.e., $\kappa_1 \neq \kappa_2$, $\Delta\beta_1 \neq \Delta\beta_2$, etc.) is obvious.

Equation (4-2) can be written as

$$r_1(\omega)\, r_2(\omega)\, e^{2gL_2}\, e^{-i(\phi_1 + \phi_2 + 2\Delta\beta L_2 + 2\beta_o L_2)} = 1$$

Hence the oscillation frequency (i.e., $\Delta\beta$ at oscillation) and threshold gain are obtained by equating the phase and amplitude on both sides of the last equation

$$g = \frac{1}{2L_2} \ln \frac{1}{r_1 r_2} \qquad (4\text{-}4a)$$

$$\Phi \equiv \phi_1 + \phi_2 + 2\Delta\beta L_2 + 2\beta_o L_2 = 2n\pi \qquad (4\text{-}4b)$$

where $n = 0, \pm 1, \pm 2, \cdots$.

In a given distributed Bragg reflector structure we can use equation (2-32) to find r_1, r_2, ϕ_1 and ϕ_2 as functions of $\Delta\beta$. The round trip phase delay

$$\Phi = \phi_1 + \phi_2 + 2\Delta\beta L_2 + 2\beta_o L_2$$

can thus be plotted as a function of $\Delta\beta$. The intersections of this curve with the horizontal lines $\Phi = 2n\pi$ determine the set of oscillation frequencies $\Delta\beta_n$. The corresponding $r_1(\Delta\beta_n)$ and $r_2(\Delta\beta_n)$ are then used in equation (4-4a) to find the corresponding values of the threshold gain g_n . This procedure is illustrated in Fig. 4-2 for the special case $L_1 = L_3 = L$, $L_2 = 2L$, $\kappa L = 3.0$ and $\beta_o L_2 = 2N\pi$. Under these conditions equations (4-4a) and (4-4b) reduce to

$$g = \frac{1}{2L} \ln \frac{1}{r} \qquad (4\text{-}4c)$$

$$\Phi = \phi + 2\Delta\beta L = n\pi \qquad (4\text{-}4d)$$

$\Phi = \phi + 2\Delta\beta L$ and $\Phi = n\pi$ are plotted in Fig. 4-2(a) The intersections are at $\Delta\beta L = \pm 0.67, \pm 2.00, \pm 3.22, \pm 4.14$, etc. The corresponding reflectivities are obtained from Fig. 4-2(b) and used in equation (4-4c) to calculate the threshold gains $2gL = 0.0050$, 0.0127, 0.0830, and 1.2629, etc. It is seen that although the effective reflectivity of the modes at $\Delta\beta L = \pm 2.00$ (0.974) is only slightly smaller than that of the modes at $\Delta\beta L = \pm 0.67$ (0.989) the threshold for the modes at $\Delta\beta L = \pm 2.00$ is more than twice as big as that of the modes at

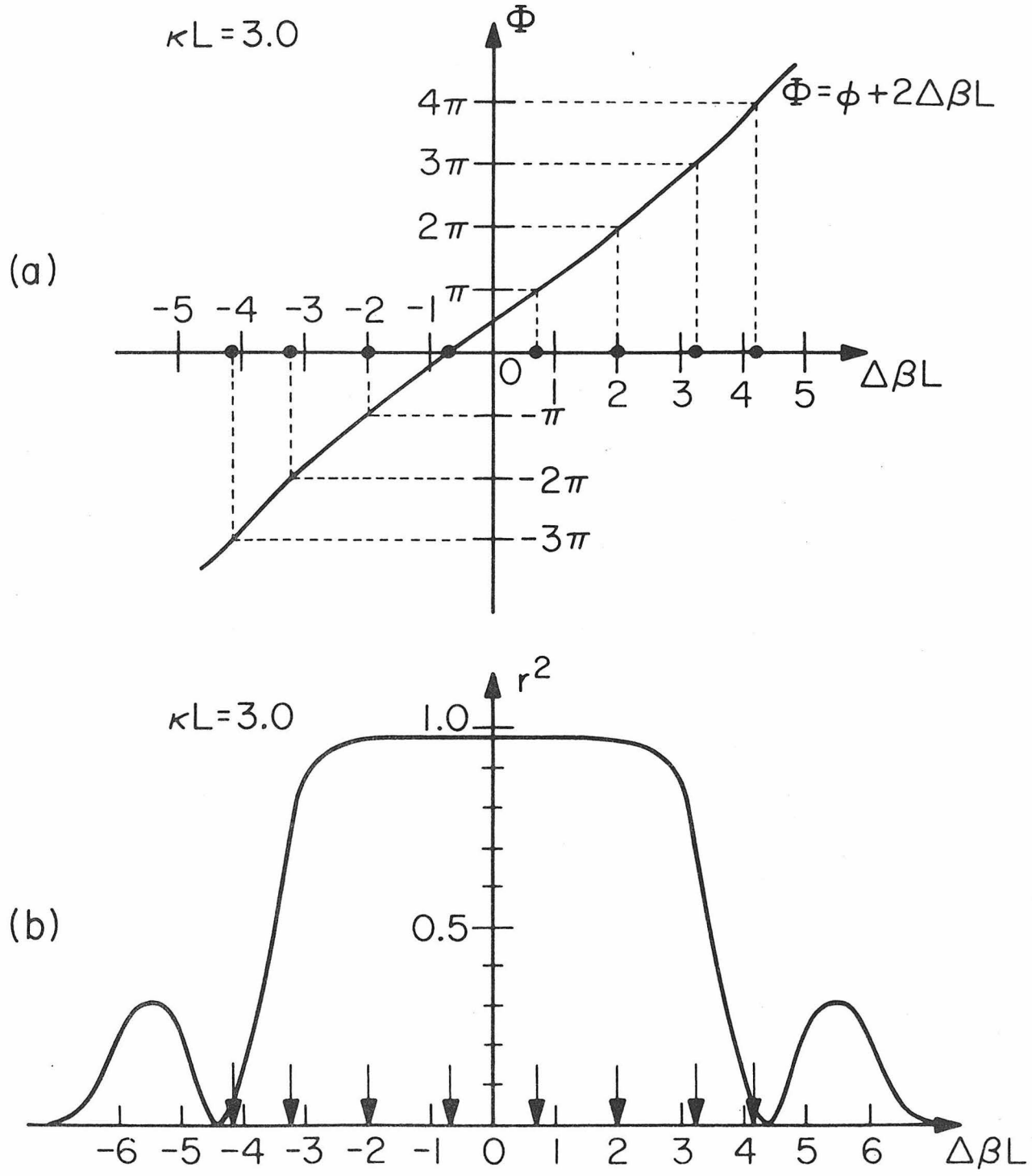

Fig. 4-2 Graphical method of determining oscillation condition of a distributed Bragg reflector laser.

$\Delta\beta = \pm 0.67$. This clearly illustrates the longitudinal mode selectivity of distributed Bragg reflector lasers.

4-3 Determination of Mode Structure

To obtain the actual oscillation wavelength from the solutions of $\Delta\beta_n$ we recall that

$$\Delta\beta_n = \beta - \beta_o = \frac{2\pi n_{eff}}{\lambda} - \frac{\pi}{\Lambda}$$

therefore

$$n_{eff} = \frac{\lambda}{2}\left(\frac{1}{\Lambda} + \frac{\Delta\beta_n}{\pi}\right) \equiv \frac{\lambda}{2\Lambda_n} \tag{4-5}$$

So each longitudinal mode is represented by a straight line with slope $\frac{1}{2\Lambda_n}$ in the n_{eff}-λ plane. We can also plot the waveguide mode dispersion relation

$$n_{eff}(\lambda) = \frac{\lambda\beta(\lambda)}{2\pi}$$

on the same diagram. The intersections of this curve with the lines represented by equation (4-5) give the oscillation wavelengths of different longitudinal modes. This procedure is very similar to that described in section 3-4 for distributed feedback lasers. The longitudinal mode spacing of distributed Bragg reflector lasers, as expected, in the limit of $L_2 >> L_1, L_3$ is inversely proportional to L_2 as in the Fabry-Perot lasers.

Bragg reflectors can determine the longitudinal wave vector of the laser but do not affect directly the propagation vectors in the other two dimensions. This could result in oscillation of more than

one transverse mode. Control of modes whose transverse K vectors lie in the plane of the junction can be achieved by controlling the width of the pumped area. The quenching of transverse modes (k vectors normal to the junction plane) can be obtained by controlling the height of the laser waveguide. For small enough heights the effect of mode dispersion causes the wavelength at which the Bragg condition is satisfied by a higher order transverse mode to be appreciably shorter than that of the fundamental transverse mode. It can thus be shifted far enough from the peak of the gain profile so as to exercise a substantially lower gain. To obtain the oscillation frequencies and threshold gains of a given transverse mode we repeat the procedure described above but use the appropriate dispersion $n_{eff}(\lambda)$ curve of the mode in equation (4-5) and recall that, in general, the coupling constant will be different for different modes.

We have described above how a judicious choice of the thickness of the active layer and the corrugation period could be used to obtain a single transverse mode operation. By carefully choosing the corrugation period we can cause the oscillation wavelength of the lowest order longitudinal mode to occur near the peak of the gain profile. Since this mode was found to possess the lowest threshold gain g_n, it is clear that the external pumping threshold for this mode will be lowest and one can obtain single mode operation. This kind of modal control is also similar to that of distributed feedback lasers.

4-4 The Effect of Lossy Reflectors

Up to this point we have considered lossless reflectors only.

In many real applications the reflector sections are made of the same material as the active region but are unpumped. As a result the reflectors are lossy. In this section we are going to examine the property of a section of lossy periodic waveguide and its effect on the lasing characteristics of a laser with Bragg reflectors made out of this kind of lossy waveguide.

We start with equations (3-1)

$$\frac{dA}{dz} = i\kappa B e^{-i2(\Delta\beta+i\alpha)z}$$

$$\frac{dB}{dz} = -i\kappa A e^{i2(\Delta\beta+i\alpha)z}$$

These are the coupled-mode equations describing propagation in an amplifying periodic waveguide with amplitude gain α. Now if we replace α by $-\alpha$ so that α represents the amplitude loss coefficient we obtain

$$\frac{dA}{dz} = i\kappa B\, e^{-i2(\Delta\beta-i\alpha)z} \tag{4-6a}$$

$$\frac{dB}{dz} = -i\kappa A\, e^{i2(\Delta\beta-i\alpha)z} \tag{4-6b}$$

The solutions of equation (4-6) can be obtained from equations (3-2) and (3-3) if we replace α by $-\alpha$. They are

$$E_i(z) = B(z)\, e^{-i\beta z - \alpha z}$$

$$= E_i(0)\frac{[(\alpha+i\Delta\beta)\sinh\gamma(L-z) + \gamma\cosh\gamma(L-z)]e^{-i\beta_o z}}{(\alpha+i\Delta\beta)\sinh\gamma L + \gamma\cosh\gamma L} \tag{4-7}$$

and

$$E_r(z) = A(z)\, e^{i\beta z+\alpha z}$$

$$= E_i(0)\,\frac{-i\kappa\sinh\gamma(L-z)e^{i\beta_o z}}{(\alpha+i\Delta\beta)\sinh\gamma L + \gamma\cosh\gamma L} \tag{4-8}$$

where $\gamma^2 = (\alpha+i\Delta\beta)^2 + \kappa^2$.

For $\Delta\beta = 0$, we have

$$|E_i(z)|^2 = \left|\frac{\alpha\sinh\gamma(L-z) + \gamma\cosh\gamma(L-z)}{\alpha\sinh\gamma L + \gamma\cosh\gamma L}\right|^2 \tag{4-9}$$

and

$$|E_r(z)|^2 = \left|\frac{\kappa\sinh\gamma(L-z)}{\alpha\sinh\gamma L + \gamma\cosh\gamma L}\right|^2 \tag{4-10}$$

Equation (4-9) and (4-10) are plotted in Fig. 4-3 for $\kappa L = 8.0$, $\alpha L = 0$ and $\alpha L = 2$. We see that the power distribution along the waveguide carried by the incident wave does not vary much for $\kappa >> \alpha$ from that in the lossless ($\alpha=0$) case. The reflected wave, on the other hand, is seen to undergo attenuation. The intensity reflectivity in this case is reduced from $\sim$1.0 at $\alpha=0$ to roughly $\left|\frac{\kappa}{\alpha+\kappa}\right|^2$. For $\kappa L = 8.0$, $\alpha L = 2.0$ the reflectivity is down to $\sim$0.64. The effective distance penetrated by the wave into the waveguide taken as the $1/e^2$ point of the forward power is $\sim L/8$ for our lossy waveguide. This is due to the strong coupling rather than the attenuation. (Note that $\frac{1}{\kappa} = \frac{L}{8}$). In Fig. 4-4 we plot $|E_i(z)|^2$, $|E_r(z)|^2$ for $\kappa L = 2.0$ with $\alpha L = 0$ and $\alpha L = 2.0$. Since now κL and αL are comparable we would expect the effective penetration depth to be

$$L_{eff} \simeq \frac{1}{\sqrt{\kappa^2+\alpha^2}} = 0.354\ L$$

This is easily verified from the figure. Also, the maximum intensity reflectivity is reduced to around

$$\left|\frac{\kappa}{\alpha+\sqrt{\kappa^2+\alpha^2}}\right|^2 = 0.172$$

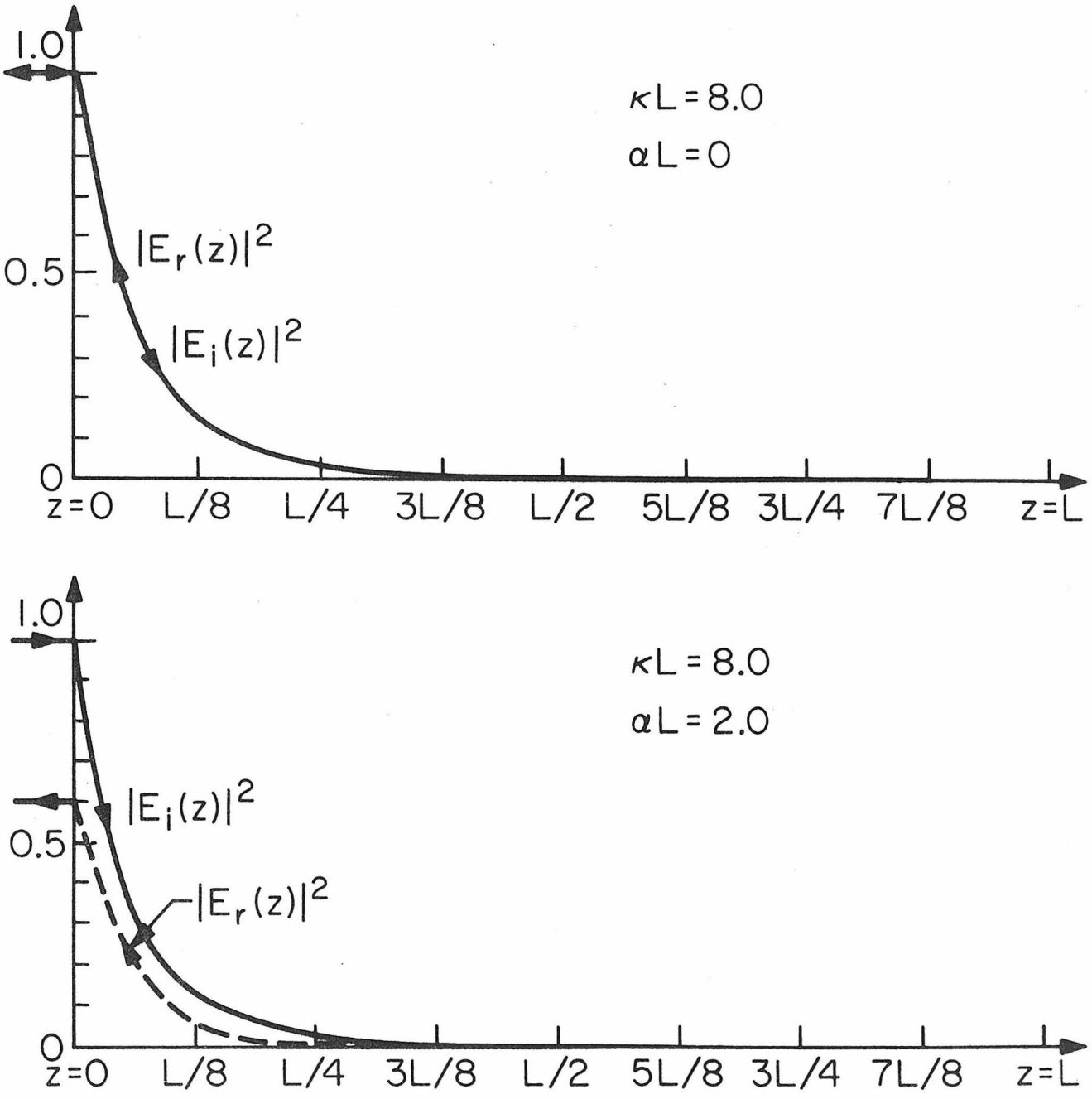

Fig. 4-3 Plots of $|E_i(z)|^2$ and $|E_r(z)|^2$ for $\kappa L = 8.0$ and (a) $\alpha L = 0$ (b) $\alpha L = 2.0$.

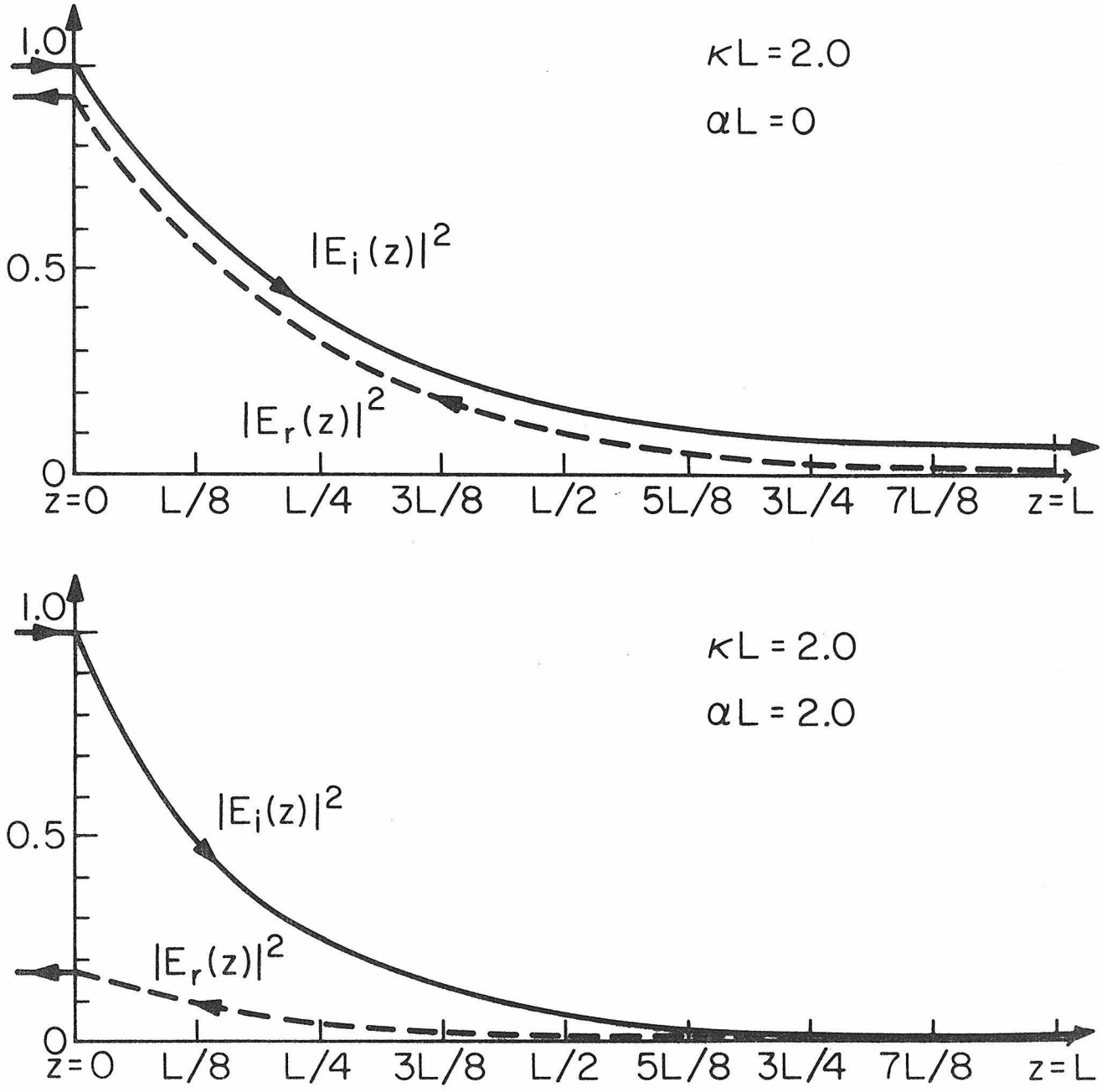

Fig. 4-4 Plots of $|E_i(z)|^2$ and $|E_r(z)|^2$ for $\kappa L = 2.0$ and (a) $\alpha L = 0$ (b) $\alpha L = 2.0$.

The third case $\alpha >> \kappa$ is plotted in Fig. 4-5 with $\kappa L = 0.5$ and $\alpha L = 0$ and 2.0. The maximum reflectivity is now

$$\sim \left|\frac{\kappa}{2\alpha}\right|^2 = 0.016$$

The effective penetration length is

$$L_{eff} \sim \frac{1}{\alpha} = 0.5L$$

For the general case of $\Delta\beta \neq 0$, we can write the reflectivity as

$$R = \frac{E_r(0)}{E_i(0)} = \frac{-i\kappa \sinh\gamma L}{(\alpha+i\Delta\beta)\sinh\gamma L + \gamma\cosh\gamma L} = re^{-i\phi} \qquad (4\text{-}11)$$

A plot of r^2 for $\kappa L = 3.0$, $\alpha L = 1.0$ is shown in Fig. 4-6(a). We also plot the curve with $\alpha L = 0$ for comparison. The magnitude of the reflectivity in the presence of waveguide loss is substantially lower than that of the loss-free case. In addition, the sidelobe "oscillation" is smoothed out. In this case the reflectivity is still a strong function of the incident wave frequency. The loss not only changes the magnitude of the reflectivity r but also changes the phase ϕ. This is shown in Fig. 4-6(b). For $\alpha L = 1$ the behavior of ϕ is such that it almost follows the curve for $\alpha L = 0$ when $\Delta\beta L$ is small. As $\Delta\beta L$ increases, $\phi_{\alpha L=1}$ gradually falls off the $\alpha L = 0$ curve and stays nearly constant.

Now consider the case where two lossy sections serve as the reflectors of a laser. The oscillation condition (4-3) is modified to

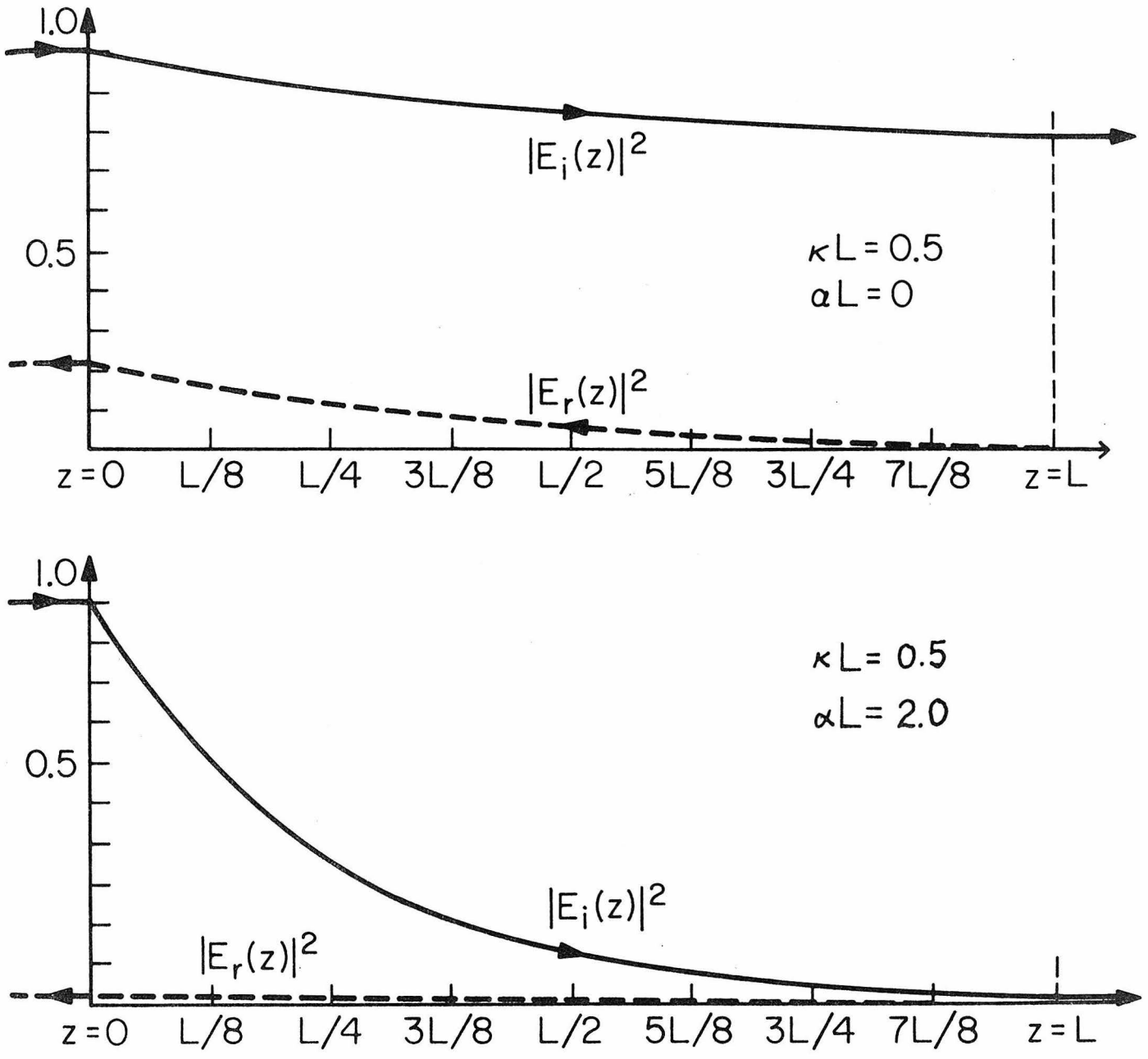

Fig. 4-5 Plots of $|E_i(z)|^2$ and $|E_r(z)|^2$ for $\kappa L = 0.5$ and (a) $\alpha L = 0$ (b) $\alpha L = 2.0$.

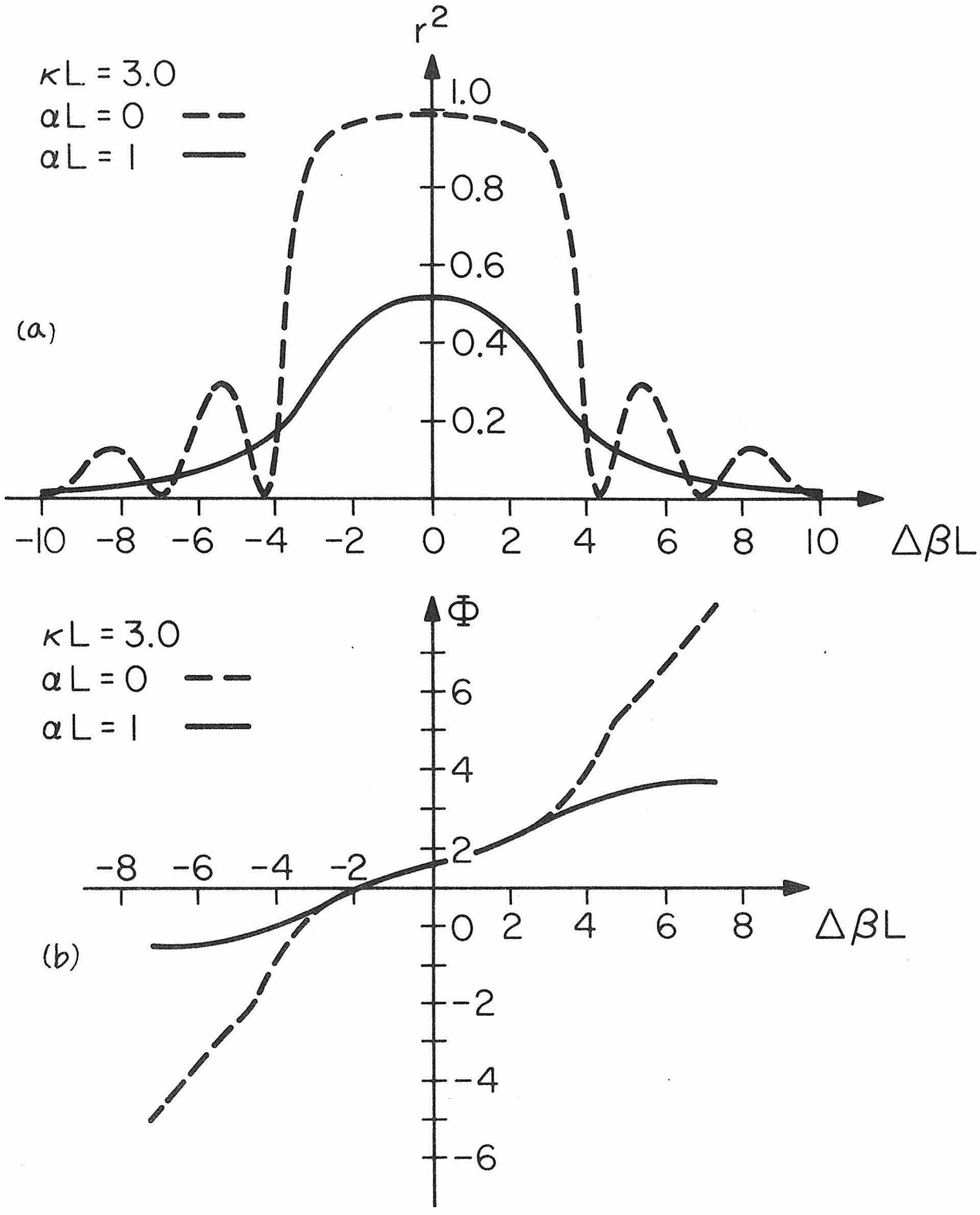

Fig. 4-6 Plots of (a) the intensity reflectivity (b) the phase of the reflectivity of a Bragg reflector with and without loss.

$$-\kappa^2 e^{2(g-i\beta)L_2} = [(\alpha+i\Delta\beta) + \gamma\coth\gamma L_1][(\alpha+i\Delta\beta) + \gamma\coth\gamma L_3] \qquad (4\text{-}12)$$

where $\gamma^2 = (\alpha+i\Delta\beta)^2 + \kappa^2$. Let us consider, as an example, the special case $L_1 = L_3 = L$, $L_2 = 2L$, $\kappa L = 3.0$, $\beta_o L_2 = 2N\pi$ considered previously, but take $\alpha L = 1.0$. The phase shift diagram is shown in Fig. 4-7(a). The lasing frequencies are at $\Delta\beta L = \pm 0.67, \pm 2.00, \pm 3.36, \pm 4.85$, etc. We note that as compared to the lossless case described in section 4-2 the lasing frequencies of the lower order modes hardly change. Because of the substantial reduction of the reflectivities, the thresholds however, are much higher. They are $2gL = 0.3367, 0.4077, 0.6813, 1.0814$, etc.

In a GaAs distributed Bragg reflector laser the unpumped corrugated sections will absorb laser radiation. Also, if we use higher order corrugations to provide the feedback ($\Lambda = \ell \frac{\lambda}{2n_{eff}}$, $\ell=2,3,\cdots$) there will exist radiation loss due to the coupling between the guided modes and the radiation modes through the lower harmonics of the corrugation. Theoretically, the use of fundamental mode ($\Lambda = \frac{\lambda}{2n_{eff}}$) should make it impossible to couple to radiation modes. Deviations from perfect periodicity, however, will always introduce some scattering loss. We can account for these losses in the analysis by a distributed loss coefficient α_{rad} so the loss factor α that appears in equation (4-11) consists of two parts

$$\alpha = \alpha_{bulk} + \alpha_{rad}$$

A typical value of α as estimated in our experiments is $\sim 15\ cm^{-1}$.

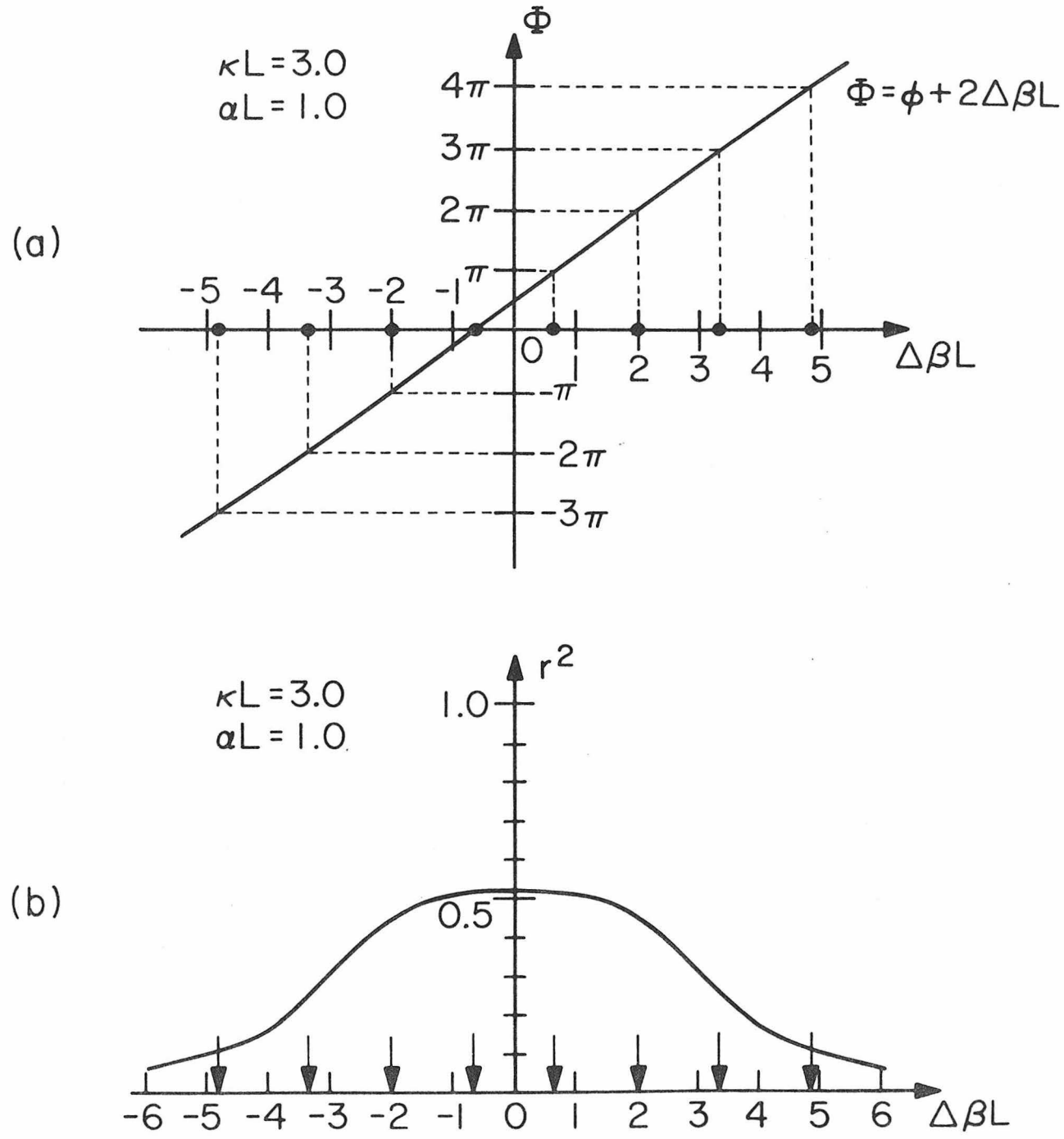

Fig. 4-7 Graphical method of determining oscillation condition of a distributed Bragg reflector laser with lossy reflectors ($\alpha L = 1.0$).

4-5 Comparison of Distributed Feedback and Distributed Bragg Reflector Lasers

The distributed Bragg reflector lasers and the distributed feedback lasers are very similar in several respects. They both utilize corrugations to provide the feedback and thus have the same degree of modal control as discussed earlier. The main difference between them is that in distributed feedback lasers the gain and the feedback region are not separated while in the distributed Bragg reflector lasers the gain and the feedback regions can be separated. One important consequence is that in distributed Bragg reflector lasers it is possible to have oscillation at or very near the center of the "stop band" where the reflectivity is maximum leading to very low threshold. While in distributed feedback lasers no oscillation can occur for $|\Delta\beta| < \kappa$. For $\Delta\beta$ outside the stop band the reflectivity is lower. Therefore distributed feedback lasers possess higher thresholds.

The threshold gain of a distributed Bragg reflector laser, from equation (4-4a), is

$$\alpha_{th}^{DBR} = \alpha_{bulk} + \frac{1}{2L_2} \ell n \frac{1}{r_1 r_2}$$

and the loss coefficient that is used to obtain r_1 and r_2 is $\alpha = \alpha_{bulk} + \alpha_{rad}$. It is clear that the effect of radiation loss in this kind of laser can be reduced by making L_2 large, i.e., to use a longer active region. This is to be compared with the threshold of a distributed feedback laser [equation (3-21)]

$$\alpha_{th}^{DFB} = \alpha_{th}^{o}\ (\kappa,L) + \alpha_{o} + \alpha_{rad}$$

where the effect of α_{rad} is to increase α_{th}^{DFB} by an amount equal to α_{rad} to compensate for the radiation loss.

Another major advantage of distributed Bragg reflector lasers over distributed feedback lasers is that the corrugations are separated from the active region so that there will be no degradation of the carrier recombination efficiency as observed in distributed feedback lasers. And as described in section 3-9 the fabrication of GaAs-GaAlAs distributed feedback laser diodes requires that the liquid phase epitaxy process be interrupted in order to make the corrugation. And then the second growth process is carried out on the corrugated surface, which is a difficult procedure. In distributed Bragg reflector lasers, on the other hand, it is possible to perform liquid phase epitaxial growth in one step as in the fabrication of ordinary injection lasers. A disadvantage of distributed Bragg mirror lasers is that in order to have the corrugation close to the optical wave we need to etch the wafer so that a mesa structure is obtained as shown in Fig. 1-3(b). The corrugations are then fabricated on both sides of the mesa. It is more difficult to obtain a high quality corrugation on this kind of "nonsmooth" surface especially at the region immediately next to the mesa.

4-6 Experiments with Optically Pumped GaAs Distributed Bragg Reflector Lasers

Fig. 4-8 shows the cross section of a typical optically pumped GaAs waveguide distributed Bragg reflector laser used in our experiment. Two layers of GaAlAs and GaAs were grown on an n-GaAs substrate by liquid phase epitaxy to form a waveguide structure.

Photoresist grating mask was then laid over the whole surface of the wafer by holographic photolithography. Part of the grating was covered by a stripe mask so that subsequent chemical etching through the photoresist grating resulted in a gap of length L_2 between the two corrugated end sections. Third order gratings $\Lambda = 3\lambda/2n_{eff}$ were used. The wafers were then saw-cut at one end for access to the laser output. Typical dimensions are $L_1 \sim 250$ μm, $L_2 \sim 500$ μm, $L_3 \sim 3$ mm and $L_4 \sim 3$ mm. The relatively large lengths of sections L_3 and L_4 which are lossy at the laser wavelength is to ensure that there is only negligible reflection from the far face of the sample.

Samples were cooled to liquid nitrogen temperature (77°K) and pumped optically by a repetitively pulsed dye laser tuned to ∿6300Å. The pumping beam was focused by a cylindrical lens onto the sample. During the pumping the corrugations could be totally or partially covered in order to study the effect of lossy reflectors. It was found that with the corrugations pumped the laser threshold decreased by a factor of 2-3 while the spectrum did not change significantly. Both observations are in agreement with the theory.

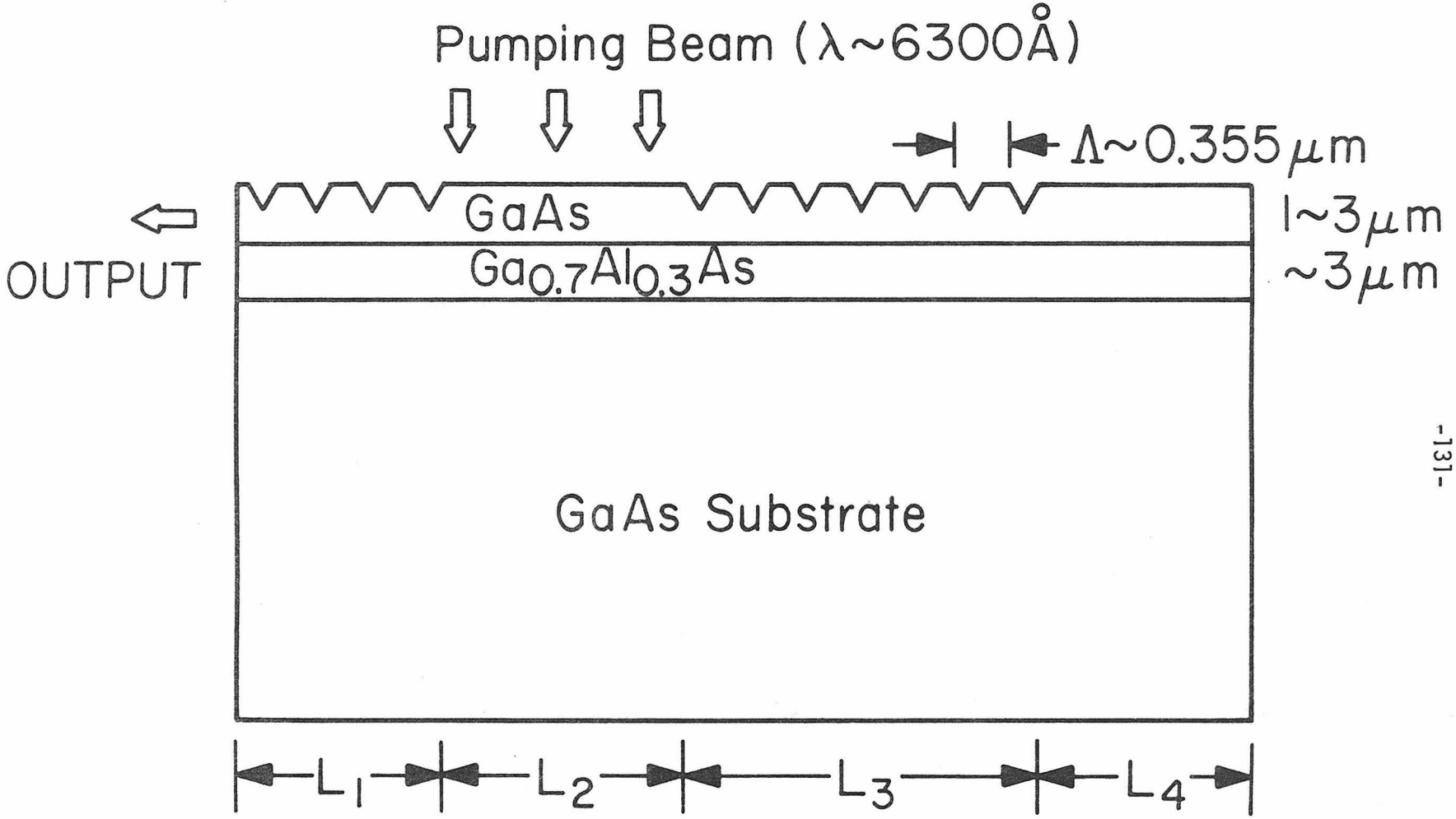

Fig. 4-8 Cross section of an optically pumped GaAs distributed Bragg reflector laser.

Fig. 4-9 is a spectrum from one of the lasers which shows single mode operation up to two times the threshold pumping intensity. In this case the corrugations were not pumped. In waveguides of larger height the mode selectivity, discussed in section 4-3, decreases and it is possible to have several transverse modes oscillating simultaneously. An example of such a spectrum is shown in Fig. 4-10. Three peaks are shown which belong to different transverse modes. They are separated by 12Å and 24Å, and have TE polarization (electric field parallel to the junction plane). In some lasers, with a somewhat thinner top layer, transverse mode spacings as large as 40Å were observed.

Because of the coexistence of several transverse modes in our laser there is a possibility of intermode coupling leading to hybrid laser modes[8,9]. For example, the right-going m=0 mode can couple to the left-going m=1 mode and vice versa. This kind of hybrid mode will oscillate at a wavelength roughly halfway between the m=0 and m=1 mode wavelength. Fig. 4-11 shows one example of this phenomena where we have m=0, m=1, m=2 modes and the hybrid mode between m=0 and m=2 designated as (0,2).

The distributed Bragg reflector structure also offers a possible solution to the difficult problem of coupling a waveguide laser output into fibers. It is suggested that one can fabricate a Bragg reflector laser with fundamental grating on one side of the active region and a second order grating on the opposite side. It is well known that a second order grating couples light in first order in a direction perpendicular to the grating plane[10,11,12]. We

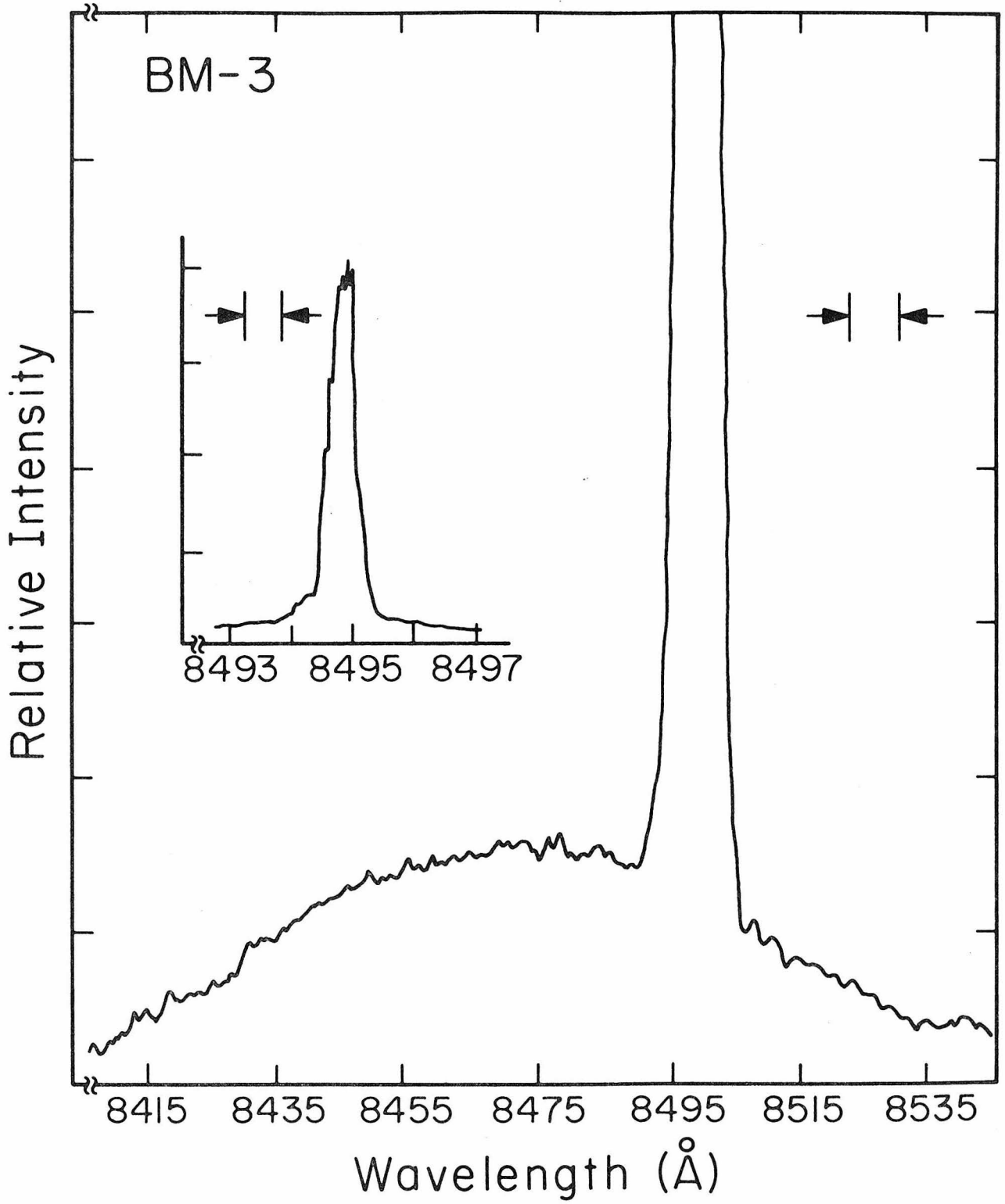

Fig. 4-9 Single mode oscillation spectrum of an optically pumped GaAs distributed Bragg reflector laser.

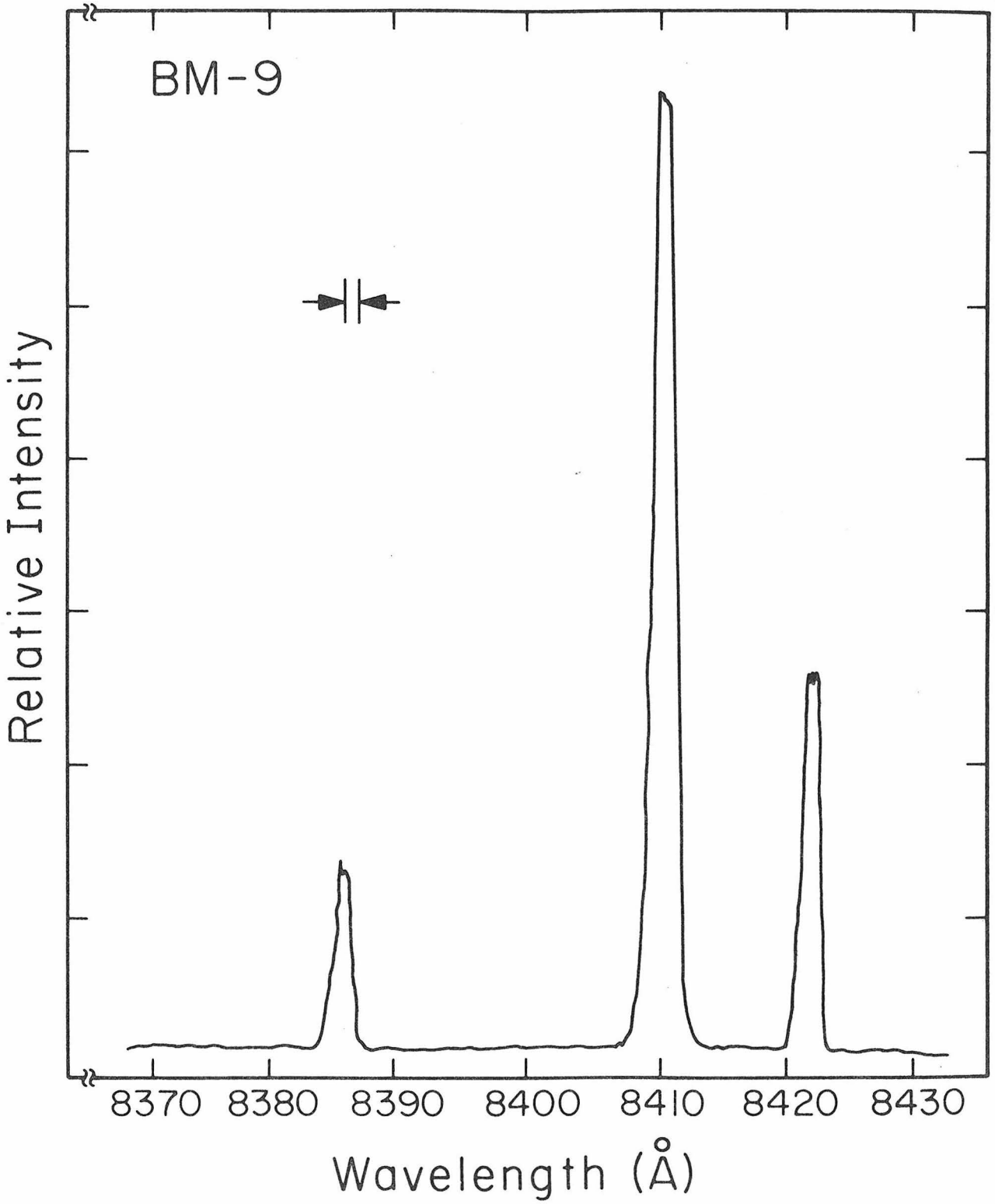

Fig. 4-10 Multi-transverse mode oscillation spectrum of a GaAs waveguide distributed Bragg reflector laser.

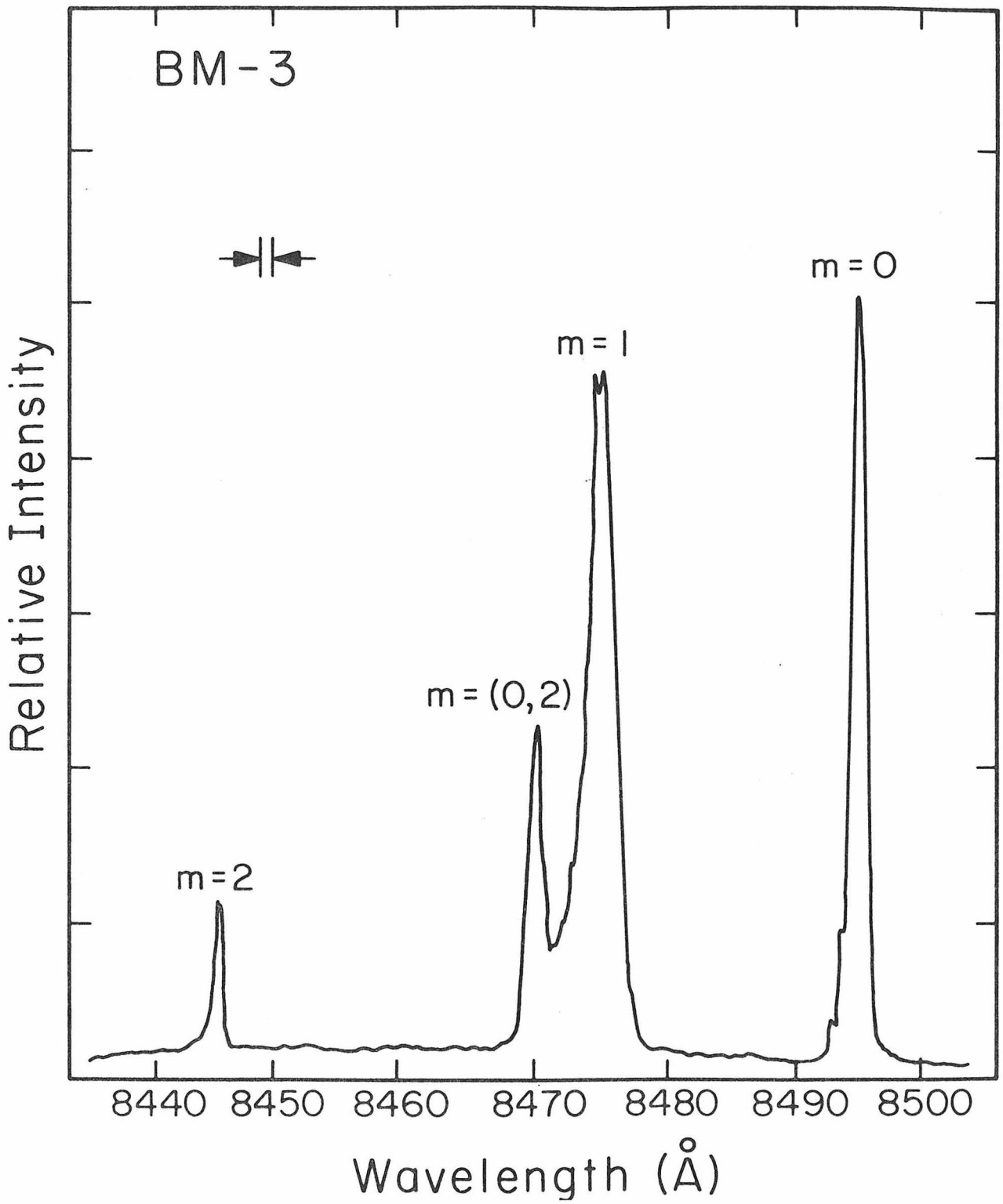

Fig. 4-11 Spectrum shows hybrid mode oscillation in a multi-transverse mode distributed Bragg reflector laser.

can fix one end of a fiber to the grating and thus couple the laser light into the fiber as illustrated in Fig. 4-12. The coupling efficiency can be made large by adjusting the corrugation depth so as to obtain an effective radiating aperture with cross sectional dimensions which approximate those of the fiber. A modulator section can be inserted between the grating and the active region to modulate the output intensity.

Some preliminary experimental results on this scheme were obtained. This was done by fabricating lasers with one cleaved end face and one second order Bragg reflector, optically pumped at both 77°K and 300°K. One end of the fiber was held against the corrugation next to the pumped region, the other end was held against the entrance slit of a spectrometer. Although the measured output power from the fiber was low, it demonstrated the feasibility of this scheme. More work on the optimal design of this type of structure is needed to improve the coupling efficiency.

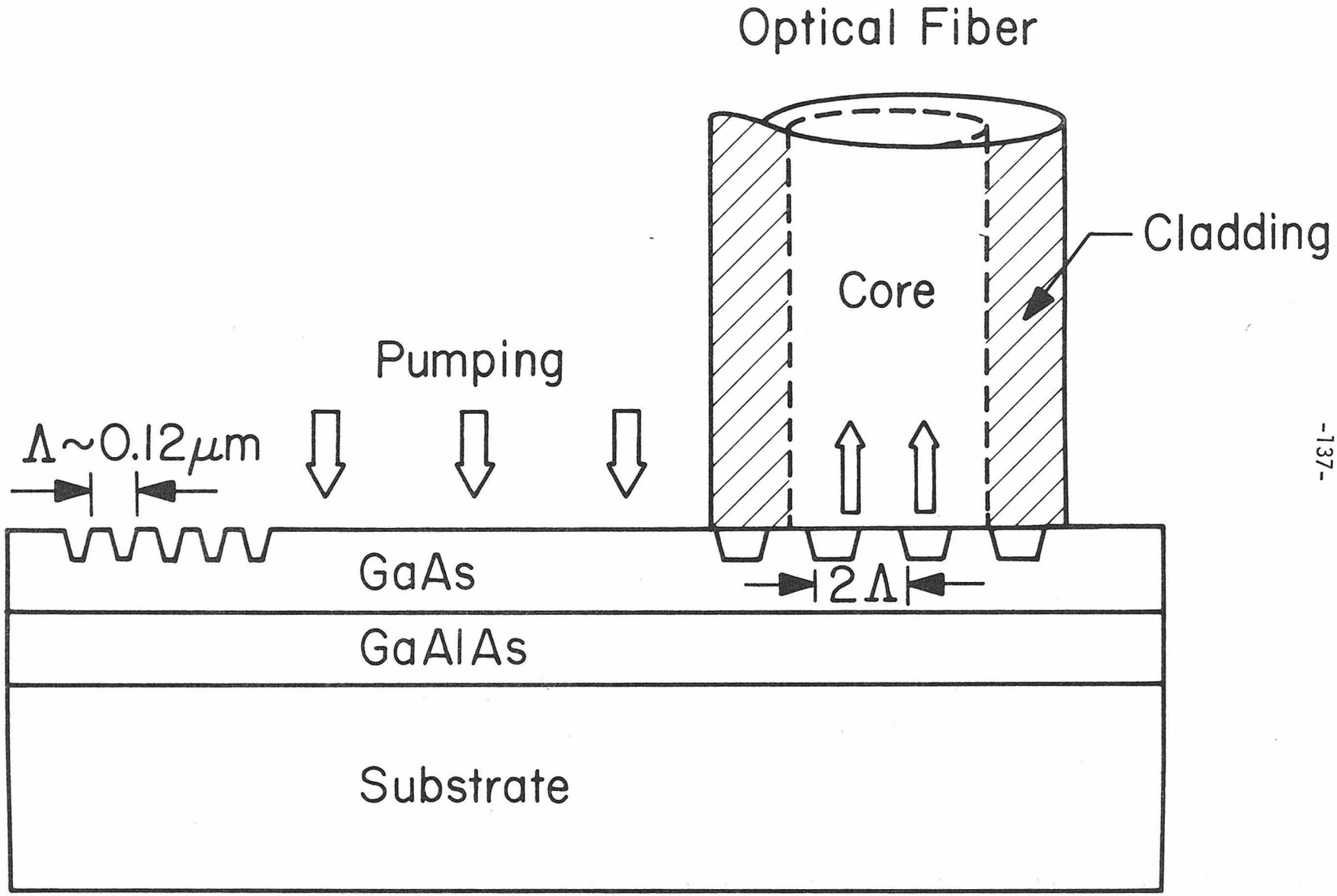

Fig. 4-12 Sketch of the proposed scheme of coupling laser light into optical fiber.

CHAPTER 4 REFERENCES

(1) M. Nakamura, K. Aiki, J. Umeda, A. Katzir, A. Yariv, and H. W. Yen, "GaAs-GaAlAs double-heterostructure injection lasers with distributed feedback," IEEE J. Quantum Electron. 11, 436 (1975).

(2) R. Shubert, "Theory of optical-waveguide distributed lasers with nonuniform gain and coupling," J. Appl. Phys. 45, 209 (1974).

(3) S. Wang, "Principles of distributed feedback and distributed Bragg-reflector lasers," IEEE J. Quantum Electron. 10, 413 (1974).

(4) F. K. Reinhart, R. A. Logan, and C. V. Shank, "GaAs-$Al_xGa_{1-x}As$ injection lasers with distributed Bragg reflectors," Appl. Phys. Lett. 27, 45 (1975).

(5) H. W. Yen, A. Yariv, and W. Ng, "Optically pumped GaAs waveguide lasers with Bragg reflectors," Integrated Optics Conference-Technical digest, Salt Lake City, Utah, Jan. 1976.

(6) W. T. Tsang and S. Wang, "GaAs-$Ga_{1-x}Al_xAs$ double heterostructure injection lasers with distributed Bragg reflectors," Integrated Optics Conference - Technical digest (post-deadline paper) Salt Lake City, Utah, Jan. 1976.

(7) H. Kogelnik and C. V. Shank, "Coupled-wave theory of distributed feedback lasers," J. Appl. Phys. 43, 2327 (1972).

(8) P. Zory, "Laser oscillation in leaky corrugated optical waveguides," Appl. Phys. Lett. 22, 125 (1973).

(9) H. Kogelnik, C. V. Shank, and J. E. Bjorkholm, "Hybrid scattering in periodic waveguides," Appl. Phys. Lett. 22, 135 (1973).

(10) Zh. I. Alferov, S. A. Gurevich, R. F. Kazarinov, M. N. Mizerov, E. L. Portnoi, R. P. Seisyzn, and R. A. Suris, "Semiconductor laser with extremely low divergence of radiation," Sov. Phys.-Semicond. 4, 541 (1974).

(11) R. D. Burnham, D. R. Scifres, and W. Streifer, "Low divergence beams from grating-coupled composite guide heterostructure GaAlAs diode lasers," Appl. Phys. Lett. 26, 644 (1975).

(12) P. Zory, and L. D. Comerford, "Grating-coupled double-heterostructure AlGaAs diode lasers," IEEE J. Quantum Electron. 11, 451 (1975).

CHAPTER 5

EXPERIMENTAL TECHNIQUES

5-1 Introduction

Due to the short wavelength and the small size of optical fibers, the dimensions of the optical circuit components which need to interface with them are typically on the order of a few microns. The requirements on the precision and definition of devices are thus very strict. For example - in fabricating a dielectric waveguide, the smoothness of the sidewalls and the uniformity of the guiding layer thickness will determine whether the guide is lossy or not. This is due to the fact that the nonuniformity of the waveguide structure causes mode scattering, radiation losses, and other undesirable consequences[1]. Generally speaking - the tolerance on the waveguide sidewall smoothness should be much smaller than the guided wavelength. Another example is the fabrication of optical gratings for filters[2,3], polarizers[4], Bragg reflectors etc. where the period can be as small as 0.1 μm and is required to be uniform across a considerable length. Conventional photolithography is not suitable for this purpose. Hence new technique had to be developed to meet these requirements.

Another requirement regarding the fabrication of optical circuits is that the fabrication processes be compatible with planar technology. This will be important in integrating several optical components on one common substrate.

In this chapter we describe some of the important techniques used and developed during the course of studying GaAs distributed feedback and distributed Bragg reflector lasers. These include

liquid phase epitaxial crystal growth, holographic photolithography, chemical and ion beam etching of GaAs crystals, and some optical measurements.

5-2 Liquid Phase Epitaxy in GaAs-GaAlAs System

Liquid phase epitaxy (LPE) by definition, is the precipitation from a liquid phase of a crystalline layer onto a parent substrate where the crystallographic orientation of the layer is determined by that of the parent substrate. It is a very common method of growing semiconductor thin films for optical, acoustical, and microwave devices. The basic principle is described as follows. The solution and the substrate are kept apart in the growth apparatus (a graphite boat) prior to the growth. The solution is saturated with the growth material and heated up to a prescribed temperature. Then the solution is brought into contact with the substrate surface and allowed to cool down at a constant rate for an appropriate length of time depending on the thickness of the layer desired. If the substrate is single crystalline and the lattice constant of the precipitating material is the same or nearly the same as that of the substrate, the precipitating material forms a layer on the substrate surface which is an extension of the single crystal body of the substrate. For example in the GaAs-GaAlAs system a GaAs single crystal wafer is used as substrate and layers of GaAs or $Ga_{1-x}Al_xAs$ are grown on it. Because of the close match of the lattice constants between AlAs and GaAs, it is possible to grow layers of $Ga_{1-x}Al_xAs$ on GaAs

and vice versa with relatively low defect density.

A typical liquid phase epitaxial growth set-up is shown in Fig. 5-1(a), which consists of three major parts; a furnace, a quartz tube, and a graphite boat. The graphite boat consists of a housing unit and a slide. There are recessed areas in the slide for holding the substrates. In the housing unit there are several wells for the different melts. As an example, to fabricate a GaAs-GaAlAs double heterostructure injection laser as shown in Fig. 5-1(b) we have to grow four layers successively on an n-GaAs substrate. The wells in the graphite boat are filled with melt materials in the following sequence. Well no. 1 contains Ga, GaAs seeds, Al, and Sn. Well no. 2 contains Ga, GaAs, and Ge. Well no. 3 contains Ga, GaAs, Al and Ge. Well no. 4 contains essentially the same materials as well no. 2 except for a larger quantity of Ge. The amount of each element in the wells depends on the composition and the carrier concentration of the layer grown from it. Before the growth, the boat is assembled, the substrate and the melt materials are loaded. The boat is then inserted inside the quartz tube roughly at the center of the furnace. A quartz "pushing rod" is connected to the slide so that the latter can be moved from the outside. After purging the tube thoroughly with hydrogen the furnace is turned on and heated up to around 825°C. A constant flow of hydrogen is maintained through the tube at all times. As the temperature stabilizes and the melts are in thermal equilibrium states a biasing circuit is turned on to slowly lower the temperature of the boat

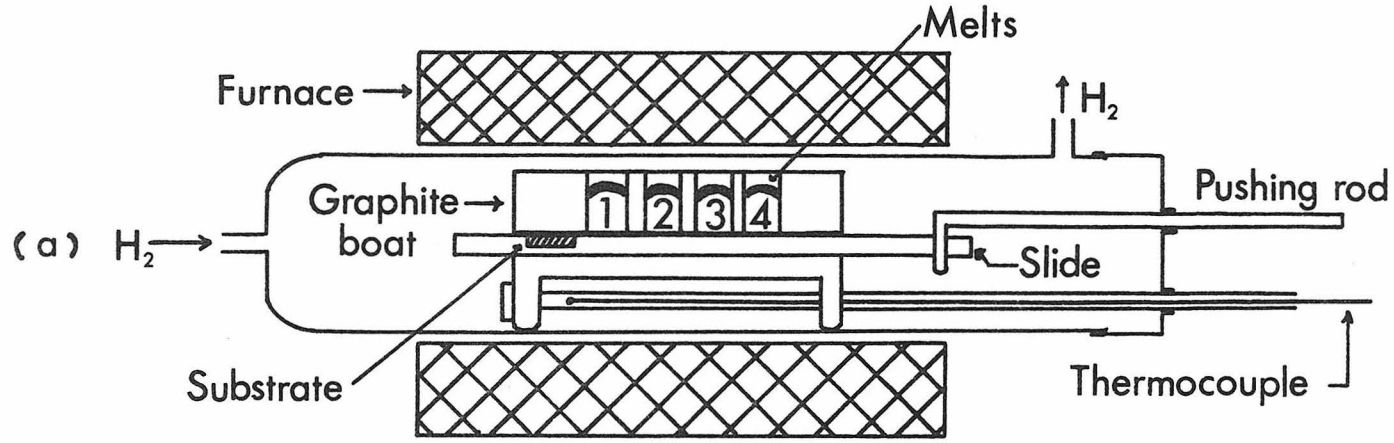

(b)

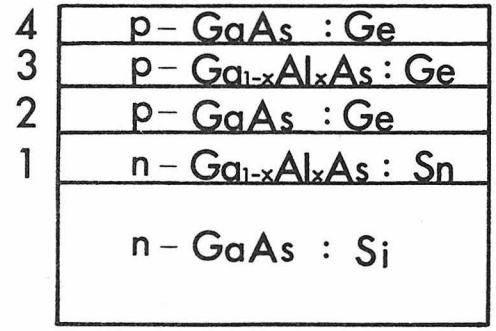

Fig. 5-1(a) A typical liquid phase epitaxial crystal growth system using horizontal three-zone furnace and sliding graphite boat.

(b) A double heterostructure GaAs injection laser structure grown by LPE.

(which is monitored by a thermocouple placed underneath the graphite boat). The cooling rate ranges from a few tenth of a degree per minute to a few degrees per minute. As the temperature drops to a prescribed value, for instance 820°C, (this is called the contact temperature) the substrate is pulled into position under the first melt. It is kept there for a period of time appropriate for the thickness of the first layer to be grown and then is moved to the next solution, and so on until the multilayer structure is grown. The substrate is then moved away from the last melt and the boat is cooled down to room temperature.

One of the main difficulties involved in crystal growth is keeping oxygen out of the growth system when the heating stage begins. At high temperatures the surface of the melts and the substrate can be easily oxidized which would prevent the growth. Also the preparation of the substrate and the melt materials has to be done carefully. Any undesirable impurity will degrade the growth. Successful crystal growth is probably the main key to the fabrication of long life cw GaAs injection lasers and other electronic devices based on GaAs epitaxy.

To fabricate a double heterostructure distributed feedback injection laser as shown in Fig. 3-23 we have to corrugate the surface of the p-GaAs active layer before growing the p-GaAlAs layer and the p-GaAs top layer. This involves the challenging problem of growing an epitaxial layer over a corrugated surface without destroying the corrugations. It has been pointed out that during epitaxial growth there is always some meltback of the substrate.

This presents a serious problem if growth over shallow corrugations is desired. We thus carried out a series of experiments by growing a layer of GaAlAs on corrugated GaAs substrates with different growth temperatures and cooling rates to determine the dependence of the amount of meltback on the growth conditions. After growth, part of the GaAlAs layer was etched away by HF and the GaAs substrate surface was examined by using scanning electron microscope (SEM) and by laser beam diffraction experiment to see whether the corrugation survived the growth. The results are summarized in Table 5-1. It was found that the epitaxial GaAlAs layer grown above 700°C on the corrugated substrate had a mirrorlike finish. A great deal of improvement in reducing the amount of meltback was achieved by lowering the contact temperature from 820°C to 700°C. A small improvement was also obtained by increasing the cooling rate from 1 to 5°C/min. The depth of the corrugation can be directly measured from the SEM pictures. It can also be estimated by measuring the relative intensity of the various orders of diffracted light from the corrugation after removing the epitaxial layer. In our work a He-Ne (6328Å) laser was used for this purpose. The diffraction efficiency, i.e., the ratio of the first order diffraction intensity to that of the input intensity in a number of samples grown under varying conditions is listed in Table 5-1. Fig. 5-2 is an SEM picture of sample A-5 after partial removal of the GaAlAs layer. The corrugation survived almost intact with only minimal meltback. The irregular edge and the small holes were caused by the penetration of HF through imperfect photoresist mask. Fig. 5-3 shows the

Sample Number	Growth Temperature Range (°C)	Cooling Rate (°C/min)	Final Corrugation Height Peak to Peak (Å)	Diffraction Efficiency
A-1	820 - 810	1	< 100	5×10^{-4}
A-2	820 - 810	5	100	1×10^{-3}
A-4	750 - 720	5	400	4×10^{-2}
A-5	700 - 670	5	500	8×10^{-2}
Before Growth			580	1×10^{-1}

Table 5-1 Summary of the Experimental Results of Liquid Phase Epitaxy on Corrugated Substrate.

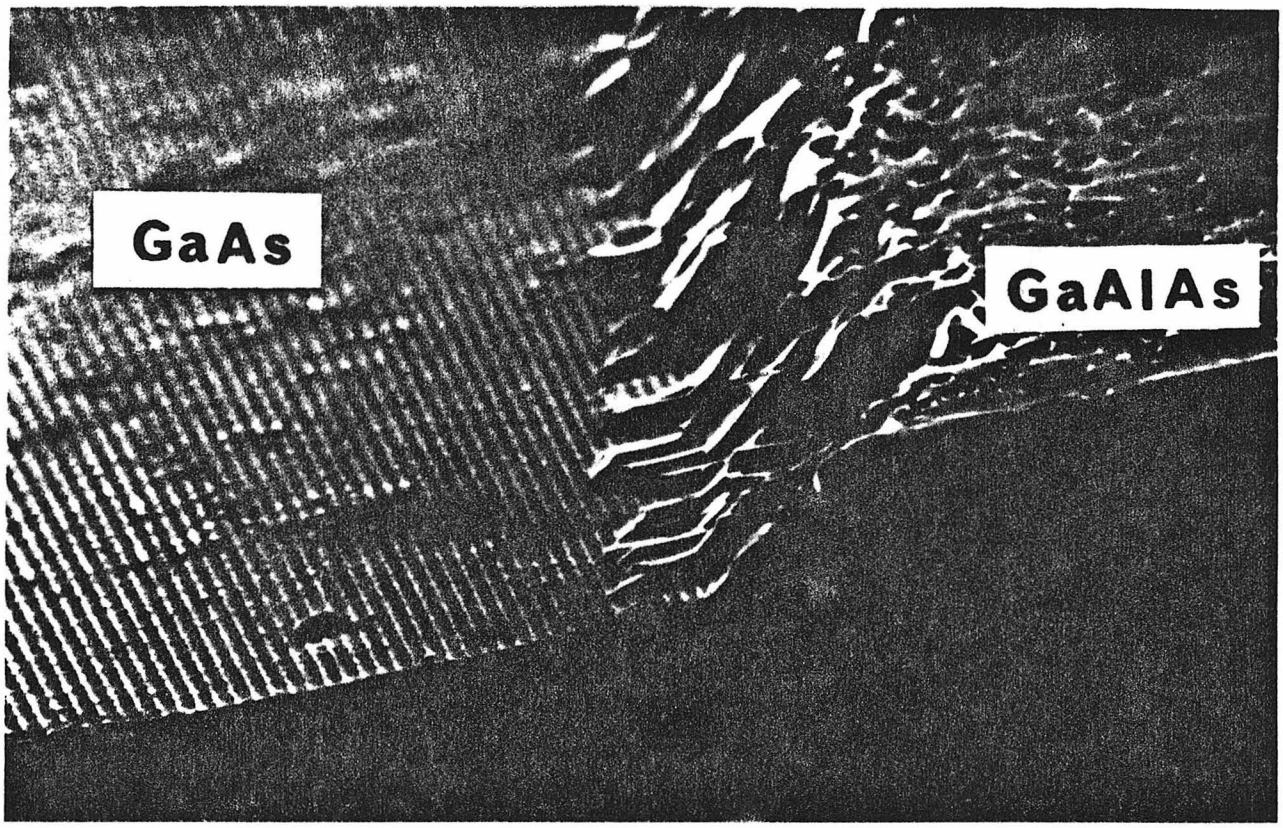

Fig. 5-2 An SEM picture of sample A-5 with the top GaAlAs layer partially etched away.

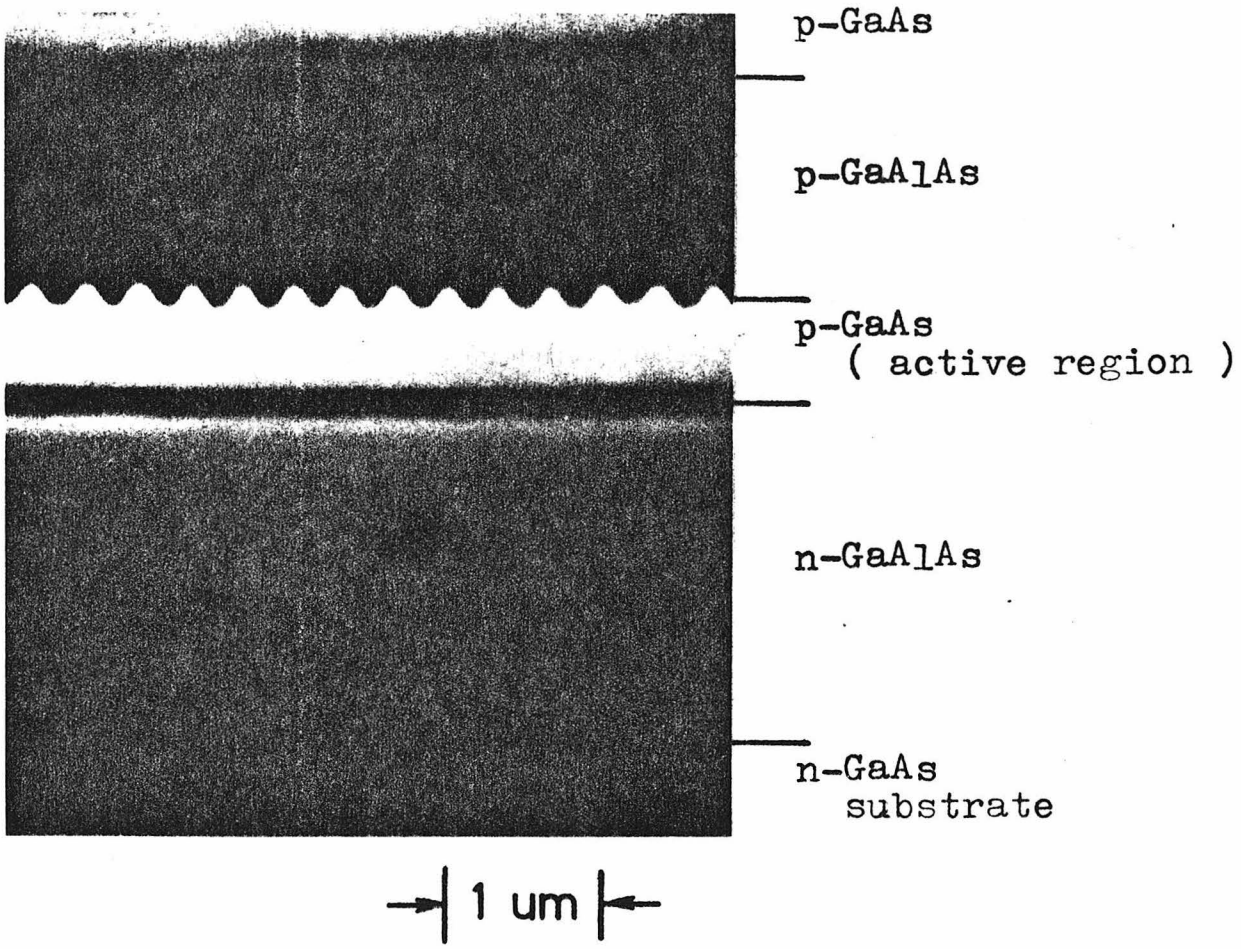

Fig. 5-3 Cross section of a double heterostructure GaAs-GaAlAs distributed feedback laser grown by LPE.

cross section of a completed double heterostructure distributed feedback injection laser which shows excellent growth interfaces.

5-3 Grating Fabrication by Holographic Photolithography

Small period (<1 μm) gratings have been widely used in integrated optics as couplers, filters, and reflectors. For these applications the grating period ranges from ∿0.1 μm to ∿1 μm. It is difficult for ordinary photolithography to fabricate this kind of pattern because of the tight spacing. Hence a maskless exposure process--holographic photolithography[5] was developed for this purpose and is described in what follows.

Two plane waves of the same frequency and of amplitudes E_1 and E_2 are incident upon a smooth surface at an angle 2θ as shown in Fig. 5-4. Taking the complex amplitudes of the waves across the surface as

$$E_1 = Ae^{-ik(x\sin\theta - y\cos\theta)}$$

$$E_2 = RAe^{-ik(-x\sin\theta - y\cos\theta) - i\phi}$$

respectively we find that the intensity on the surface is

$$|E_1+E_2|^2_{y=0} = |A|^2\{(1-R)^2 + 4R\cos^2(kx\sin\theta-\phi)\}$$

$$= |A|^2\{1 + R^2 + 2R\cos 2[kx\sin\theta-\phi]\} \qquad (5\text{-}1)$$

The intensity is thus modulated in the x direction with a period

$$\Lambda = \frac{2\pi}{2k\sin\theta} = \frac{\lambda}{2n\sin\theta} \qquad (5\text{-}2)$$

where n is the index of refraction of the medium in which the waves meet over the surface and λ is the vacuum wavelength of the waves. Equation (5-1) shows that as long as ϕ, the phase difference between E_1 and E_2 is constant (not a function of time) the interference pattern will remain stationary in space. Furthermore if R = 1, i.e., E_1 and E_2 have equal intensities, then

$$|E_1+E_2|^2_{y=0} = 4|A|^2\cos^2(k\sin\theta x-\phi)$$

This means that the intensity modulation is 100%. If $R \neq 1$ there will be a lift-up of the nodes plus a reduction of the peak to valley intensity difference. Fig. 5-4(b) shows the intensity distribution of the interference pattern with different values of R. If we place a sample coated with photoresist at the y = 0 plane, the photoresist will be exposed by the interference fringes whose intensity is shown in Fig. 5-4(b). The intensity distribution associated with R = 1 is ideal for this purpose. After developing the exposed photoresist we obtain a grating pattern.

So far we have not considered the effect of the substrate. Most of the substrates used in practice are highly reflective. As a result we have to consider the total field of two incident waves and their reflected waves. Assuming the substrate has 100% reflectivity, for incident waves with electric field polarized in the z direction the total intensity is given by[6]

$$I \propto \sin^2\left(\frac{2\pi n\cos\theta y}{\lambda}\right)\cos^2\left(\frac{2\pi n\cos\theta x}{\lambda}\right)$$

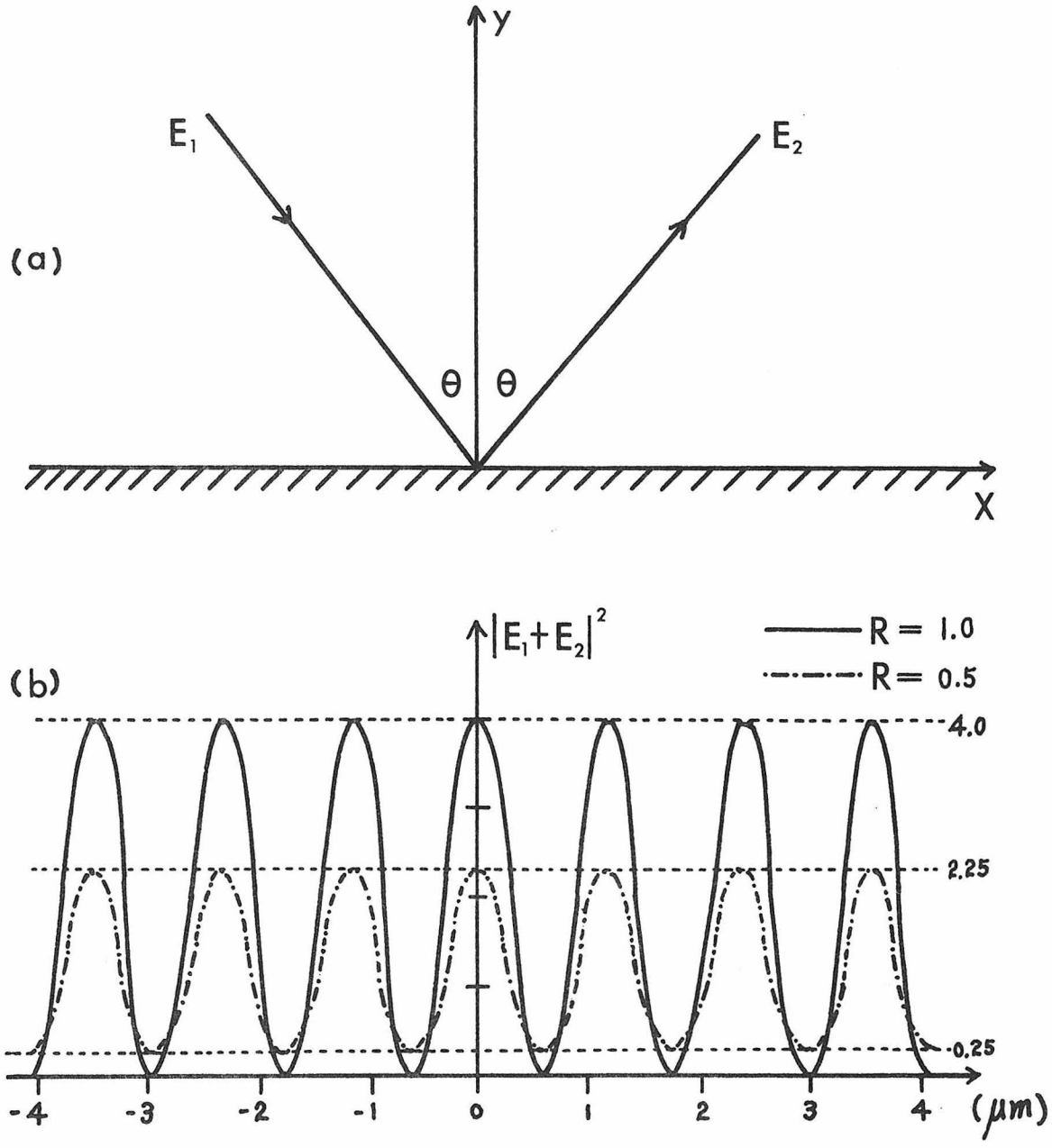

Fig. 5-4 (a) The coordinate system that describes the interference of two plane waves.

(b) Plots of intensity distribution $|E_1+E_2|^2_{y=o}$ along x. The parameters are taken as $\phi = 0$, $\theta = 11°$, $\lambda = 0.4416$ μm, and $|A| = 1$.

Which consists of a standing wave in the y-direction, in addition to that in the x direction, with a period

$$\Lambda_y = \frac{\lambda}{2n\cos\theta}$$

This periodic intensity variation in the y-direction has an important effect on the exposure time of the photoresist. If the photoresist surface is close to one of the nodal planes, there will be no fringes recorded on the surface of the photoresist. The subsequent development will not give a grating pattern. Ideally the photoresist thickness should never exceed

$$t = \frac{\lambda}{2n\cos\theta} = \Lambda_y$$

Otherwise it is difficult to develop the photoresist down to the substrate surface.

Fig. 5-5 is a schematic diagram of the experimental set-up used to fabricate the gratings. The output of a He-Cd laser is divided into two beams by a dielectric beam splitter. Each beam is reflected from a mirror and passes through a spatial filter. The mirrors are set so that the laser beams intersect at an angle 2θ at the sample holder. A spatial filter is inserted after each mirror. The spatial filter consists of a quartz lens and a 12.5 μm diameter pinhole. The beam is focused by the lens and made to pass through the pinhole which is located at the focal point of the lens. The purpose of the spatial filters is to ensure that the beams coming out of the pinholes possess a high degree of spatial coherence. (This is achieved by limiting the transmission to essentially the lowest order Gaussian

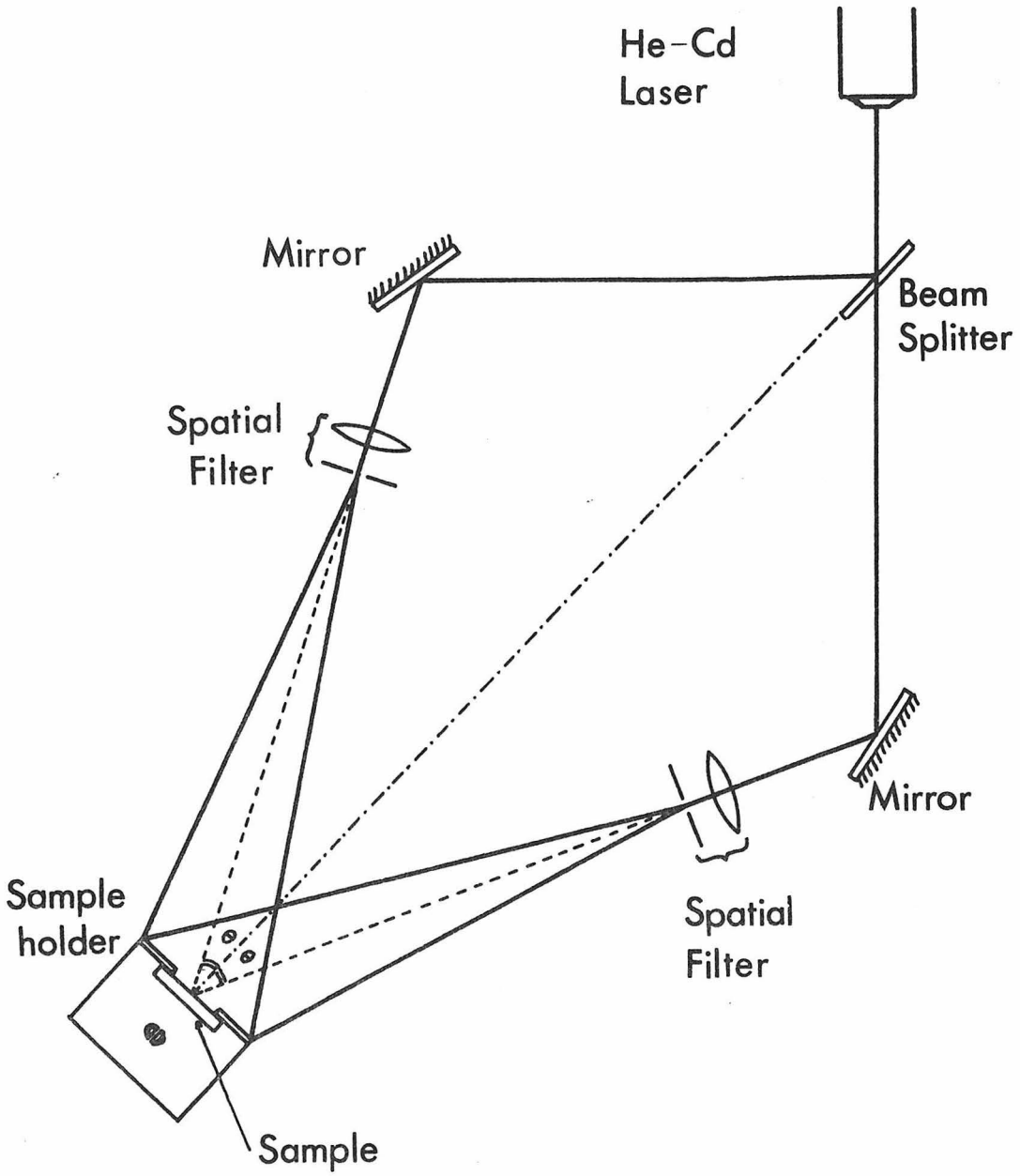

Fig. 5.5 A schematic diagram of the grating exposure set-up.

transverse component). The beams emerging from the pinholes are divergent. In most experimental situations the distance between the pinholes and the sample is large and the sample area is small so that at the sample surface the beams have essentially planar wavefronts. The advantage of this arrangement is that it does not require very high quality mirrors since mirror defects are "cleaned up" by the spatial filters. This is especially important at shorter laser wavelengths where high quality mirrors do not exist. A drawback, however, is that each time that the angle 2θ is changed the spatial filters need to be realigned. If spatial filters are placed in front of the mirrors the problem of angle changes is alleviated but high quality mirrors must be used.

The key for obtaining high quality grating patterns is good optical alignment (i.e. equal incidence angles for both beams). This can be checked by putting a highly reflective test sample in the sample holder. If the system is well aligned, the reflected beam of one of the incident beams from the test sample will coincide with the other incident beam and vice versa.

As an example, to make a grating of $\Lambda = 3500\text{Å}$ the angle θ is determined from equation (5-2). If we use the blue output of an He-Cd laser λ is 4416Å hence $\theta = 39.1°$. Theoretically the smallest grating period that can be made by this interference method is $\Lambda = \frac{\lambda}{2}$ when $\theta = 90°$.

The shortest wavelength cw laser available to date is $\lambda = 3250\text{Å}$ from an He-Cd laser. Thus the smallest Λ obtainable is 1625Å. In section 3-7 we showed that for the first order distributed feedback

oscillation in GaAs a period Λ = 0.1184 μm is required. The shortest obtainable period Λ = 0.1625 μm is thus too big for our purpose. However the above limitation exists only for exposures performed in air (or vacuum). If one uses a medium with an index n then the shortest Λ is $\lambda/2n$. For example one can use a quartz block or a bath of high index liquid[7,8,9]. Fig. 5-6(a) shows a configuration in which a quartz block is used for producing 0.11 μm period grating. The quartz prism is attached to the sample with the help of some index matching fluid (immersion oil, xylene, etc) so that the light can couple out of the prism. The index of refraction of the quartz $n_q \approx 1.5$. Using λ = 3250Å, θ = 70° we have Λ = 1153Å. A variation of this method is shown in Fig. 5-6(b). Here the sample is immersed in a tank filled with xylene ($n \sim 1.5$). The tank has two low loss optical flats, one on each side, for the access of the incident beams.

Before depositing the grating photoresist mask on GaAs wafers we first have to thoroughly clean the surface of the GaAs samples. This is usually done by rinsing in warm trichloroethylene (TCE) acetone, 2-propanol, and deionized water. The samples are subsequently etched slightly in H_2SO_4:H_2O:H_2O_2(4:1:1) solution. After dry blowing the samples are kept in a dust free dish and baked in an oven (90°C) for about 10 minutes.

Shipley photoresist (AZ 1350B) is diluted (one part photoresist to two parts thinner) and coated on the samples by spinning. The thickness of the photoresist layer is estimated to be ~1500Å. The photoresist-coated samples are then prebaked for about 10 minutes at 90°C. In our exposure system the typical optical intensity at

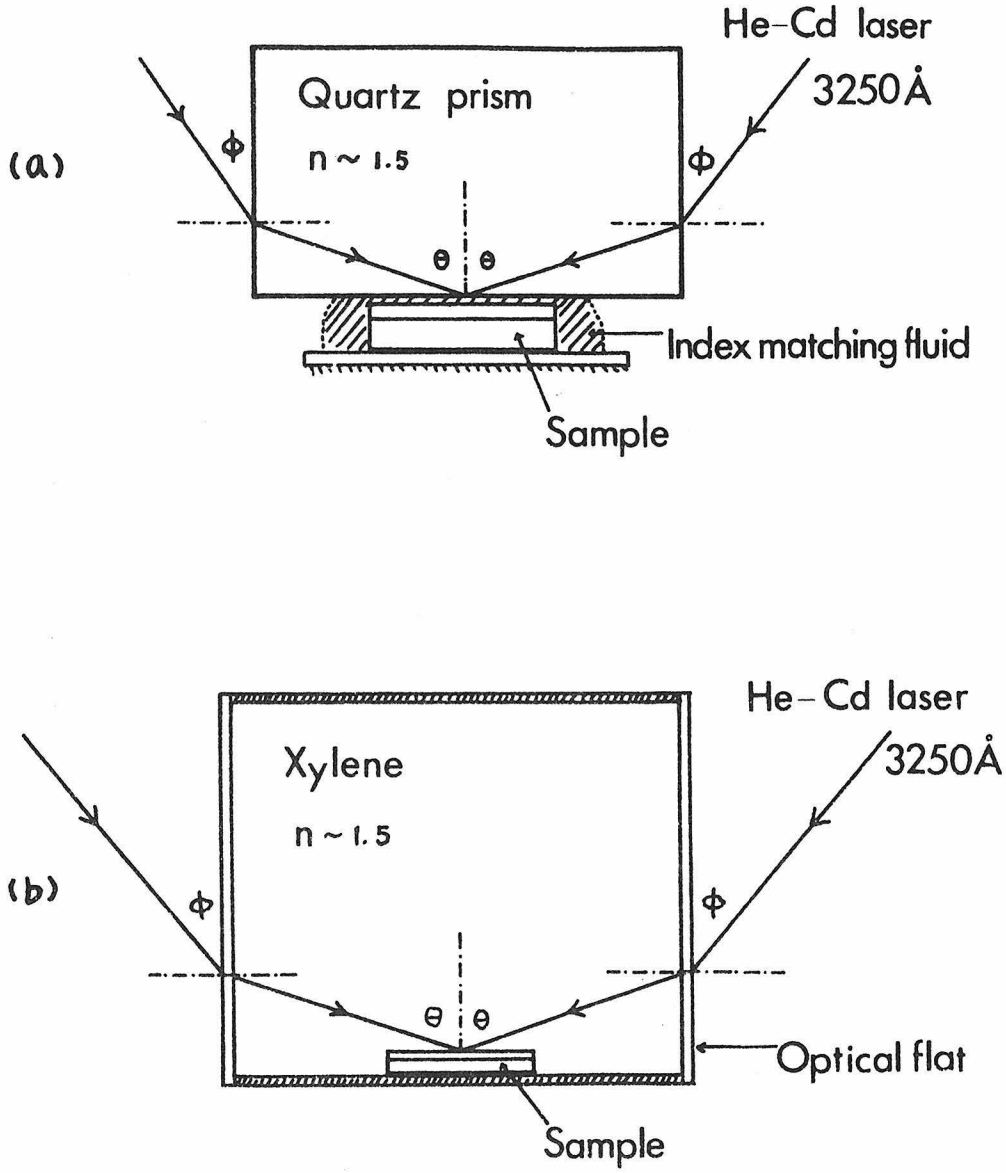

Fig. 5-6 Experimental configurations for producing gratings with periods from 0.1 μm to 0.16 μm.

the sample is ∿4 mw per beam. The exposure time is around 15 seconds. The developing time is fixed at 10 seconds. In some cases the photoresist gratings are slightly over-exposed in order to develop the fringe patterns all the way to the substrate surface. This leads to better result during the subsequent chemical etching or ion beam etching. Grating quality can be determined by visual inspection of the film color or by measuring the efficiency as a diffraction grating.

5-4 Ion Beam Milling and Chemical Etching of GaAs Gratings

We employed two methods of transferring a photoresist grating onto a GaAs substrate. One is a dry process while the other is a wet process. In the dry process ion beam etching[5,10,11,12] is used and in the wet process chemical etching is used. The basic principle of ion beam etching is as follows. An inert gas (e.g. Argon) is fed into a high vacuum chamber and ionized through an electrical discharge. These heavy ions are collimated and accelerated to impinge on the sample surface. The high energy (typically 0.5 keV - 5 keV) particles cause sputtering ejection of the sample material. The samples can be masked to allow the etching of different patterns. If the masking material has a lower etching rate than the substrate material, patterns can be transferred from the mask to the substrate.

The relative etching rates of photoresist and GaAs have been studied by several investigators[10,11,12]. Typical values reported are around a 1 to 3 ratio. With this differential etching rate it is possible to etch patterns into GaAs using photoresist as a mask.

Photoresist masks are usually baked prior to the etching process to increase their strength. The samples are mounted on a stainless steel plate using Ni clips or vacuum grease. During etching, a motor is used to provide a translational motion of the samples across the ion beam for uniform etching. With an ion current density of $\sim$1 mA/cm^2 and an accelerating voltage of $\sim$0.7 kv the typical etching time for GaAs gratings is 3-5 minutes.

The photoresist mask subjected to the ion beam etching sometimes becomes very hard and difficult to dissolve by the conventional immersion in acetone. However, it can be removed by scrubbing with a swab soaked with acetone or by immersing in a mixture of AZ-303 developer ($\sim$20 c.c.) and KOH (a few drops).

Typical SEM photographs of GaAs gratings fabricated by ion milling through photoresist masks are shown in Fig. 5-7 and 5-8. Fig. 5-7 shows a surface corrugation with a period $\sim$0.35 μm. It has well defined patterns with a corrugation depth estimated to be around 700Å. In Fig. 5-8 we show a grating with a period $\sim$0.115 μm produced by ion milling through a photoresist mask. The poor surface quality is probably due to the nonuniformity in the photoresist mask after development.

In general, the results of ion beam etched gratings are quite satisfactory. There are some methods that one can use to increase the depth of the corrugation. For example one can "shadow" the photoresist grating by evaporating a thin film of some low etching rate metal at a shallow angle. This can increase the endurance time of the mask.

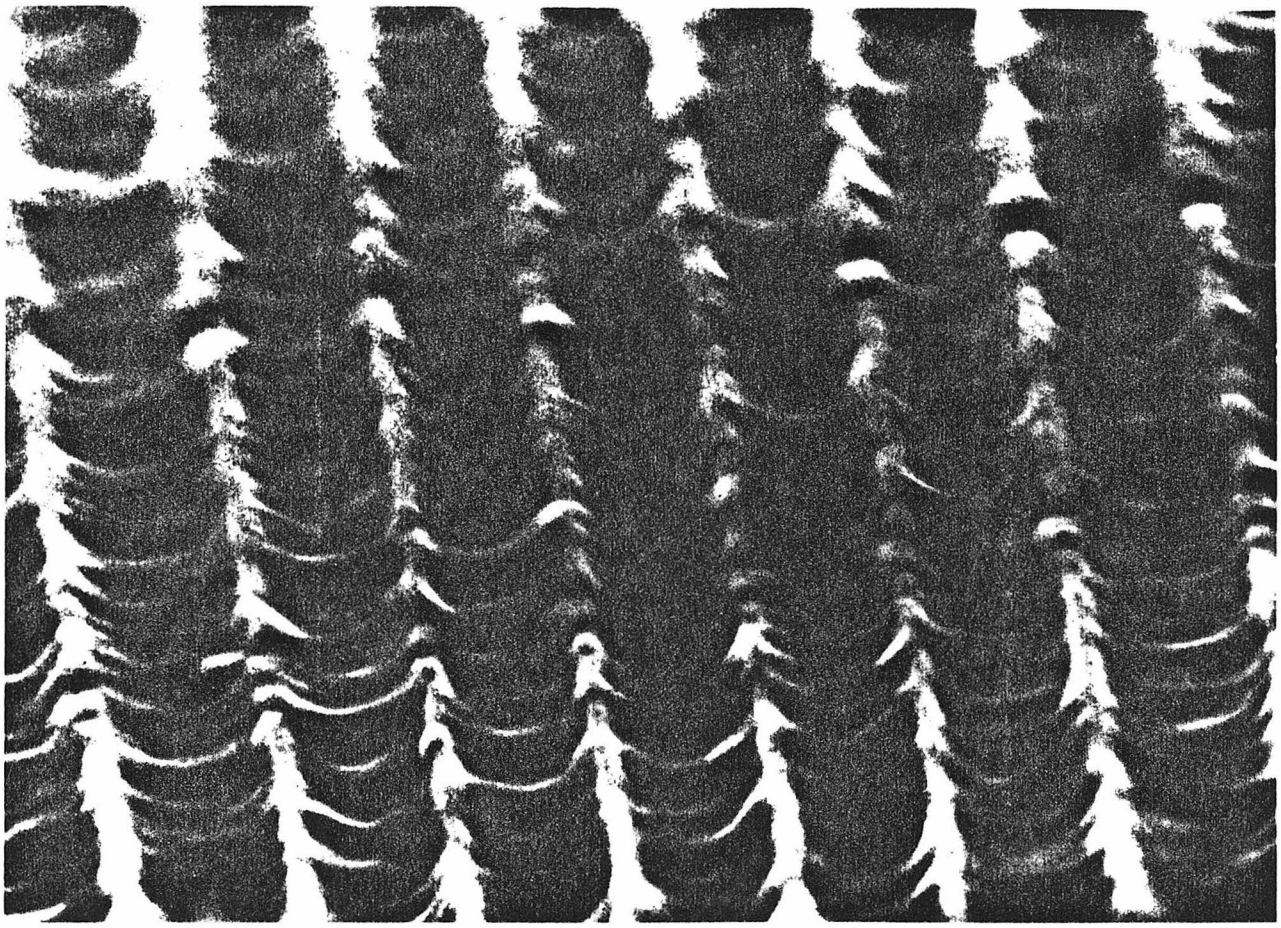

Fig. 5-7 An SEM picture of a GaAs surface corrugation produced by ion beam etching through a photoresist mask. The period is $\sim$ 0.35 μm.

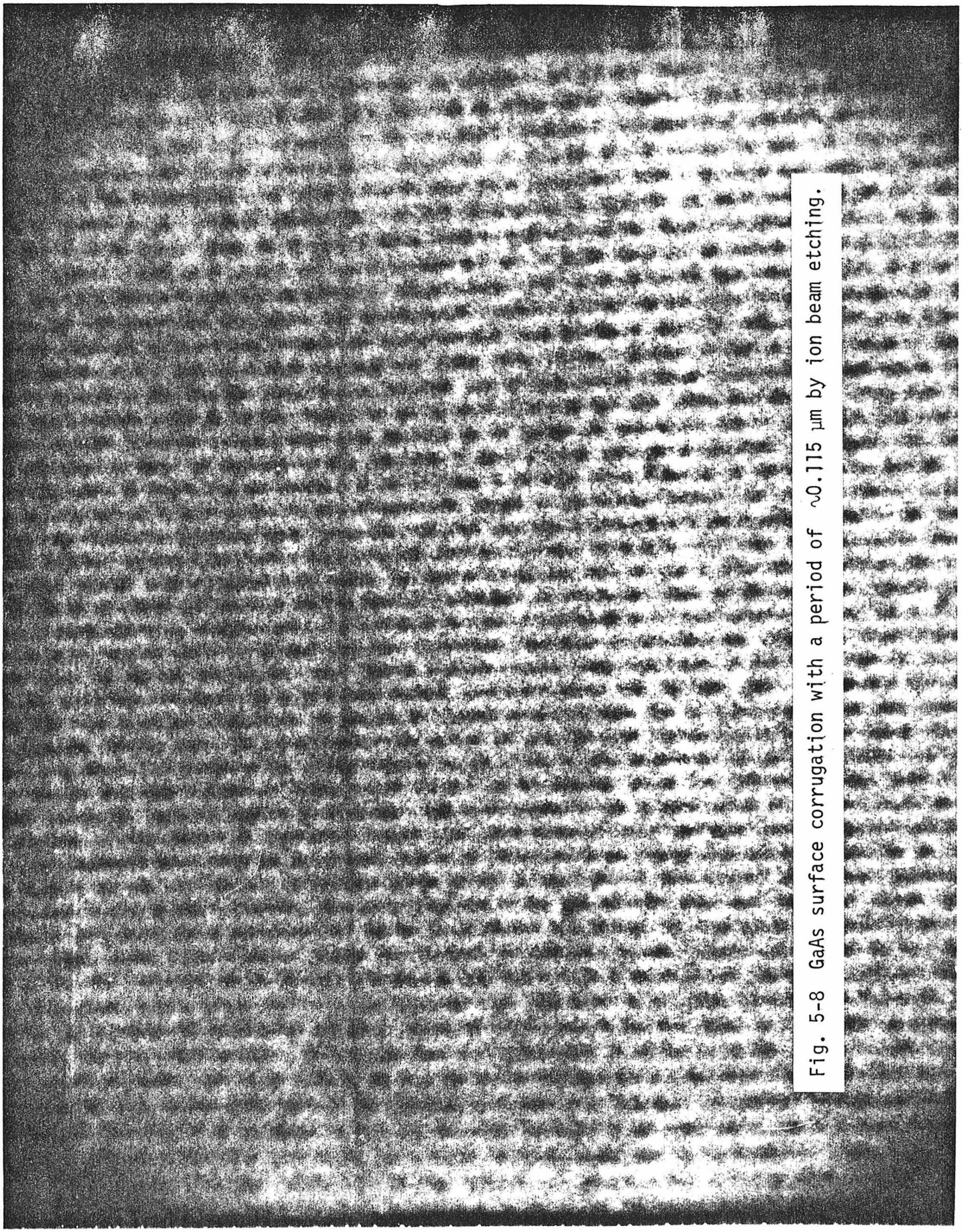

Fig. 5-8 GaAs surface corrugation with a period of ~0.115 μm by ion beam etching.

In ion milling the removal of material is achieved by bombardment with energetic particles. As a result the process introduces a high density of defects in the samples. These defects cause an increase in the threshold current of the GaAs double heterostructure distributed feedback lasers as described in Chapter 3. As an alternative approach we investigated the possibility of using chemical etching. The selective chemical etching properties of GaAs crystal have been studied extensively[13,14]. It has been found that the Br_2-CH_3OH (1:1000 in volume) system gives good results in preferential etching of GaAs. If a slot mask is deposited on a GaAs crystal {100} plane and aligned parallel to one of the two cleavage faces ({01$\bar{1}$} or {0$\bar{1}\bar{1}$}) the etched pattern can have one of two different types of groove profiles depending on the orientation of the mask. This is illustrated in Fig. 5-9(a). In these two types of grooves the side walls are all A{111} crystal planes of GaAs. This is because the etching rate of this plane is much lower than any other low Miller indices planes. As a result the v-shaped groove is essentially self-terminating while the other kind of groove diverges. For the purpose of grating fabrication we prefer the v-groove profile[15]. The direction of the mask slots for this groove can usually be determined by etching a "cross" pattern in a small part of the sample. The A{111} planes make an angle of 54°44' with the {100} planes. Hence in making gratings by chemical etching the maximum depth achievable is roughly

$$h = \frac{\Lambda}{2} \tan 54°44'$$

or

$$h = 0.71\Lambda$$

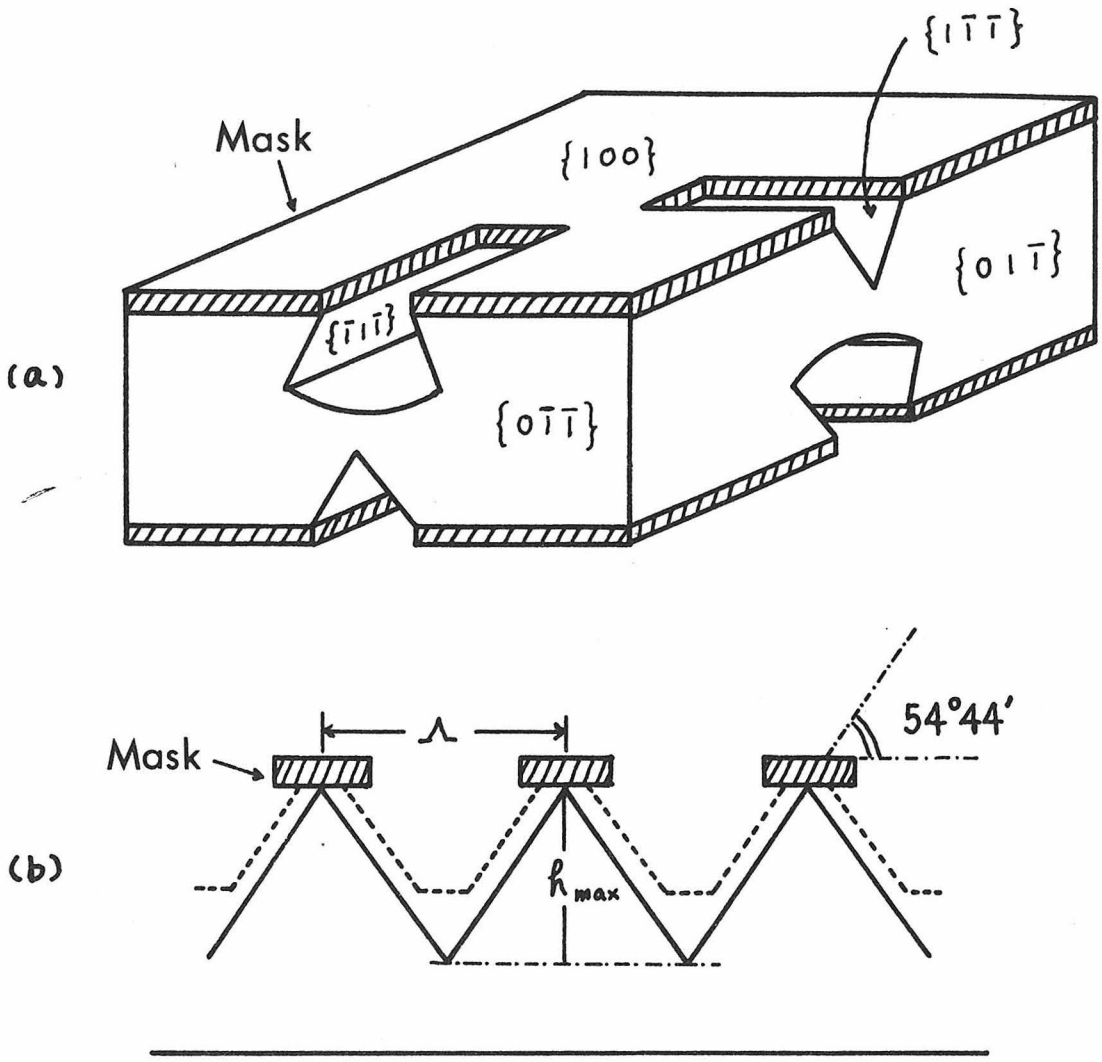

Fig. 5-9 (a) The preferential etching patterns on the {100} face of a GaAs crystal.

(b) A schematic diagram shows the relation between the grating period Λ and the V-shaped groove maximum depth h_{max}.

For Λ = 0.35 μm, this comes out to be ∿2500Å and for Λ = 0.11 μm, h_{max} is ∿780Å as illustrated in Fig. 5-9(b). This is based on the assumption that we can get a symmetrical triangular profile. Some of the corrugations fabricated by this method are shown in Fig. 5-10 and 5-11. Fig. 5-10 is an SEM picture of a GaAs grating with a period of ∿0.345 μm and depth of ∿0.18 μm. It shows clearly the crystal planes and the etched v-shaped profile. Fig. 5-11 is a picture of a grating with period ∿0.11 μm which shows good surface quality as compared to the ion-milled grating (Fig. 5-8). The depth of this grating is estimated to be ∿500Å. Although Br_2-CH_3OH system attackes photoresist, it is still possible to etch gratings into GaAs with deep grooves without a special treatment. One can also shadow the photoresist for better results[15]. Other etching solutions that do not attack photoresist can also be used.

Regardless of the etching method employed it is important that the photoresist grating mask be developed down to the surface of the sample for best result. It has been explained in section 5-3 that because of the large index of refraction of GaAs the standing wave pattern in the y-direction [see Fig. 5-4(a)] has a minimum at the surface of the substrate. As a result the photoresist cannot be developed away completely and a thin film is left between fringes as illustrated in Fig. 5-12(a). If the grating period is large (e.g. $\Lambda \sim$ 3500Å) we can over develop the photoresist slightly to obtain a mask as shown in Fig. 5-12(b). In fabricating the very short 0.11 μm gratings this procedure is difficult to control. However we can use ion beam milling to shape the photoresist grating prior to chemical

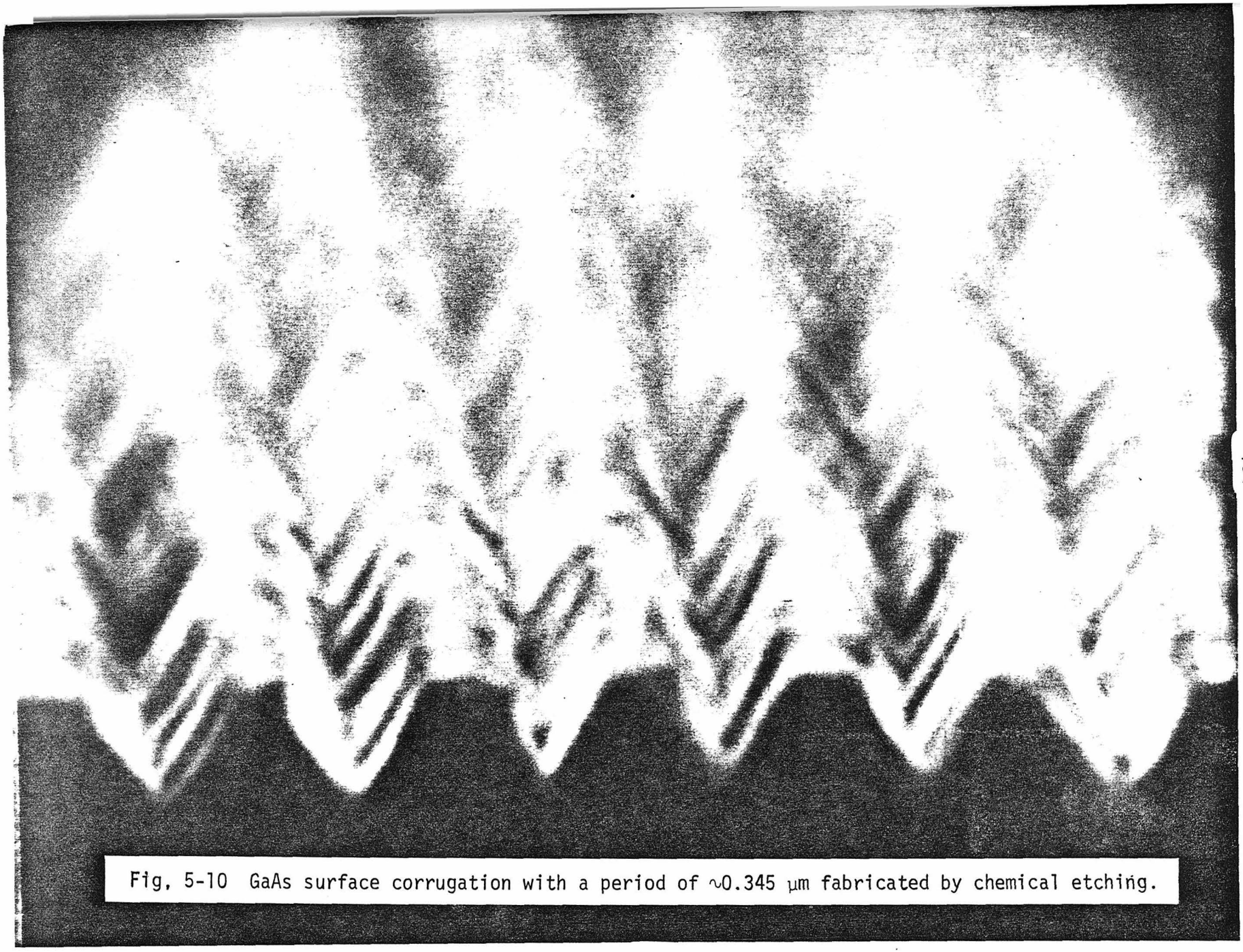

Fig. 5-10 GaAs surface corrugation with a period of ~0.345 μm fabricated by chemical etching.

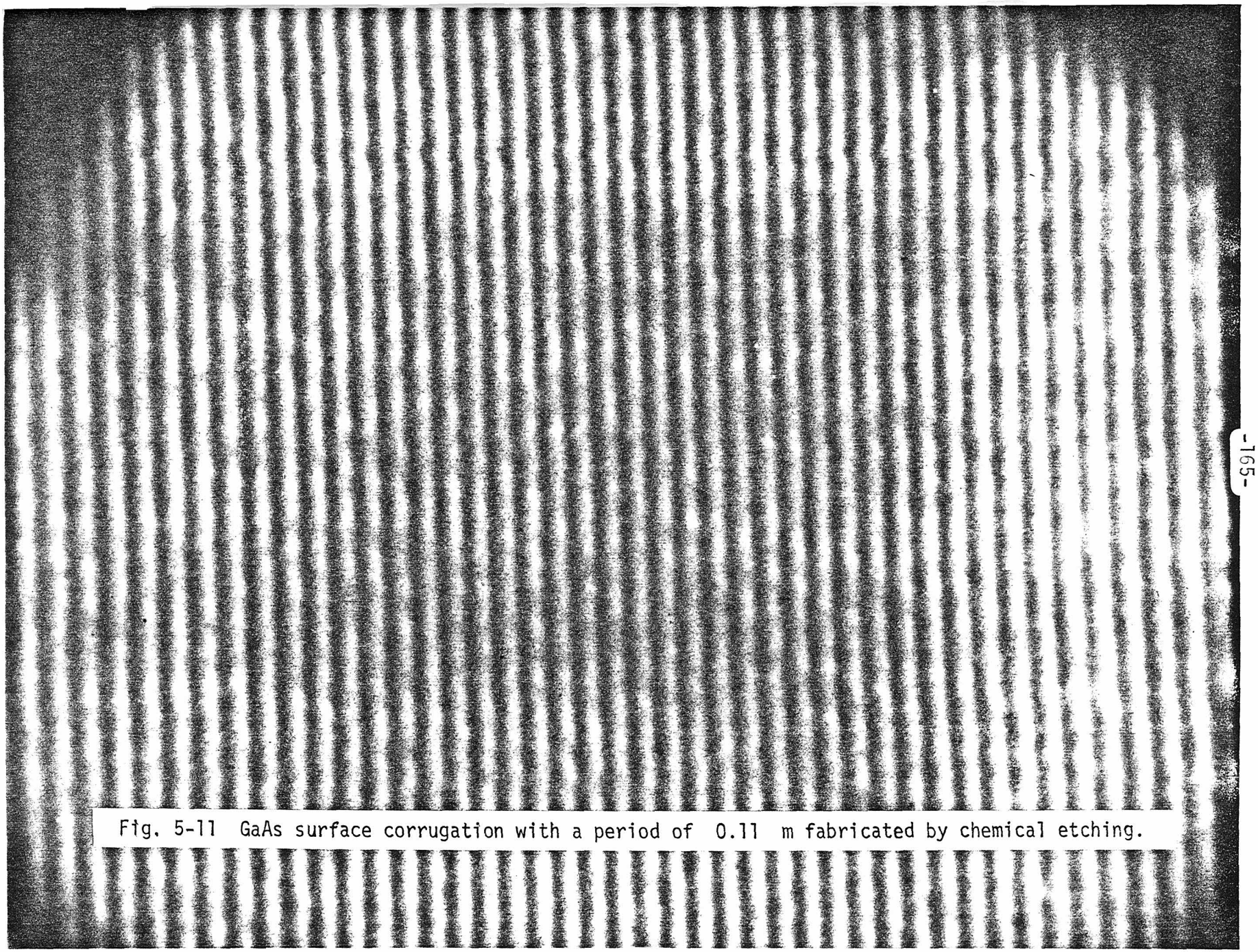

Fig. 5-11 GaAs surface corrugation with a period of 0.11 m fabricated by chemical etching.

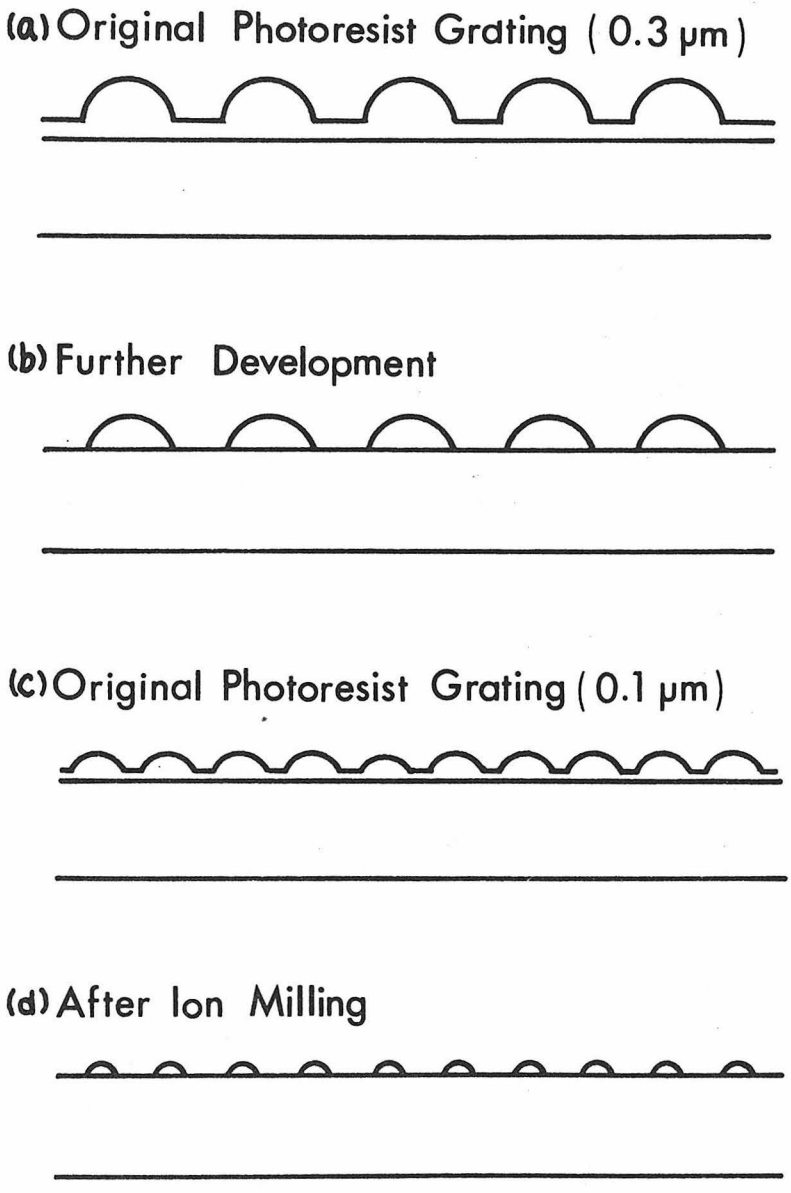

Fig. 5-12 Schemes of shaping photoresist gratings mask for chemical etching.

etching. This is illustrated in Fig. 5-12 (c) and (d).

5-5 Optical Measurements

In this section we describe a few important measuring techniques used in our study of GaAs distributed feedback and distributed Bragg reflector lasers. These include the characterization of GaAs epitaxial layers as an active device material, the determination of the aluminum content in a GaAlAs layer, the determination of GaAs distributed feedback laser parameters, and the measurement of grating period by laser beam diffraction.

Photoluminescence measurement is a very common technique for material characterization in semiconductors. By measuring the spectral location of the luminescence peak we can obtain information concerning the energy band structure of the sample. Since the bandgap energy of GaAlAs is a function of the mole fraction of Al in the material we can thus apply the luminescence measurement results to obtain an estimate of the amount of Al in the material. This process is important because a precise control of the Al content in an epitaxial layer is difficult. An example of determining the composition of a multi-layer structure is shown in Fig. 5-13(a). We first etch a small part of the sample so as to obtain a "staircase" as in Fig. 5-13(b). Each step corresponds to one of the layers. We next measure the photoluminescence spectrum from each step in a system similar to that shown in Fig. 3-18. The pumping beam is focused by a convex lens to a small spot on the sample surface which is tilted at an angle of $\sim 45°$ with respect to the pumping beam. The output from the surface of the sample is collected

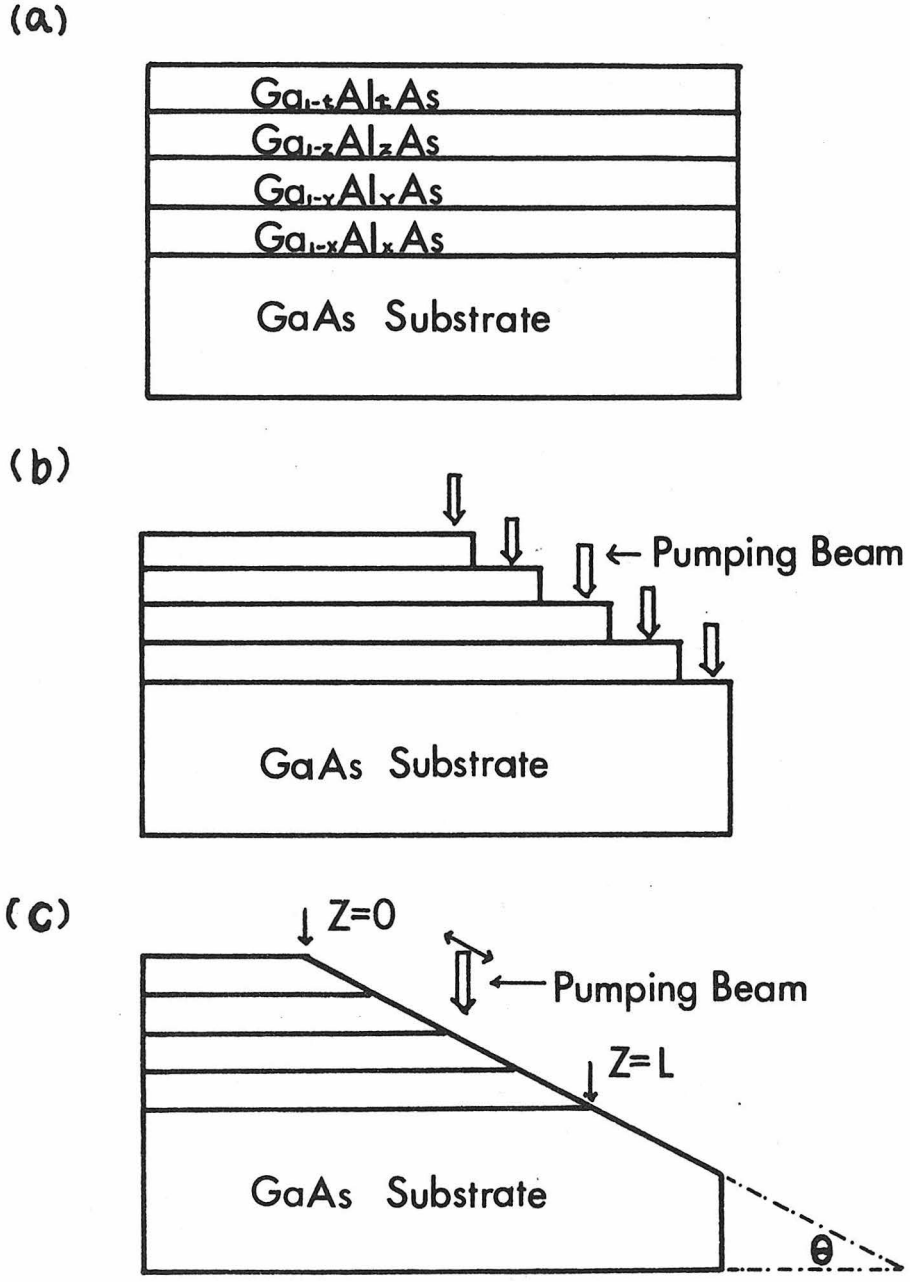

Fig. 5-13 Schematic diagrams showing two different ways of preparing samples for photoluminescence measurement.

by a lens and guided into a spectrometer. If the composition profile of each layer is needed we can perform angle lapping of the sample so that the thickness of the layer is "amplified" by a factor of $1/\sin\theta$ where θ is the angle of lapping. This is illustrated in Fig. 5-13(c). The small pumping spot is scanned from $z = 0$ to $z = L$ and the corresponding luminescence spectra are used to obtain the concentration of Al as a function of z. This information is then used to obtain the profile of Al content within each layer. The dependence of peak luminescence wavelength on the mole fraction of Al is given[16] in Fig. 5-14.

As mentioned in section 3-7, given a GaAs waveguide prior to fabricating a distributed feedback laser we need first to take a luminescence measurement in order to locate the center of the gain spectrum. At the same time, by measuring the magnitude of the luminescence output intensity we obtain an indication of the relative internal quantum efficiency of the sample. A low radiative recombination efficiency usually means that the sample contains a high density of defects which act as traps of the carriers. Thus by scanning the pumping spot across the surface of a sample we can map the relative defect density of the sample.

In the next paragraph we will describe how the optical pumping method can be used to determine some distributed feedback laser parameters.

Recall in section 3-7 that we gave the threshold gain of a distributed feedback laser as

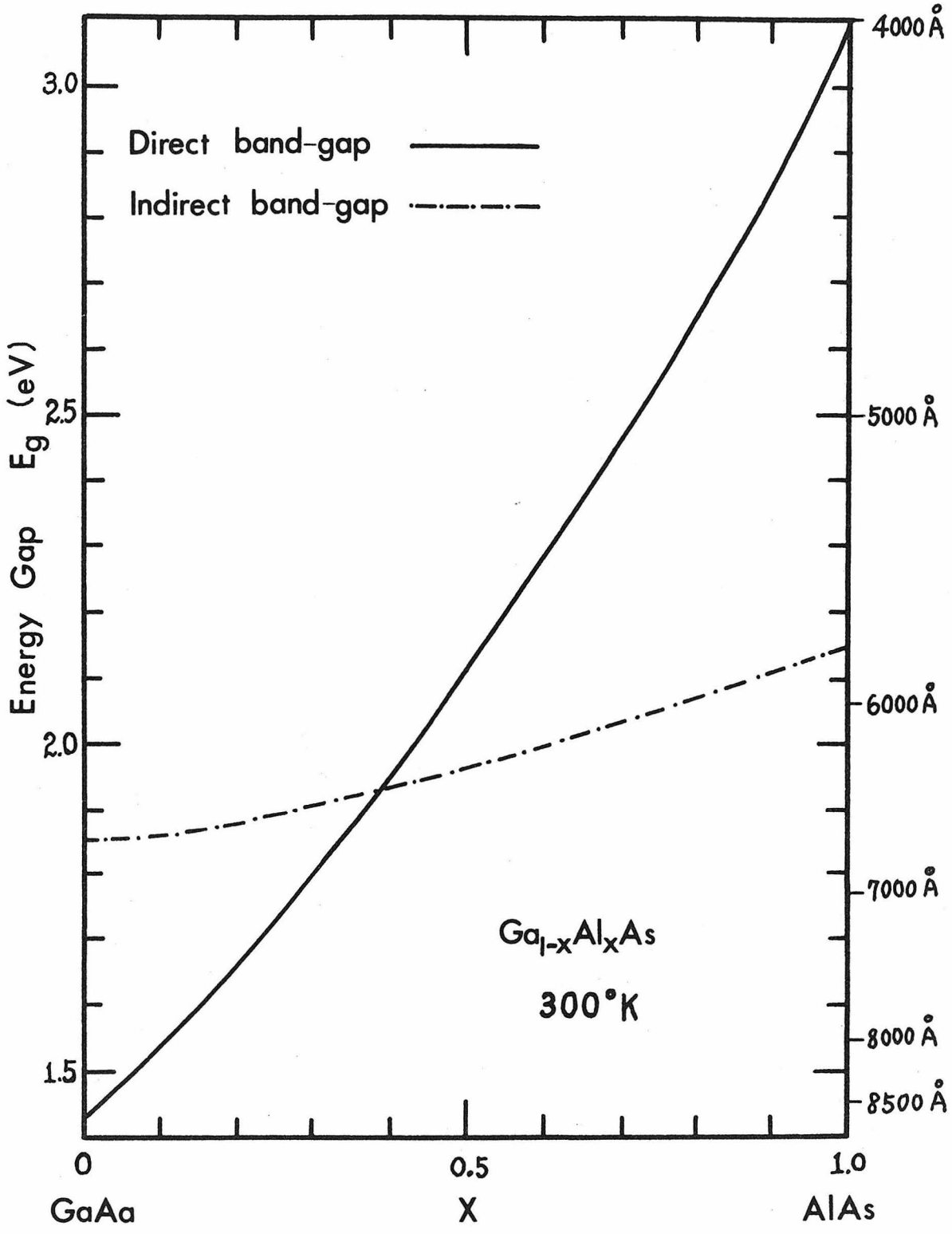

Fig. 5-14 Band-gap energy of $Ga_{1-x}Al_xAs$ against composition.

$$\alpha_{th} = \alpha_{th}^{o}(\kappa,L) + \alpha_{bulk} + \alpha_{rad}$$

where $\alpha_{th}^{o}(\kappa,L)$ is the intrinsic threshold gain of a distributed feedback laser, α_{bulk} and α_{rad} are the amplitude absorption and radiation coefficients respectively. In an experiment we measure α_{th} as the "true" threshold of our laser. In order to compare with the theory we have to know α_{bulk} and α_{rad} (at the lasing wavelength). As shown in Fig. 5-15(a) we optically pump a corrugated GaAs waveguide with a beam of constant width and of fixed length ℓ_o. We then measure the output power P as a function of ℓ, the distance between the crystal edge and the pumped region. The output power is related to the internally generated power P_o through the relation

$$P = P_o e^{-2\alpha_{corr}\ell}$$

where α_{corr} is the overall amplitude loss coefficient of a corrugated waveguide and can be expressed as

$$\alpha_{corr} = \alpha_{bulk} + \alpha_{rad} \qquad (5\text{-}3)$$

The magnitude of α_{bulk} is estimated in a similar manner except that an uncorrugated region is used so that $\alpha_{rad} = 0$. This is shown in Fig. 5-15(b). Another method of determining α_{bulk} is by manufacturing GaAs Fabry-Perot lasers of various lengths from the same waveguide and measuring their threshold pumping intensity. Since in a Fabry Perot laser the threshold gain is given by

$$\alpha_{th} = \alpha_{bulk} + \frac{1}{L} \ell n \frac{1}{R}$$

where L is the length of the laser and R is the intensity reflectivity of the cleaved mirrors. If we plot α_{th} as a function of 1/L we obtain

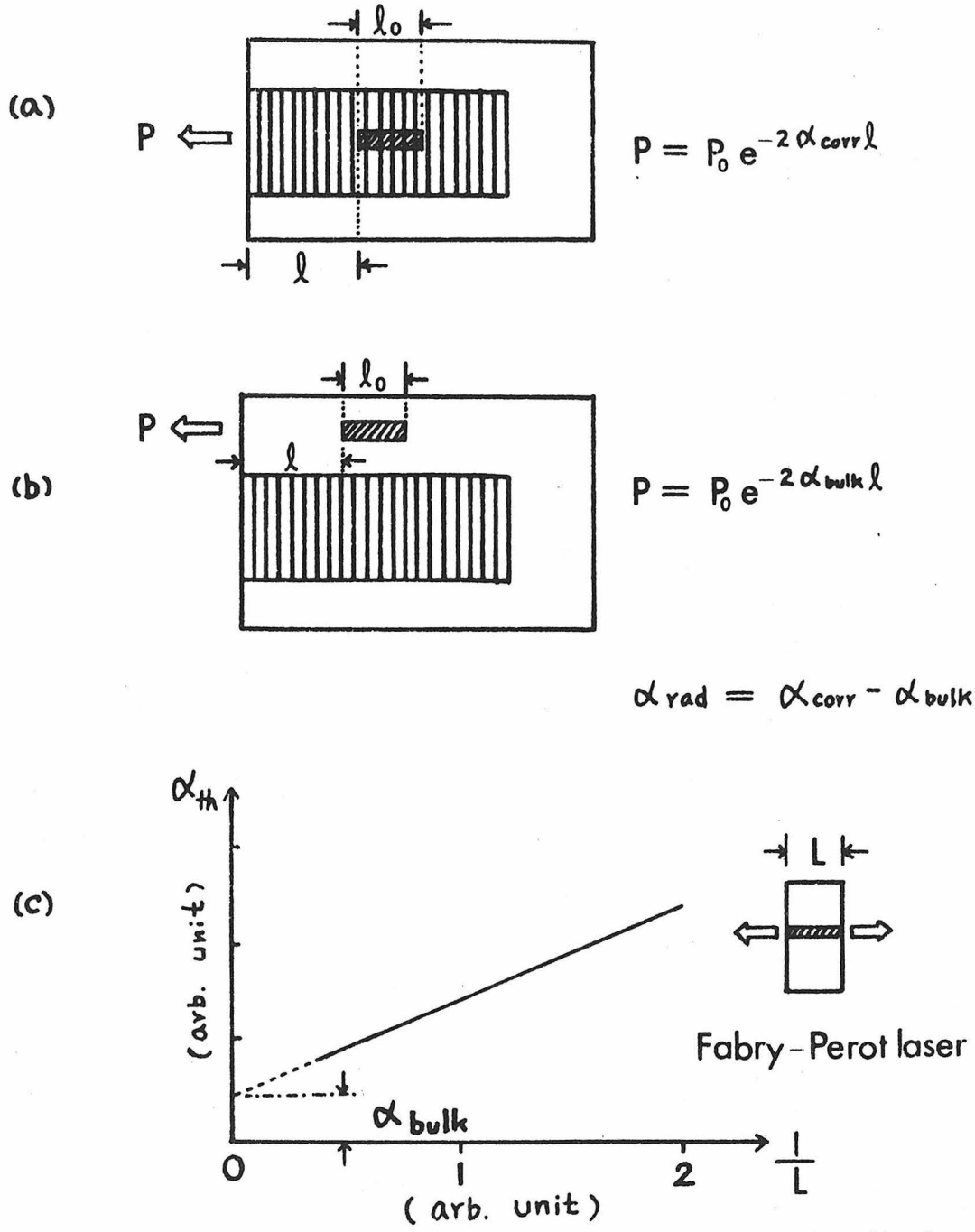

Fig. 5-15 Determination of the bulk absorption and radiation loss coefficients of a corrugated GaAs sample.

a straight line with slope $\ell n \frac{1}{R}$ and an intercept with the α_{th} axis gives α_{bulk} as illustrated in Fig. 5-15(c). Once α_{bulk} is found we can use it in equation (5-3) to determine α_{rad}. These methods are only practical with optical excitation where the changes in the excitation conditions are easily affected.

It is very important to determine accurately the period of the grating in a distributed feedback laser. This can be appreciated from the lasing wavelength equation

$$\lambda \approx 2n_{eff}\Lambda$$

where $2n_{eff} \simeq 7.2$. A change of 10Å in the grating period, say, will result in a shift of the lasing wavelength by nearly 72Å. Such a big shift can easily move the lasing wavelength from the center of the gain spectrum to the tail where the gain is low, thus increasing the threshold beyond any practical pumping level. Hence we need to determine whether the holographic exposure system is set to give the required period before exposing the GaAs samples. This is accomplished by first exposing a test sample and using a laser beam diffraction to measure its period. The sample is mounted on a rotary table and a laser beam is directed to pass through the rotating axis of the table as shown in Fig. 5-16(a). A reference angle θ_o is determined by letting the incident beam and the reflected beam coincide at normal incidence. The grating is then rotated until the Littrow reflection takes place, that is when the diffracted beam and the incident beam directions coincide. This occurs when the condition

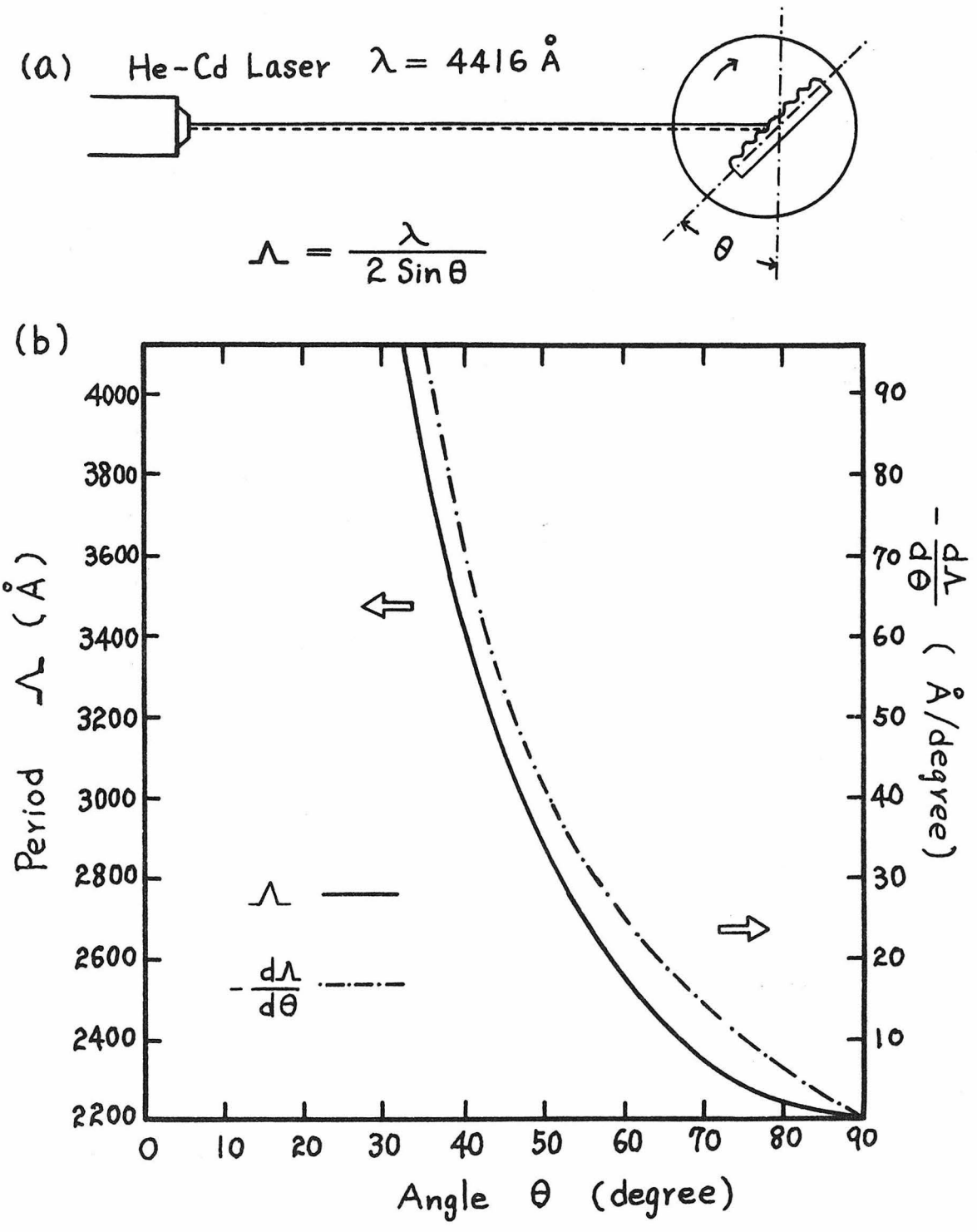

Fig. 5-16 (a) Diagram shows the geometry of the grating period measuring system.

(b) Plots of equation (5-4) and (5-5).

$$2\Lambda \sin\theta = \lambda \tag{5-4}$$

is satisfied, where θ is as indicated in Fig. 5-16(a). If the angular reading at this point is θ_1, then $\theta = |\theta_1 - \theta_0|$. Let us calculate the sensitivity of Λ with respect to a small change in θ

$$\frac{d\Lambda}{d\theta} = -\Lambda\cot\theta \tag{5-5}$$

Equations (5-4) and (5-5) are plotted in Fig. 5-16(b). The dependence of $d\Lambda/d\theta$ on θ is such that it approaches infinity when the angle is small and decreases to zero when θ is near 90°. As a typical example consider a grating with a period of 3500Å using the blue line of an He-Cd laser (4416Å). The required θ can be determined from Fig. 5-16(b) to be 39.11°. At this angle $d\Lambda/d\theta$ is ∿75.13Å/degree hence an error of 1 minute in reading the angle will result in an error of 1.25Å in Λ which is easily tolerated. A good rotary table can yield angular accuracies considerably in excess of the 1 minute figure used above.

The measurement of fundamental gratings is not as straightforward. For a grating with a period $\Lambda \sim 0.11$ μm we cannot observe diffraction using $\lambda = 3250$Å in air. Thus we have to pass the UV laser beam through a quartz prism first as shown in Fig. 5-17(a). The prism which has a rectangular base with index of refraction n is mounted on a rotary table. A sample with 0.11 μm grating is attached to one of the prism faces with xylene or immersion oil. The prism is first set so that the incident beam incident on one of the prism faces is reflected backward retracing the incident beam direction. The

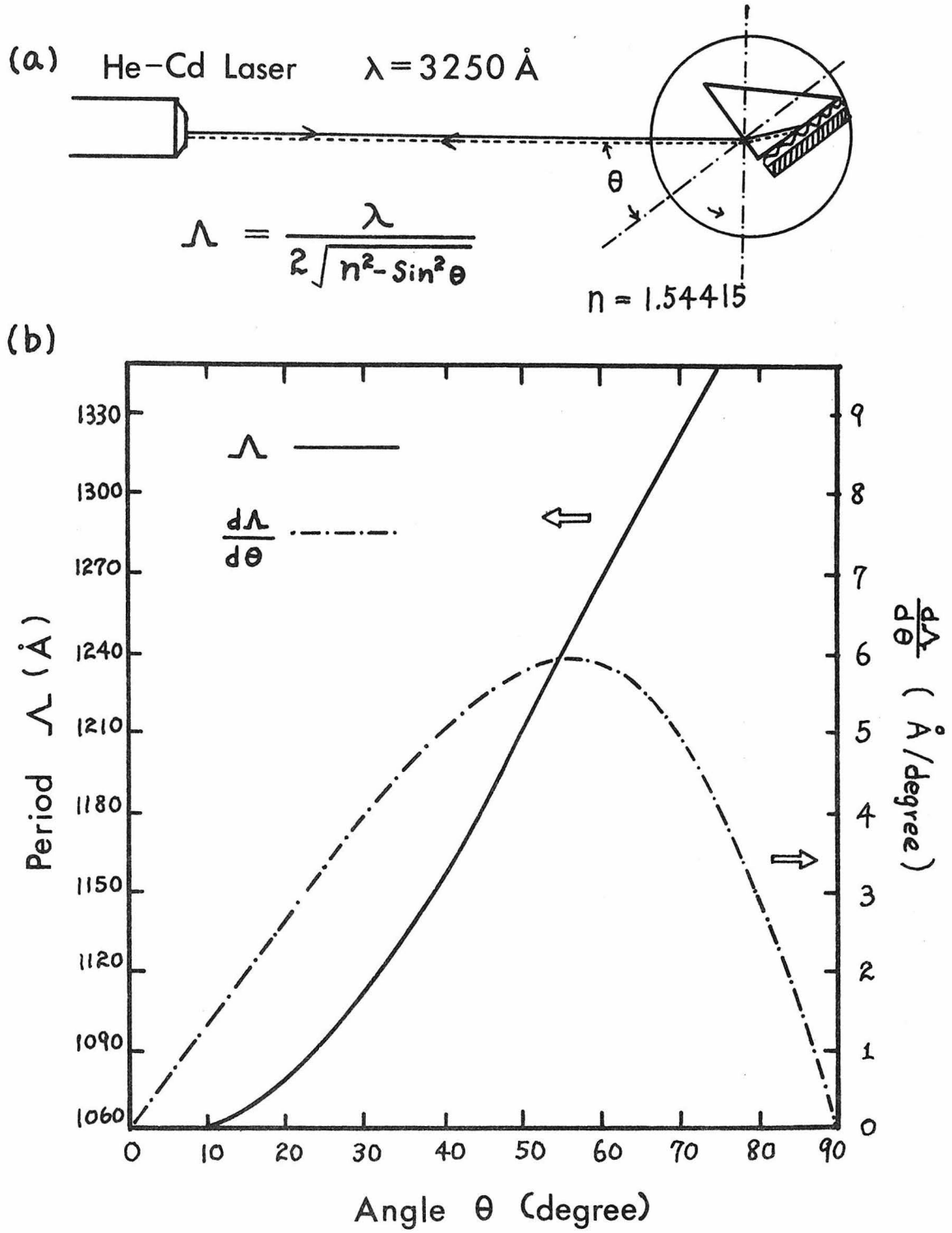

Fig. 5-17 (a) Schematic diagram of the system for measuring grating period less than 0.16 μm.

(b) Plots of equation (5-6) and (5-7).

angular reading at this position is denoted as θ_o. The prism is then rotated until the diffracted beam from the grating retraces the incident beam direction. Let the corresponding angular reading be θ_1, which means that the prism is rotated an angle of $\theta = |\theta_1 - \theta_o|$. Using the geometry shown in Fig. 5-17(a) we can find the period of the grating as

$$\Lambda = \frac{\lambda}{2\sqrt{n^2 - \sin^2\theta}} \tag{5-6}$$

If $\lambda = 3250\text{Å}$ is used we have

$$\Lambda = \frac{1625}{\sqrt{n^2 - \sin^2\theta}} \ (\text{Å})$$

where θ is the measured angle of rotation. In this formula the index of refraction of the prism n enters, so we have to know n as accurately as possible. A rough estimate of n can be obtained by a simple laser beam refraction experiment. A more accurate value is obtained by using a grating with a larger period ($\Lambda > 1700\text{Å}$) which is measurable in air using $\lambda = 3250\text{Å}$. This same grating is then attached to the prism and one looks for its diffraction in higher orders. For example if $\Lambda = 2771\text{Å}$ is measured in air, using the rough estimate of $n \sim 1.5$ we find that the Littrow reflection angles inside the prism will be $\phi \sim 61.5°$ for the first order beam and $\phi \sim 17.4°$ for the second order beam. The first order reflected beam is not observable in the forward direction because

$$\sin\theta = n\sin\phi > 1$$

However we will be able to see the second order reflected beam. Assume, for example, that the measured angle θ is 35°27', the index of refraction is then determined to very high precision as n = 1.54415 (at λ = 3250Å). This n is used in equation (5-6) to calculate the grating periods with Λ smaller than 0.16 μm. The grating period measured by this method is less sensitive to the accuracy of angular readings than the previous method. This is seen from

$$\frac{d\Lambda}{d\theta} = \frac{\Lambda}{2}\left(\frac{\sin 2\theta}{n^2 - \sin^2\theta}\right) \tag{5-7}$$

Equation (5-7) and equation (5-6) are plotted in Fig. 5-17(b) for n = 1.54415.

CHAPTER 5 REFERENCES

(1) D. Marcuse, "Mode conversion caused by surface imperfections of a dielectric slab waveguide," Bell Syst. Tech. J. 48, 3187 (1969).

(2) D. C. Flanders, H. Kogelnik, R. V. Schmidt, and C. V. Shank, "Grating filters for thin-film optical waveguide," Appl. Phys. Lett. 24, 194 (1974).

(3) R. V. Schmidt, D. C. Flanders, C. V. Shank, and R. D. Standley, "Narrow-band grating filters for thin-film optical waveguide," Appl. Phys. Lett. 25, 651 (1974).

(4) H. L. Garvin, J. E. Kiefer, and S. Somekh, "Wire grid polarizers for 10.6 μm radiation," Conference on Laser Engineering and Applications - Digest of Technical Papers, 100 (1973).

(5) H. L. Garvin, E. Garmire, S. Somekh, H. Stoll, and A. Yariv, "Ion beam micromachining of integrated optics components," Appl. Opt. 12, 455 (1973).

(6) L. P. Boivin, "Standing wave effect in grating production by laser beam interference on resist coated highly reflecting substrates," Opt. Commun. 9, 206 (1973).

(7) C. V. Shank and R. V. Schmidt, "Optical technique for producing 0.1-μ periodic surface structures," Appl. Phys. Lett. 23, 154 (1973).

(8) H. W. Yen, M. Nakamura, E. Garmire, S. Somekh, A. Yariv, and H. L. Garvin, "Optically pumped GaAs waveguide lasers with a fundamental 0.11μ corrugation feedback," Opt. Commun. 9, 35 (1973).

(9) W. T. Tsang and S. Wang, "Simultaneous exposure and development technique for making gratings on positive photoresist," Appl. Phys. Lett. 24, 196 (1974).

(10) E. G. Spencer and P. H. Schmidt, "Ion-beam techniques for device fabrication," J. Vac. Sci. Technol. 8, S52 (1971).

(11) Per G. Glöersen, "Ion beam etching," J. Vac. Sci. Technol. 12, 28 (1975).

(12) H. L. Garvin, "High resolution fabrication by ion beam sputtering," Sol. State Tech. 31 (1973).

(13) Y. Tarui, Y. Komiya, and Y. Harada, "Preferential etching and etched profile of GaAs," J. Electrochem. Soc. 118, 118 (1971).

(14) S. Iida and K. Ito, "Selective etching of gallium arsenide crystals in H_2SO_4-H_2O_2-H_2O system," J. Electrochem. Soc. 118, 768 (1971).

(15) L. Comerford and P. Zory, "Selectively etched diffraction gratings in GaAs," Appl. Phys. Lett. 25, 208 (1974).

(16) M. B. Panish, "Heterojunction injection lasers," IEEE Trans. Microwave Theory Tech. 23, 20 (1975).